2019

Design, Synthesis, and Evaluation of GUNW-3 as a Brain Targeting Agent

Asim Najmi
South Dakota State University

DESIGN, SYNTHESIS, AND EVALUATION OF GUNW-3 AS A BRAIN TARGETING AGENT

BY

ASIM NAJMI

A dissertation submitted in partial fulfillment of the requirements for the

Doctor of Philosophy

Major in Pharmaceutical Science

South Dakota State University

2019

DESIGN, SYNTHESIS, AND EVALUATION OF GUNW-3 AS A BRAIN TARGETING AGEN

ASIM NAJMI

This dissertation is approved as a creditable and independent investigation by a candidate for the Doctor of Philosophy in Pharmaceutical Sciences degree and is acceptable for meeting the dissertation requirements for this degree. Acceptance of this does not imply that the conclusion reached by the candidate are necessarily the conclusions of the major department.

Xiangming Guan, Ph.D. Date
Dissertation Advisor

Omathannu Perumal, Ph.D. Date
Head, Department of Pharmaceutical Sciences

Dean, Graduate School Date

ACKNOWLEDGEMENTS

All the praise and thanks to Allah, for giving me the blessing and the strength to accomplish this dissertation work.

I am truly thankful to Dr. Xiangming Guan to give me the opportunity to join his lab and pursue my Ph.D. I acknowledge, with deep gratitude, for his inspiration, encouragement, valuable time, and guidance. Without his help, support, and suggestion, this work could not be completed. Thereafter, I am deeply grateful to my committee members: Dr. Teresa Seefeldt, Dr. Hemachand Tummala, and Dr. Stephen Gent, for their support and suggestion during my Ph.D. journey. I would like to thank my labmates Shenggang Wang, Yue Huang, and Dr. Yahya Alqahtani for their contribution to this work through experiments and scientific discussion. I appreciate the time we spent together: teamwork, late night experiments, scientific discussion, and nonscientific interactions. All those moments were enjoyable and unforgettable.

I would like to thank Jazan University, Saudi Arabian Cultural Mission, and the government of Saudi Arabia for funding my academic journey.

I am truly thankful to my parents Yahya Najmi and Eysh Najmi for their unconditional love, support, and prayers. My thanks also to my brothers, sisters, and all relatives for their support. Special thanks to my loving and unbelievable supportive wife, Nawal Akkur, who has stood by me through all this journey. Without her amazing patience, help, encouragement, and taking care of the family nothing would be accomplished. Nawal made countless sacrifices to help me reach this point. There is no word to convey how much I appreciate her existence in my life. My thanks to my

daughter, Walife, for all the nights she felt asleep while she was waiting for me and for her continuous call to ask “are you still working dad?”. Thanks to my son, Yahya, who was always trying to discover what I was doing while I was writing. Thanks to Walife and Yahya for bringing the joy to our family.

TABLE OF CONTENTS

LIST OF FIGURES ix

LIST OF TABLES xii

ABSTRACT xiii

Chapter 1. Introduction 1

1.1 Brain 1

1.2 Blood Brain Barrier 3

1.2.1 History 3

1.2.2 Structure of the BBB 5

1.2.3 Function of the BBB 7

1.3 Pathways to across the BBB 8

1.4 Strategies to overcome the BBB 11

1.5 Transporter dependent brain targeting agents 19

1.6 GSH transporter for brain targeting 24

Chapter 2 Design, Synthesis, and Characterization of GUNW-3 27

2.1 Introduction 27

2.2 Design of GUNW-3 as a brain-targeting agent 27

2.3 Experimental Section 31

2.3.1 Material and instruments 31

2.3.2 Synthesis of GUNW-3 32

2.3.3 Purification and chemical stability of GUNW-3 34

2.3.4 In-vitro toxicity study 35

2.3.5 In-vivo toxicity study 35

2.4 Result and Discussion 35

2.4.1 Synthesis of GUNW-3 35

2.4.2 Purity and stability of GUNW-3 38

2.4.3 Confirmation of *S*-link isomer vs *N*-link isomer 40

2.4.4 Cell viability test of GUNW-3 44

2.4.5 In-vivo toxicity 45

Chapter 3 Brain Targeting of GUNW-3 Micelles 48

3.1. Introduction 48

3.1.1 Micelles 48

3.1.2 Micelles in drug delivery 49

3.1.3 Micelles for Brain Targeting 50

3.1.3a Ligand-Micelle-Based Active Brain Targeting 50

3.1.3.b Passive Targeting 51

3.1.4 GUNW-3 micelles 52

3.2 Experimental Section 54

3.2.1 Materials and instruments 54

3.2.2 Procedures 54

3.2.2.1 The Critical micellar concentration of GUNW-3 54

3.2.2.2 Preparation and characterization of GUNW-3 DiR micelles..... 55

3.2.2.3 Preparation of control DiR liposomes..... 55

3.2.2.4 Determination of DiR encapsulation efficiency and loading capacity 56

3.2.2.5 Stabilities of GUNW-3 DiR micelles and control DiR liposomes 56

3.2.2.6 Whole body fluorescence imaging of mice 57

3.2.2.7 EX-vivo brain and organs imaging 57

3.2.2.8 Statistics 58

3.3 Result and Discussion..... 59

3.3.1 The critical micellar concentration (CMC) of GUNW-3 micelles... 59

3.3.2 Preparation and characterization of GUNW-3 DiR micelles 61

3.3.3 Preparation and characterization of control DiR liposomes..... 62

3.3.4 Determination of DiR encapsulation..... 64

3.3.5 Stabilities of GUNW-3 DiR micelles and control DiR liposomes... 64

3.3.6 Whole-body fluorescence imaging 67

3.3.7 Ex-vivo imaging. 72

Chapter 4 Brain-Targeting of GUNW-3 Liposomes 84

4.1 Introduction 84

4.1.1 Classification of liposomes 85

4.1.2 Liposomes for brain targeting 86

4.1.3 GUNW-3 liposomes for brain targeting 87

4.2 Experimental section 91

4.2.1 Material and instruments 91

4.2.2 Procedures 91

4.3 Result and Discussion 95

4.3.1 Liposome preparation 95

4.3.2 Liposome stability 98

4.3.3 In-vivo imaging 100

4.3.4 Ex-vivo imaging. 102

Chapter 5. Conclusion, Significance, and Future Direction 108

5.1 Conclusion 108

5.2 Limitation 109

5.3 Significance 109

5.4 Future direction 110

References 111

LIST OF FIGURES

Figure 1.1 Brain. 2

Figure 1.2 Illustration for Glodmann's discovery of the BBB[9]. 4

Figure 1.3 Basic structure of tight junction of the BBB[8]. 6

Figure 1.4 Pathways to across BBB[10]. 10

Figure 1 5 Trans-cranial brain drug delivery[24] 12

Figure 2.1 Schematic drawing of chemical structure GUNW-3 and its formation of GUNW-3 micelles……29

Figure 2.2 Schematic drawing illustrating GUNW-3 as a part of the components of liposomes. 30

Figure 2.3 Synthetic schemes of GUNW-3. 37

Figure 2.4 Representative HPLC chromatogram of GUNW-3 at concentration of 1 mg/ml and the blank solvent. 38

Figure 2.5 Stability of GUNW-3 in a solution of methanol-ammonium water (1:1 ratio, pH:10.8). 39

Figure 2.6 Chemical structures of GUNW-3 and its N-link isomer 40

Figure 2.7 FITR spectra of GSH (A) and GUNW-3 (B) 41

Figure 2.8 Mass spectrum of GUNW-3 obtained from LC/MS/MS on a positive mode. 43

Figure 2.9 Dose-response curves for the determination of IC_{50} values of GUNW-3 with NCI-H226 cell line (A) and CV-1 cell line (B) (mean ±SD). 44

Figure 2.10 The report from the Animal Disease Research & Diagnostic Laboratory for a pathological examination of mice treated with GUNW-3 micelles or GUNW-3 liposomes 46

Figure 3.1 Chemical Structure of GUNW-3……..53

Figure 3. 2 A plot of I_3/I_1 versus concentration of GUNW-3. 60

Figure 3. 3 Preparation of GUNW-3 micelles. 61

Figure 3.4 Particle size and size distribution of GUNW-3 DiR micelles. 63

Figure 3.5 (A) Stabilities of GUNW-3 DiR micelles and control DiR liposome in the absence of FBS. (B) GUNW-3 DiR micelles stability in the presence of FBS. (C) control DiR liposomes stability in the presence of serum..... 66

Figure 3. 6 In-vivo whole-body fluorescence imaging of mice at 15 min, 1 h, 24 h, and 48 h..... 69

Figure 3. 7 Lateral image for each group at 1h. 70

Figure 3.8 Fluorescence intensity from the brains of mice treated with GUNW-3 DiR micelles, control DiR liposomes, or free DiR at different time points. 71

Figure 3.9 Ex-vivo imaging of the brains at 1 h after a single dose IV injection by tail vein injection..... 73

Figure 3.10 Ex-vivo imaging of the brains at 48 h after a single dose IV injection by tail vein injection 75

Figure 3.11 Ex-vivo imaging of the major organs collected 1 h after a single dose IV injection 78

Figure 3.12 Ex-vivo imaging of the major organs 48 h after a single dose IV injection.. 81

Figure 4.1 A graphic description of a liposome[82]……..85

Figure 4.2 Chemical structure of Lecithin. 88

Figure 4.3 Chemical structure of cholesterol..... 88

Figure 4.4 Chemical structure of dimethyldoioctadecylammonium bromide (DDAB) ... 89

Figure 4.5 Chemical structure of GUNW-3..... 89

Figure 4.6 Graphic description of the preparation of GUNW-3 DiR liposomes and control DiR liposomes using the thin hydration method..... 95

Figure 4.7 Particle size and size distribution of control DiR liposomes (A), and GUNW-3 DiR liposome (B)..... 97

Figure 4.8 Stability of GUNW-3 DiR liposomes and control DiR liposomes. A: storage stability at 4 C for 7 days; B: GUNW-3 DiR liposomes; C: Control DiR liposomes stability in the presence of proteins (FBS) at 37 ˚C for 7 days..... 99

Figure 4.9 In-vivo whole-body imaging of mice at 15 min, 30 min, 60 min, and 180 min. A: control DiR liposomes; and B: GUNW-3 DiR liposomes..... 101

Figure 4.10 In-vivo semi-quantitative fluorescence intensity of brains.. 102

Figure 4 11 Ex-vivo imaging of the brains at 1 h after a single dose IV injection of A: control DiR liposomes or B: GUNW-3 DiR liposomes. D: Semi-quantitative fluorescence intensity of brains 103

Figure 4.12 Ex-vivo imaging of the major organ 1h after (i.v) injection of the (A) Control DiR liposomes (B) GUNW-3 DiR liposomes. 105

Figure 4.13 Semi-quantitative fluorescence intensity from different organs 106

LIST OF TABLES

Table 1.1 BBB disruption after the intracarotid arterial infusion[24] 13

Table 1.2 Summary of Receptor-mediated transport (RMT) and Carrier-mediated transport (CMT) dependent brain targeting [33] 20

Table 3.1 Micelles formulations in clinical trials……..50

Table 3.2 Nanoparticle parameters of GUNW-3 DiR micelles and control DiR liposomes. 63

Table 3 3 Comparison of fluorescence intensity from the brains of mice with different treatments as presented in Figure 3.8..... 74

Table 3.4 Comparison of fluorescence intensity from the brains of mice with different treatments as presented in Figure 3.9..... 76

Table 3.5 Comparison of fluorescence intensity from the brains of mice with different treatments as presented in Figure 3.11..... 79

Table 3.6 Comparison of fluorescence intensity from the brains of mice with different treatments as presented in Figure 3.12..... 82

Table 4.1 Parameters of control DiR liposomes and GUNW-3 liposomes…….. ……97

ABSTRACT

DESIGN, SYNTHESIS, AND EVALUATION OF GUNW-3 AS A BRAIN TARGETING AGENT

ASIM NAJMI

2019

The blood brain barrier (BBB) is a barrier in the brain that separates the peripheral blood circulation system from the central nerve system (CNS). The barrier effectively protects the brain from xenobiotics. The BBB serves as a physical barrier through the tight junction of endothelial cells that were found to be 50-100 times tighter than that of normal endothelial cells. Different drug efflux pumps such as P-glycoproteins and multidrug-resistance proteins are found to be overdistributed on the BBB. These drug efflux pumps help pump xenobiotics out if they enter the cells and serv as an additional mechanism to prevent xenobiotics from entering the CNS. The tight junction, drug efflux pumps, and other features of the BBB prevent almost 98% of small molecules, such as most therapeutics, and almost all large molecules such as biologics, recombinant genes and proteins from entering the brain. The inability to reach the therapeutic concentration caused by the barrier is often the major cause of treatment failure for brain diseases.

Although the BBB blocks foreign compounds from entering the CNS, endogenous compounds, such as glucose, amino acids, peptides, neurotransmitters, and glutathione (GSH), enter the CNS readily through their corresponding receptors or transporters present in the BBB. Some of these receptors or transporters have been

targeted for facilitating therapeutics, diagnostics, and other compounds to cross the BBB to reach the CNS.

GSH is an endogenous three amino acid peptide. It plays various roles in the body: as a major antioxidant, a compound that removes toxic compounds, and a compound involved in other cellular functions. GSH crosses the BBB through a Na-dependent GSH transporter. Recently, GSH transporters have been found effective in facilitating crossing of compounds through the BBB to reach the CNS. To achieve GSH transporter-mediated BBB crossing, GSH has been linked to a therapeutic agent (GSH-Drug) to form a prodrug. The prodrug crosses the BBB by binding the GSH part to a GSH transporter followed by internalization of the prodrug. GSH has also been linked to polyethylene glycol (PEG) which is connected to a phospholipid (P) to form GSH-PEG-P or polyethylene glycol connected to vitamin E to form GSH-PEG-E. GSH-PEG-P and GSH-PEG-E have been coated on the surface of liposomes (GSH-PEGylated liposomes) to facilitate crossing of the liposomes through the BBB using the mechanism of binding the GSH moiety to a GSH transporter followed by internalization of the liposomes through endocytosis or transcytosis. The GSH-PEGylated liposomes have been shown to safely enhance the delivery to the brain by approximately 3-folds.

We have developed GUNW-3 as a GSH-transporter dependent brain targeting agent. GUNW-3 was designed by connecting a hydrophilic GSH molecule to a hydrophobic cholesterol molecule through a two ehthylene glycol unit linker with a hope that the GSH part can serve as a brain-targeting structure through binding to the GSH transporter and facilitate the entry into the brain. This dissertation describes the design,

synthesis, and fully characterization of GUNW-3. The dissertation also describes the ability of GUNW-3 to form micelles by itself (GUNW-3 micelles), the ability of GUNW-3 micelles to cross the BBB to reach the brain, and the ability of GUNW-3 micelles to carry a dye (DiR) to the brain. Further, the dissertation shows the ability of GUNW-3 helps guide liposomes to the brain by forming GUNW-3 liposomes and the ability of GUNW-3 liposomes to deliver a dye (DiR) to the brain. Below is a brief description of the findings in this dissertation.

GUNW-3 was synthesized in 4 steps from cholesterol and other commercially available reagents. GUNW-3 was found to be relatively stable. A cytotoxicity study of GUNW-3 revealed IC_{50} values of 0.65 mM and 0.47 mM for CV-1 cells (monkey kidney cells) and NCI-H226 cells (human lung cancer cells) respectively.

GUNW-3 was found to form micelles by itself with a CMC value of 3.9 μM. CMC is a critical micelle parameter to reflect the stability of micelles and is also a parameter to determine if the micelles are stable enough to be used for a clinical application. The CMC of micelles need to be in μM concentration so that the micelles are stable enough to remain as micelles once being diluted in the blood stream. The CMC in low μM (3.9 μM) of GUNW-3 suggests that GUNW-3 micelles can be used for a therapeutic application. Further, the CMC of GUNW-3 is much lower than the IC_{50} values of the molecule indicating that GUNW-3 is not cytotoxic. For brain targeting, our data with ex-vivo imaging of the brains shows that the brain uptake of DiR, a dye, delivered by GUNW-3 micelles were 5 times higher than that of the control liposome and 12 times higher than that of free DiR at the first hour. After 48 h, the brain uptake of DiR

delivered by GUNW-3 micelles was 6.5 times higher than that of the control liposome and 14 times higher than that of free DiR.

GUNW-3 was also found to help deliver liposomes to the brain most likely by embedding the hydrophobic cholesterol part into the liposome double lipid layer and the hydrophilic GSH part floating on the surface of the liposomes for brain targeting. Our data from ex-vivo imaging of the brains demonstrate that GUNW-3 liposomes were able to significantly (>3 folds) improve the delivery of DiR to the brain and retain in the brain well when compared with the control liposomes.

Liposomes and micelles are known effective drug carriers that can be used to deliver various drugs or compounds such as small molecule therapeutics, DNA, RNA, and proteins (e.g., antibodies). Liposomes and micelles can encapsulate drugs and protect them from *in vivo*/*in vitro* degradation. They can also help reduce drug clearance, increase *in vivo* drug half-life, enhance the drug payload, control drug release, and improve drug solubility. The abilities to deliver DiR to the brain by GUNW-3 micelles and GUNW-3 liposomes warrantee further investigation of these two brain targeting delivery systems for delivering compounds to the brain for brain disease treatment or prevention.

In summary, we have synthesized and characterized the rationally designed GUNW-3 as a brain targeting agent. GUNW-3 micelles and GUNW-3 liposomes showed promising brain targeting abilities. GUNW-3 micelles and GUNW-3 liposomes will be promising delivery systems for therapeutic and diagnostic molecules.

Chapter 1. Introduction

1.1 Brain

The human brain is the most complex organ that is made up by ~100 billion neurons and consists of three main parts; cerebrum, cerebellum, and medulla (Figure 1.1) [1-3]. Although the brain weighs only 2% of the body weight, 15% of the blood volume and 20% of the total oxygen supply are received by the brain [4, 5].Together with the spinal cord, the brain is known as the central nervous system (CNS). The CNS functions by receiving and processing signals and sending orders to all human organs to control the activities of the body [6]. The brain is protected by head bone of skull and presence of the blood brain barrier (BBB)[7].

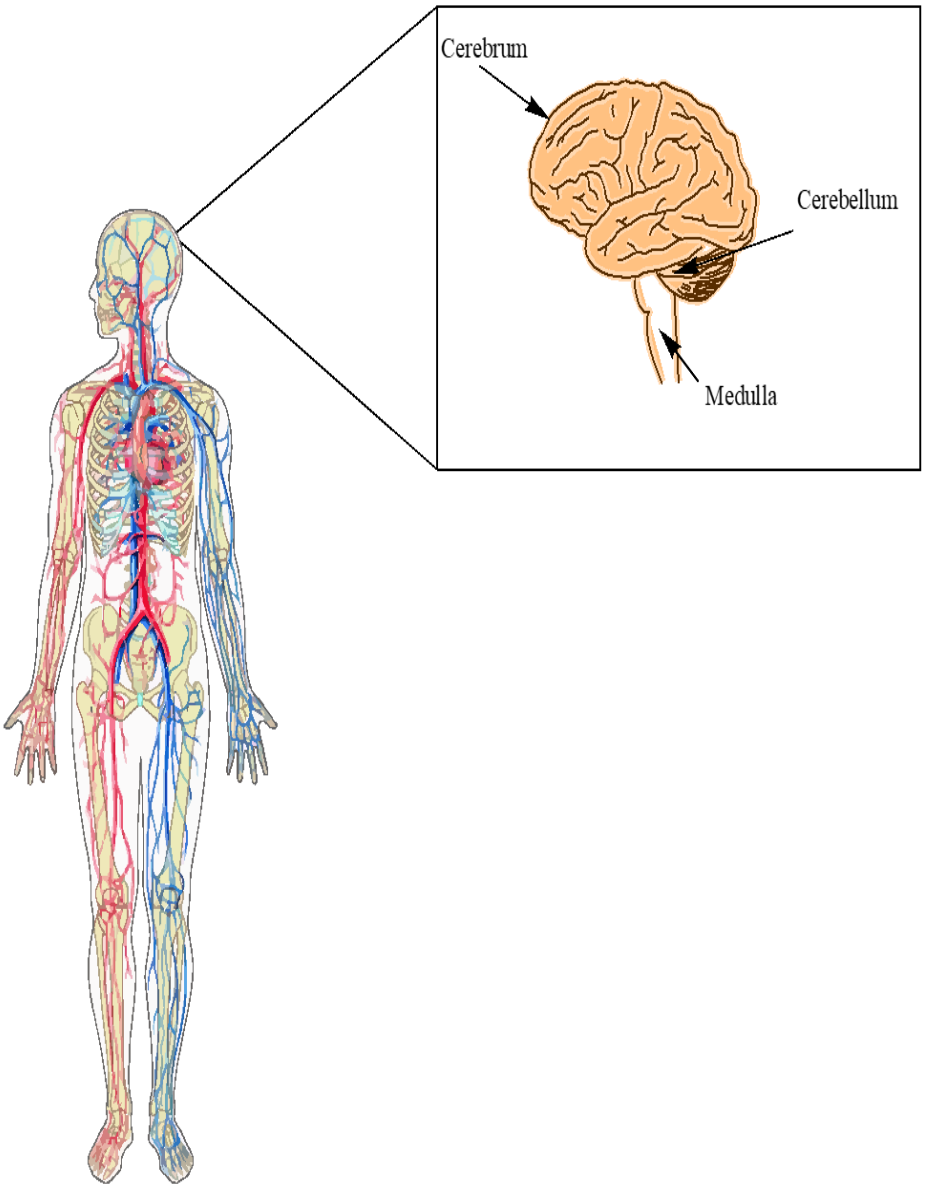

Figure 1.1 Brain.

1.2 Blood Brain Barrier

1.2.1 History

The concept of the BBB was first introduced after a series of experiments conducted by Paul Ehrlich in the late 19th century. By using a water-soluble dye, aniline, Ehrlich found that the dye stained all the tissues except the brain and spinal cord. The results of this experiment were the first piece of evidence for the presence of the BBB. However, Ehrlich incorrectly attributed his finding to the inability of the nervous system to take up the dye. Edwin Glodmann, Ehrlich's student, challenged his mentor's conclusion by designing an experiment with two parts. First, he used trypan blue injected intravenously to confirm Ehrlich's finding that all tissues except the brain and spinal cord were stained. In his second experiment Glodmann injected trypan blue directly to cerebrospinal fluid. The injection resulted in staining of the nerve tissues only. This experiment was the first piece of evidence to indicate the presence of a barrier between the brain tissue and blood (Figure 1.2). Later, an electron microscopy study in the early 1960's demonstrated the presence of a tight junction and location of the BBB to the endothelial cells not to surrounding astrocyte or basement lamina[8, 9].

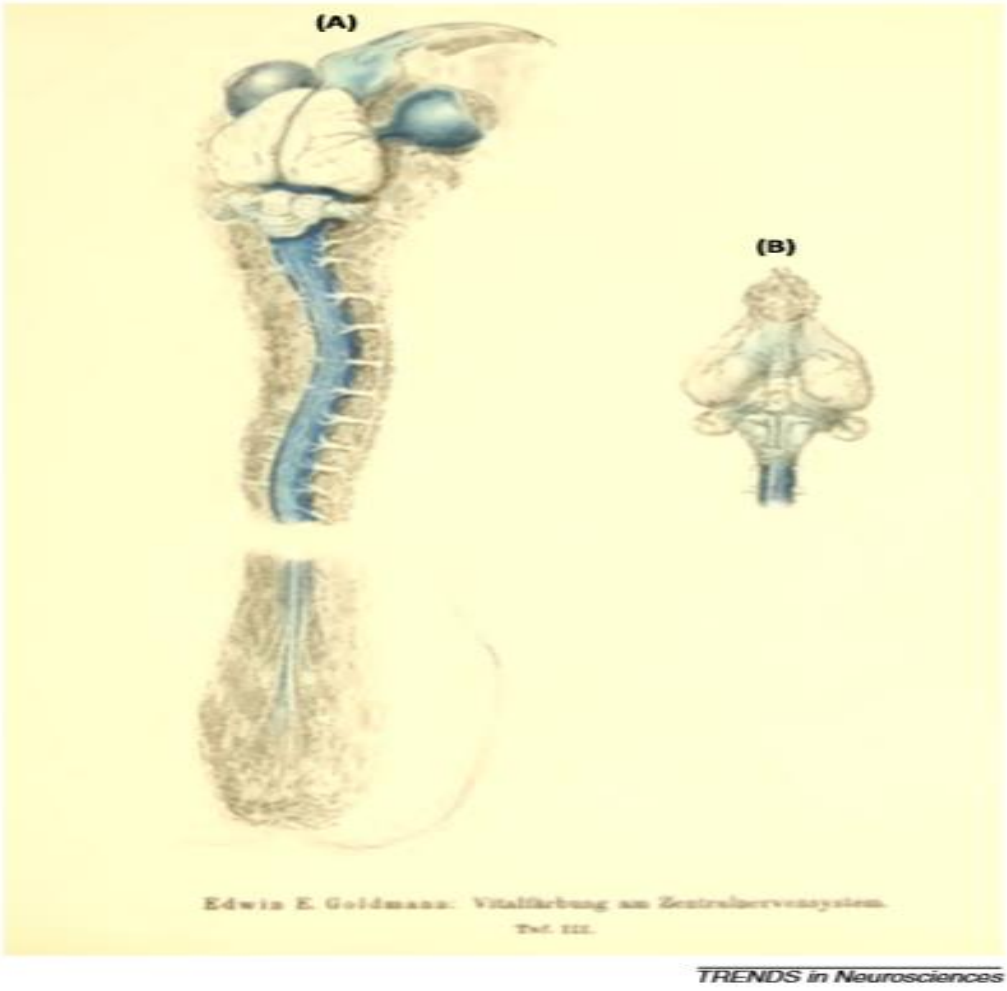

Figure 1.2 Illustration for Glodmann's discovery of the BBB[9].

1.2.2 Structure of the BBB

The BBB is a selective barrier made by endothelial cells that separates the peripheral blood circulation form the CNS [7, 10]. The BBB serves as a physical barrier through the tight junctions of endothelial cells that force molecules to go by transcellular pathway rather than the paracellular route [10].The junction of endothelial cells was found to be 50-100 times tighter than that of normal endothelial cells (Figure 1.3) [11]. Because of this reason, hydrophilic molecules are physically hampered to enter the brain due to this very tight aqueous space. Overdistribution of different drug efflux pumps such as P-glycoprotein and multidrug-resistance protein is another feature of the BBB. These efflux pumps restrict the passage of hydrophobic molecules through the brain cells [7, 12]. Studies reveals that among 6000 drugs in medicinal chemistry database that are used to treat a small number of selective brain ailments, i.e., insomnia and Alzheimer's, only 6% of them are brain active due to the presence of the BBB [13]. Interestingly, among all the drugs only 12% are active in the central nervous system, a scenario that becomes 1% if affective disorders are excluded [14]. Therefore, enabling a therapeutic to cross the BBB is a great challenge in the treatment of CNS disorders.

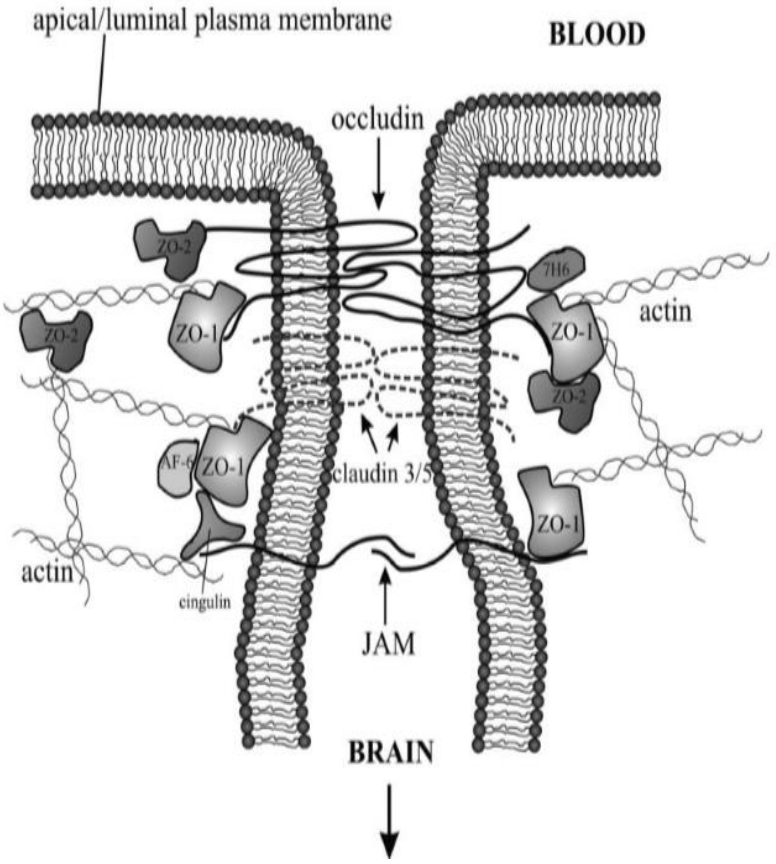

Figure 1.3 Basic structure of tight junction of the BBB[8].

1.2.3 Function of the BBB

Through its unique barrier feature, the BBB helps control and regulate substances from entry into the CNS to maintain proper functions of the CNS.

A- Ion regulation

The BBB not only provides a stable environment for neural function, but also keeps the ionic composition optimal for synaptic signaling by a combination of specific ion channels and transporters. The BBB keeps ions in plasma and CNS as two different pools and prevents CNS ion pools from the fluctuation of plasma ion pools. Thus the concentration of potassium in mammalian plasma is approximately 4.5 mM, but in CSF and brain interstitial fluid (ISF) this is maintained at ~2.5–2.9 mM, in spite of changes that can occur in plasma potassium following exercise, a meal, or any other factors [15, 16]. Ca^{2+}, Mg^{2+} and pH are also actively regulated at the BBB and BCSFB [17, 18]

B- Neurotransmitters

Blood plasma contains high levels of the neuroexcitatory amino acid glutamate which fluctuate significantly after the ingestion of food. If glutamate is released in an uncontrolled manner into the brain ISF, as in the case of hypoxic neurons during ischemic stroke, neural tissues can be damaged considerably and irreversibly. Since the central and peripheral nervous systems use many of the same neurotransmitters, the BBB helps separate these two neurotransmitter pools separate to minimize ‘crosstalk’[18, 19].

C- Neurotoxins

The BBB functions as a protective barrier which protects the CNS from neurotoxic substances in the blood. These neurotoxins can be endogenous metabolites

and proteins, xenobiotics ingested from the diet or acquired from the environment. A number of ABC energy-dependent efflux transporters (ATP-binding cassette transporters) actively pump many of these compounds out of the brain. One of the features related to the adult CNS is that in adult, neurons are fully differentiated and do not have a significant regenerative capacity[18]. They are not able to divide and replace themselves if damaged under normal circumstances, though there is a continuous steady rate of neuronal cell death from birth throughout life in the healthy human brain with relatively low levels of neurogenesis [18, 20]. Any acceleration in the natural rate of cell death resulting from an increased access of neurotoxins into the brain would become prematurely debilitating.

D- Brain nutrition

The BBB has low passive permeability to many essential water-soluble nutrients and metabolites required by the CNS. Specific transport systems therefore are expressed in the BBB to ensure an adequate supply of these nutrients. The differentiation of the endothelium into a barrier layer begins during embryonic angiogenesis[18].

1.3 Pathways to across the BBB

There are four pathways for compounds to cross the BBB: (i) passive diffusion which depends on the lipophilicity and concentration gradient of a drug. Passive diffusion includes paracellular diffusion and transcellular diffusion; (ii) adsorptive-mediated endocytosis (AMT) which occurs through nonspecific electrostatic interactions between the anionic micro domains on the brain capillary endothelial cell membrane and a cationic drug delivery system such as chitosan, gelatin, or cationic liposomes; (iii) transporters-mediated transcytosis (TMT); and (iv) receptor-mediated endocytosis

(RME)[21]. The last two pathways are the basis for a number of endogenous compounds to cross the BBB despite their unfavorable lipophilicity or molecular sizes for passing through the BBB (Figure1.4)[10]. Below is a brief description of these four pathways.

A. Paracellular diffusion

Paracellular diffusion occurs between the junction space of two cells. The space is an aqueous space and allows small water-soluble molecules to pass through. However, the tight junction of the BBB limits this pathway for aqueous molecules.

B. Transcellular diffusion

Transcellular diffusion is a process where a molecule goes through the cell by passing through the cell membrane. Since the cell membrane is lipophilic, this pathway requires a molecule to be lipophilic. This pathway is limited by the presence of drug efflux pumps in the BBB. Lipophilic or hydrophobic molecules are usually a good substrate for P-glycoprotein (PGP) or multidrug drug resistance proteins (MDR). As a result, a hydrophobic drug may pass through the BBB but could be pumped back to the bloodstream resulting in no net distribution to the brain.

C. Receptor-mediated endocytosis

Large endogenous molecules that are needed for brain activities, such as proteins like insulin (5808 Da) and transferrin (MW=80kDa), are transported by their corresponding receptors. The protein binds to its receptor and enters the brain through endocytosis.

D. Transporter-mediated transcytosis

Small endogenous molecules such as glucose, amino acids, and short peptides such as glutathione are transported through their corresponding transporters in the BBB. These endogenous molecules bind to their corresponding receptors before being transported into the brain.

E. Adsorptive-mediated endocytosis

Since the cell membrane is negatively charged, cationic molecules can enter the brain through nonspecific electrostatic interactions with the anionic micro domains on the brain capillary endothelial cell membrane. Cationic liposomes enter the brain through this mechanism. Cationic liposomes are used in this dissertation as one of the controls for brain targeting.

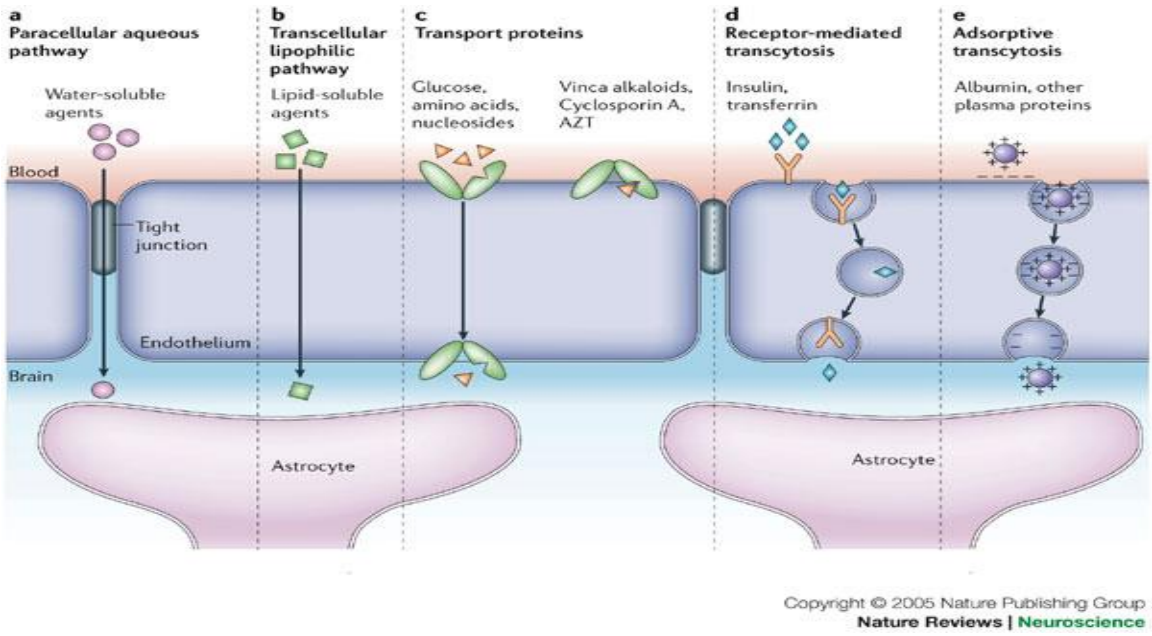

Figure 1.4 Pathways to across BBB[10].

1.4 Strategies to overcome the BBB

To overcome the BBB, three strategies has been developed. These three strategies are invasive approach, chemical property-based approach, and physiological-based approach.

A-Invasive approach

Invasive approach includes trans-cranial brain drug delivery and reversible BBB disruption.

i). Trans-cranial brain drug delivery

Trans-cranial brain drug delivery approaches bypass the BBB through intracerebral implantation, intracerebroventricular (ICV) infusion, or convection enhanced diffusion (CED).

The factor that limits the intracerebral implantation and ICV infusion is that both methods rely on drug diffusion to penetrate into the brain from the depot site. Solute diffusion decreases with the square of the diffusion distance. The concentration of drug decreases logarithmically with each millimeter of brain tissue that was removed from the injection site (in the case of intracerebral implantation) or from the ependymal surface of the brain (in the case of ICV infusion[22]. The concentration of a small molecule was decreased by 90% at a distance of only 0.5 mm from the intracerebral implantation site in rat brain [23, 24].

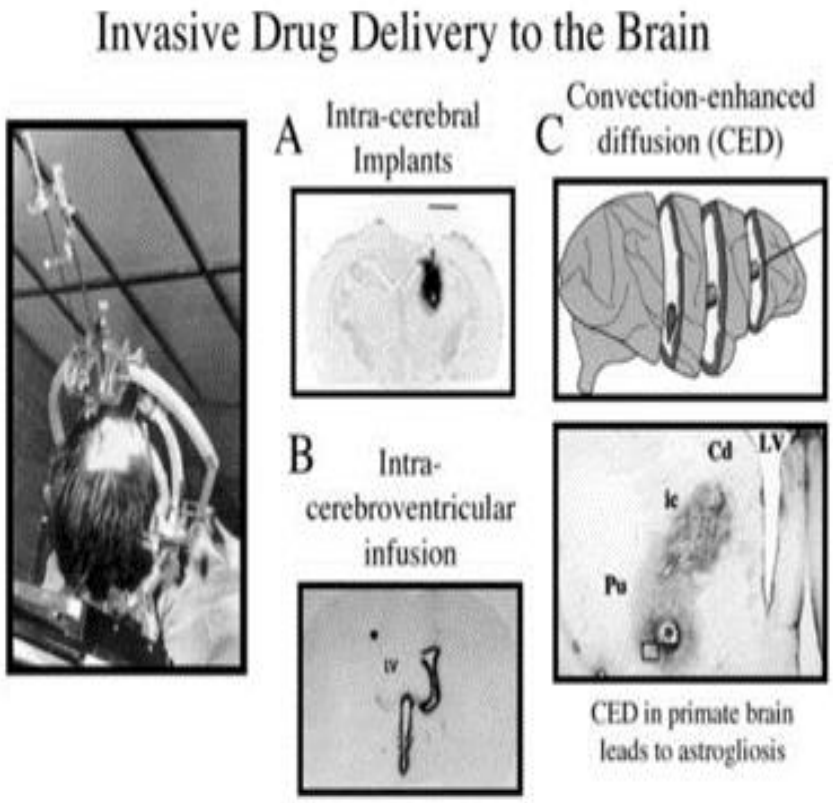

Figure 1.5 Trans-cranial brain drug delivery[24]

ii). Reversible BBB disruption

A significant effort was made in delivering drugs to the brain through BBB disruption after the intracarotid arterial infusion of vasoactive agents such as those listed in Table 1.1 The intracarotid arterial infusion of 2 M concentrations of poorly diffusible solutes such as mannitol causes disruption of the BBB owing to osmotic shrinkage of the endothelial cells. This approach is associated with severe vasculopathy[25] and chronic neuropathologic changes in rodent models and is also associated with seizures in either humans or animal models. Plasma proteins such as albumin are toxic to brain cells,[26] and BBB disruption allows for the uptake of plasma into the brain[24].

Table 1.1 BBB disruption after the intracarotid arterial infusion[24]

Method	Comment
Hyperosmolar	Leads to chronic neuropathologic changes and vasculopathy in the brain and seizures
Vasoactive agents	Examples are bradykinin, histamine, and multiple other vasoactive compounds; opens BBB in brain tumor to greater extent than normal brain
Solvents	BBB is solubilized with high dose ethanol, DMSO, SDS, Tween 80 (polysorbate-80)

Alkylating agents	Examples are etoposide and melphalan; may alkylate key sulfhydryl residues similar to mercury
Immune adjuvants	Freunds adjuvant opens BBB to IgG for weeks; enable IgG uptake into brain in rodent vaccine models, such as Alzheimer's disease
Ultrasound	The combination of administration of high-dose air bubbles (2–4 m) and high-dose ultrasound (10–1000 watt/cm2) can induce BBB disruption
Cytokines	Intracerebral interleukin-1 or CXC chemokines can attract white cells from blood and cause BBB disruption
Miscellaneous	Intracarotid acid pH, cold temperatures, or high-dose free fatty acid all cause BBB disruption

B-Chemical property-based strategy

Chemical property-based strategy mainly involves small molecules and prodrugs

i) Small molecules

Small molecule drugs can pass the BBB if it is lipid soluble, not avidly bound by plasma proteins, not a substrate for an active efflux transport system at the BBB, and has a molecular mass less than 400 Da [24]. The BBB permeation of a drug does not increase in proportion to drug's lipid solubility when the molecular weight of the drug is increased. BBB permeation drops 100-fold as the surface area of the drug increases from 52 Angstroms [27] (e.g., a drug with molecular mass of 200 Da) to 105 Angstroms [27] (e.g., a drug of 450 Da) [24, 28]. Drug diffusion through a biological membrane is not analogous to drug diffusion through water. In contrast to water, diffusion of a drug through a biological membrane depends on the volume of the drug. The classical Overton rules that relate membrane permeation to solute lipid solubility predict poorly the molecular weight threshold effect. As noted by Leib and Stein nearly 20 years ago,9 the molecular weight threshold effect was best predicted by the "hole-jumping" model of Trauble,10 which posits that solutes undergo a form of molecular "hitch hiking" in crossing a biological membrane by moving through small holes in the membrane formed by kinking of the mobile unsaturated fatty acyl side chains in the phospholipid bilayer[24].

ii). Prodrug

Poor lipophilicity is often a cause for a hydrophilic molecule not able to cross the BBB. Prodrug is one of approaches to address this issue. By connecting a hydrophobic

structure to a hydrophilic drug molecule through an enzyme-cleavable bond to form a hydrophobic prodrug, it provides a compound that is hydrophobic enough to pass the BBB. The drug will be regenerated from the prodrug once the enzyme-cleavable bond is cleaved by the endogenous enzyme. Fatty acid, glyceride, and phospholipid have been used as a hydrophobic structure to increase hydrophobicity for BBB permeation. These structures have been linked to a hydrophilic drug molecule through an enzyme cleavable bond such as an ester or amide bond. Prodrug approaches were investigated for a variety of drugs that contain a group capable of forming an ester or amide, such as an acidic group [29]. Problems associated with prodrugs include poor selectivity and poor tissue retention [30].

C- Physiological-based approach

The BBB exhibits a very high resistance owing to the tight junctions, which tighten adjacent endothelial cells together. Due to the presence of the tight junctions, paracellular pathway for solute distribution into brain interstitial fluid from blood cannot occur. Circulating molecules can only pass brain interstitium via a transcellular route through the brain capillary endothelial membranes. A blood circulating molecule may reach the brain by lipid-mediated free diffusion if it is lipid soluble, not avidly bound by plasma proteins, not a substrate for an active efflux transport system at the BBB and has a molecular mass less than 400 Da as discussed earlier. Circulating molecules may also reach the brain via certain endogenous transport systems within the brain capillary endothelium if they have affinity for the transporter. These endogenous transporters can be broadly classified into three categories: 1) Carrier-mediated transport (CMT); 2) active efflux transport (AET); and 3) receptor-mediated transport, or RMT [24].

i) CMT systems

CMT systems are for hexoses, monocarboxylic acids such as lactic acid, neutral amino acids like phenylalanine, basic amino acids like arginine, quaternary ammonium molecules such as choline, purine nucleosides such as adenosine, and purine bases such as adenine. CMT systems are all members of the Solute Carrier (SLC) gene family. The glucose carrier in the BBB is GLUT1 (glucose transporter type 1), which is a member of the SLC2 family; the monocarboxylic acid transporter in the BBB is MCT1, which is a member of the SLC16 family; the large neutral amino acid and cationic amino acid transporters in the BBB are LAT1 and CAT1 respectively, which are members of the SLC7 family; LAT1 and CAT1 are the light chains of heterodimeric proteins, and the heavy chain of the dimer is 4F2hc, which is a member of the SLC3 family; the adenosine transporter in the BBB is CNT2, which is a member of the SLC28 family. Each of the SLC families represent many common genes of overlapping nucleotide identity and some of the SLC families are made up of over 100 different genes. BBB adenosine transporter is sodium dependent on the blood side of the endothelium, [31] which rules out the role of Equilibrative nucleoside transporters (ENT) carrier in mediating uptake of circulating adenosine. In addition, there are many other CMT genes expressed at the BBB, which enable the transport of water-soluble vitamins, thyroid hormones, and other compounds through BBB. All of these BBB CMT systems, which can be in the dozens, are potential portals of entry for drugs to reach the brain. The CMT systems are highly stereospecific pore-based transporters and have high structural requirements for affinity. Therefore, it is essential to turn a drug molecule into a structure that is still a substrate of the transporter in order to achieve the purpose of taking the drug into the brain through the transporter in

the BBB. Understandably, the drug has to be regenerated from the structure once in the brain. One such example is dopamine which is used to treat Parkinson's disease. Dopamine is a very hydrophilic molecule and not able to pass through the BBB. Carboxylation of dopamine results in the formation of L-DOPA, and L-DOPA is a substrate for the BBB LAT1. Once across the BBB, dopamine is regenerated through decarboxylation by aromatic amino acid decarboxylase [24].

ii) AET

P-glycoprotein is a drug efflux pump and the prototypic AET system at the BBB. It contributes to the active efflux of molecules from the brain to blood direction. P-glycoprotein is a product of the ABC-B1 gene and one of many members of the ATP binding cassette (ABC) gene family of transporters. There are several multidrug resistance protein (MRP) transporters that belong to the ABC gene family. These drug efflux pumps contribute to the failure of a large number of drugs to reach the brain. One strategy to increase these drugs' ability to reach the brain is to develop "co-drugs" that inhibit BBB AET systems to allow BBB penetration of these therapeutic drugs. The same strategy can be also applied to overcome drug efflux caused by organic anion transporter polypeptide (OATP), or organic anion transporter (OAT) transporters [24].

iii) RMT

Certain large-molecule peptides or proteins cross the BBB via RMT. There are at least three different classes of BBB receptor systems. The transferrin receptor (TfR) is a bidirectional RMT system that leads both the receptor-mediated transcytosis of holotransferrin from the blood to brain direction, and the reverse transcytosis of apo-

transferrin from the brain to blood direction. The neonatal Fc receptor (FcRn) is a reverse RMT system that functions only to mediate the reverse transcytosis of IgG from the brain to blood direction, not the other way around. The type 1 scavenger receptor (SR-VI) is a receptor-mediated endocytosis system that is engaged in the uptake of modified low-density lipoprotein (LDL) from the blood into the intraendothelial compartment, and this endocytosis is not followed by exocytosis into brain interstitial fluid [24, 32].

1.5 Transporter dependent brain targeting agents

Most brain targeting agents were developed using an endogenous substrate of a receptor or transporter that is highly expressed on the surface of the BBB as a brain-targeting ligand. These substrates include amino acids, glucose, nucleosides, vitamins, and GSH for transporter-mediated transport, and transferrin, low density lipoprotein, and lipoprotein for receptor-mediated transport. These endogenous substrates are presented in table 1.2 [33]

Table 1.2 Summary of Receptor-mediated transport (RMT) and Carrier-mediated transport (CMT) dependent brain targeting [33]

Transport System	Receptor /Transporter	Molecules
Receptor-mediated transport (RMT)	Insulin receptor (INSR)	Insulin
	Transferrin receptor (TFR)	Transferrin
	Insulin-like growth factor receptors (IGF1R & IGF2R)	Insulin like growth factor 1 & 2 (IGF-1 & IGF-2), mannose-6-phosphate
	Leptin receptor (LEPR)	Leptin
	Fc-like growth factor receptor(FCGRT)	IgG
	Scavenger receptor type B1 (SCARB1)	Modified lipoproteins, like acetylated low-density lipoprotein (LDL)
Carrier-mediated transport (CMT)	GLUT1 (Glucose transporter 1)	Glucose, hexose, 2-deoxyglucose, fluorodeoxy glucose (positron emission tomography [PET] scanning)
	LAT1 (large neutral amino acid transporter 1)	Large and small neutral amino acids, L-dopa (Levodopa), α- methyl-

		dopa (Methyldopa), α-methyl-para-tyrosine or gabapentin (In parkinsonism, hypertension and in delivery of antiepileptic drugs)
	CAT1 (cationic amino acid transporter 1)	Basic amino acids, like arginine or lysine
	MCT1 (monocarboxylic acid transporter 1)	Lactate, pyruvate, ketone bodies and monocarboxylic acid drugs like probenecid (In treatment of gout and urinary incontinence)
	CNT2 (concentrative nucleoside transporter 2)	Purine nucleosides, and certain pyrimidine nucleosides as uridine (In delivery of several anticancer and antiviral drugs)
	SLCs (choline transporter) (Sodium dependent)	Choline (A cholinergic agent used in experimental techniques, not as a drug)

In principle, any of these substrates can be used as a brain-targeting ligand for nanoparticles such as liposomes and micelles through coupling the ligand with the nanoparticles. An approach using a substrate associated with receptor-mediated endocytosis for brain targeting is the most studied and the most mature one. In this section we will discuss the most studied receptor-mediated transport (RMT) and carrier-mediated transport (CMT) to provide a perspective for our investigation which is related to CMT. Among the substrates for RMT and CMT, transferrin is the most investigated substrate accounting for 42% of the total publication followed by glucose which accounts for 20% [34].

i) Transferrin (Tf)

Transferrin is transported by a RMT. Transferrin was the first one studied for brain-targeting and also the most investigated one accounting for 42% of the total publication. In this first study, the human IgG3 immunoglobulin was used as a model antibody. It was found that attachment of Tf to the hinge region of IgG3 yielded the highest brain uptake, 0.3% of the injected dose reached the brain. More recently, the antiviral drug azidothymidine (AZT) has been delivered using Tf-targeted, PEGylated albumin nanoparticles (PEG-NP). The percentage of AZT recovered in the rat brain was 21.1% using the Tf-targeted PEG-NP, while non-targeted PEG-NP alone showed a 9.3% accumulation [35]. However, Tf is likely not an ideal brain delivery ligand since the TfR is nearly saturated with endogenous Tf that are present in the bloodstream at a concentration of 25 mM, meaning that a Tf-targeted drug would have to compete with a high concentration of the natural ligand [36]. As an alternative, antibodies against the TfR have been employed as a ligand for brain targeting. The mouse monoclonal antibody

(MAb) against the rat TfR, OX26, has been the most thoroughly studied one. Brain-derived neurotrophic factor BDNF was coupled to biotin (B) via PEG-hydrazide and streptavidin (SA) was coupled to OX26. OX26–BDNF was formed as a result of streptavidin/biotin (SA/B) interactions. BDNF or the OX26–BDNF conjugate were intravenously administered. It was found that rats given the OX26–BDNF conjugate had a 243% increase in motor performance when compared to BDNF alone [36]. Tf was also used to help target other nanoparticles to the brain. Liposomes coated with Tf showed around 2-5 fold increase in brain targeting compared with liposomes without Tf [37, 38].

Although the TfR has been extensively studied as an RMT system that facilitates noninvasive delivery of various therapeutics to the brain, drawbacks for the system do exist. The major drawback is the widespread expression of the TfR on peripheral organs that limits its capability for specific brain delivery. As a result, Friden and co-workers reported that only 0.44% of the injected dose reaches the rat brain in their investigation of using anti-TfR antibody (OX26) as a brain targeting ligand [39]. Similar results were obtained with the 8D3 antibody [40].The widespread expression of the TfR in non-brain tissues not only reduces the brain-targeting selectivity but also leads drug side effects to non-brain tissues. An approach to limit the drug side effects in non-brain tissues is to use a brain-specific promoter to increase TfR expression in the brain [41]. In addition, there are non-human TfR antibodies that although these particular antibodies do not recognize the human TfR, antibodies that do recognize the human TfR and transport into the primate brain [42]. Use of these antibodies can avoid the drug side effects in non-brain tissues. However, these antibodies could cause an immunogenic effect since they are not

of human origin. Strategies to overcome this hurdle will be discussed in reference to the insulin receptor RMT/anti-insulin receptor MAb system in the next section [36].

ii) Glucose

Glucose accounts for around 20% of total publication in the brain targeting field[34]. Two different types of glucose transporter are found in the BBB. The most prevalent one is the sodium-independent bi-directional facilitative transporter from the solute carrier 2 (SLC2) family of which there are 14 isoforms (GLUTs 1–14). Given the widespread distribution, GLUT1 has become one of the most extensively studied of all membrane transport proteins. At the BBB, a high density of GLUT1 is found in both luminal and abluminal membranes of endothelial cells. GLUT1 is also found in human erythrocytes. A number of neuroactive drugs have been conjugated with glucose in order to target GLUT1 for brain targeting. Four derivatives of the chemotherapy drug chlorambucil were conjugated with D-glucose to achieve brain targeting through GLUT1 [43]. However, the widespread expression of GLUT1 in other tissues especially in erythrocytes limits the brain selectivity of GLUT1 [44].

1.6 GSH transporter for brain targeting

GSH is an endogenous tripeptide [45]. GSH is the most essential endogenous antioxidant that removes reactive oxygen species (ROS) and reactive nitrogen species (RNS). Because the brain consumes about 20% of the total body oxygen and generates a large quantity of ROS, GSH is highly needed in the brain. GSH is a water-soluble and cell membrane impermeable molecule. To enter the brain, GSH has to be transported by a GSH transporter. The GSH Transporter is a Na^+-dependent transporter and localized on the luminal membrane of endothelial cells [46-49]. To accommodate the brain's need of

GSH, GSH transporters are highly expressed on the BBB surface [49-52]. Recently, GSH transporters have been found effective in facilitating crossing of compounds through the BBB to reach the CNS. To achieve GSH transporter-mediated BBB crossing, GSH has been linked to a therapeutic agent (GSH-Drug) to form a prodrug [53]. The prodrug crosses the BBB by binding the GSH part to a GSH transporter followed by internalization of the prodrug. GSH has also been used to coat the surface of nanoparticles such as PEGylated liposomes for brain targeting. GSH coated PEGylated liposomes encapsulated with doxorubicin showed better permeation in an *in vitro* BBB model compared with free doxorubicin [54]. Moreover, G-technology utilized GSH-PEGylated liposomes to provide a 3-fold increase in the delivery of a drug to the brain and the GSH-PEGylated liposomes have undergone clinical trials for brain-targeting [55]. More recently, GSH-conjugated magnetic nanoparticles served effectively as a BBB shuttle for MRI-monitored brain delivery of paclitaxel *in vivo* [56].

The aim of this dissertation was to develop a GSH transporter-based brain targeting agent. GUNW-3 was designed as a GSH transporter-based brain targeting agent. GUNW-3 is a molecule formed by connecting a hydrophilic GSH molecule to a hydrophobic cholesterol molecule through a two ethylene glycol unit linker with a hope that the GSH part can serve as a brain-targeting structure through binding to the GSH transporter and facilitate the entry into the brain. This dissertation describes the design, synthesis, and fully characterization of GUNW-3 (Chapter 2). The dissertation also describes the ability of GUNW-3 to form micelles (GUNW-3 micelles), the ability of GUNW-3 micelles to cross the BBB to reach the brain, and the ability of GUNW-3 micelles to carry a dye (DiR) to the brain (Chapter 3). Further, the dissertation shows the

ability of GUNW-3 helps guide liposomes to the brain by forming GUNW-3 liposomes and the ability of GUNW-3 liposomes to deliver a dye (DiR) to the brain (Chapter 4).

In summary, we have demonstrated a proof of concept that GUNW-3 is an effective brain targeting agent. It can form brain targeting micelles (GUNW-3 micelles) by itself and help deliver DiR to the brain. It can also help deliver liposomes (GUNW-3 liposomes) to the brain and GUNW-3 liposomes were able to deliver DiR effectively to the brain. This dissertation shows a great potential of GUNW-3 micelles and GUNW-3 liposomes in delivering a drug to the brain and provides the foundation to pursue further investigation of GUNW-3 micelles and GUNW-3 liposomes as brain targeting drug delivery systems.

Chapter 2 Design, Synthesis, and Characterization of GUNW-3

2.1 Introduction

GSH is the major antioxidant compound in the body formed by three amino acid peptides. Its roles are associated with removal of toxic compounds and involved in other cellular functions. GSH is transported to the brain through a Na-dependent GSH transporter. GSH transporters are found to be effective in facilitating crossing of compounds through the BBB to reach the brain. This chapter presents the rational design of GUNW-3 as a GSH-transporter mediated brain targeting agent, its synthesis, and full characterization of the chemical structure of GUNW-3.

2.2 Design of GUNW-3 as a brain-targeting agent

GUNW-3 was designed as a GSH-transporter dependent brain targeting agent. GUNW-3 is a molecule formed by connecting a hydrophilic GSH molecule to a hydrophobic cholesterol molecule through a two-ethylene glycol unit linker (Figure 2.1). The GSH part serves as a brain-targeting structure through binding to the GSH transporter and facilitates the entry of GUNW-3 into the brain. GUNW-3 was expected to help deliver compounds to the brain through three different ways. First, the molecule is expected to be amphiphilic due to the presence of a hydrophobic cholesterol on one end of the molecule and a hydrophilic glutathione on the other end of the molecule. The molecule is expected to form micelles (GUNW-3 micelles) with the hydrophilic GSH on the surface of the micelles and the hydrophobic cholesterol inside to form hydrophobic core. Micelles can be used to deliver hydrophobic drugs. With the GSH part being on the surface, GUNW-3 micelles are expected to be brain-targeting micelles, via the GSH transporter, to help deliver hydrophobic drugs to the brain. It has been reported that the

more GSH coated on the surface of nanoparticles, the better brain-targeting [33]. Second, since cholesterol is part of liposomes, GUNW-3 is expected to be used to prepare liposomes (GUNW-3 liposomes) with the hydrophilic GSH floating on the surface of the liposomes for brain-targeting and hydrophobic cholesterol being imbedded into the hydrophobic double lipid layer of liposomes (Figure 2.2). Liposomes are well established drug delivery systems for both hydrophobic and hydrophilic molecules. The third use of GUNW-3 is to help deliver an individual drug to the brain by linking the molecule to the individual drug. In this dissertation, the focus will be on the investigation of the brain targeting abilities of GUNW-3 micelles and GUNW-3 liposomes.

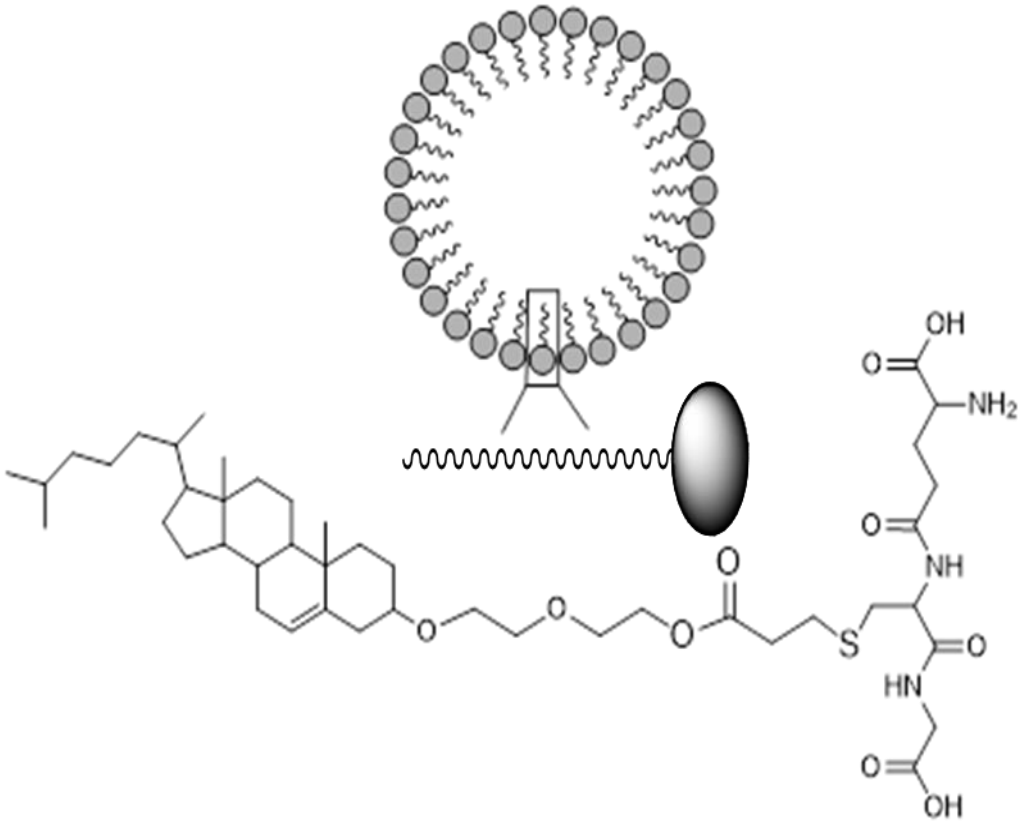

Figure 2.1 Schematic drawing of chemical structure GUNW-3 and its formation of GUNW-3 micelles.

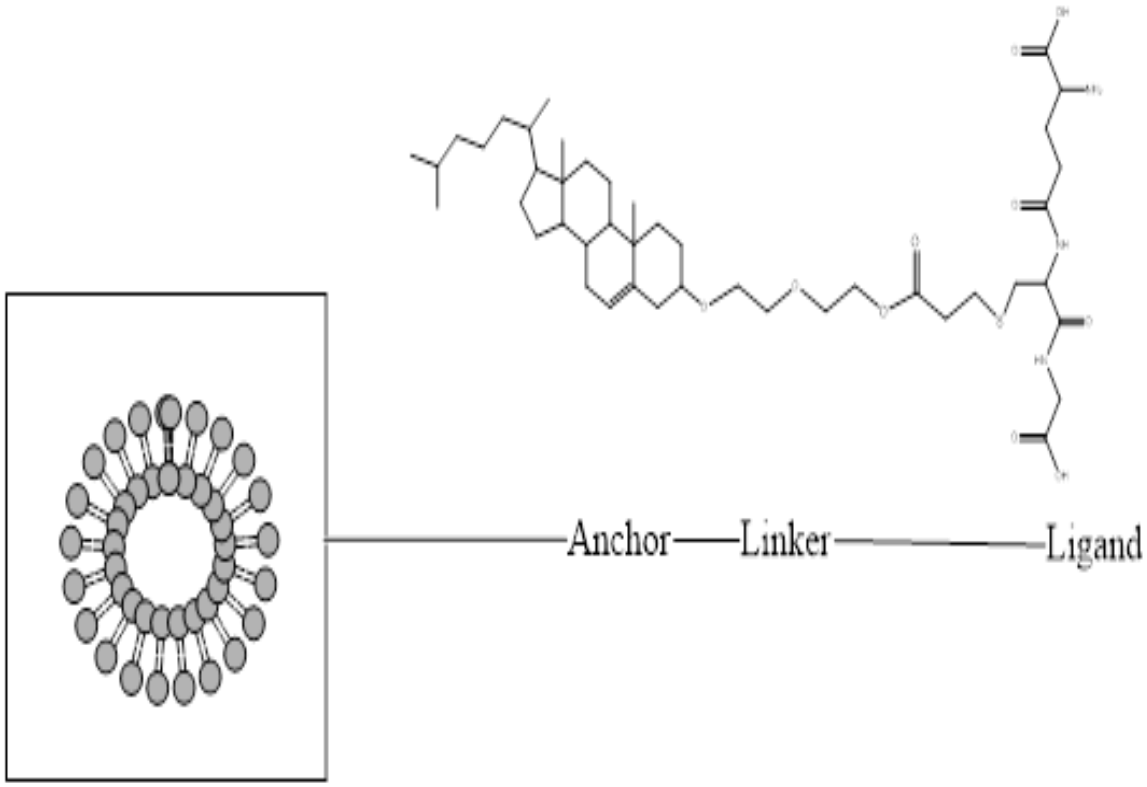

Figure 2.2 Schematic drawing illustrating GUNW-3 as a part of the components of liposomes.

2.3 Experimental Section

2.3.1 Material and instruments

Unless otherwise stated, all chemical reagents and solvents were obtained from commercial sources and used without further purification. Cholesterol, triethylamine, pyridine, ethylene glycol, acryloyl chloride, glutathione, Dulbecco's phosphate buffer saline (Gicob™DPBS, no calcium, no magnesium,1x) were purchased from Fisher Scientific (Waltham, MA, USA) and sodium carbonate was purchased from Sigma-Aldrich (St. Louis, MO, USA).

Flash column chromatography was carried out on a W-Prep 2 XY Yamazen Dual channel flush chromatography system (San Bruno, California). ^{1}H NMR spectra were recorded on a Bruker Varian 600 or 400 MHZ spectrometer in deuterated solvents as indicated. All peaks were given as chemical shift in part per million relatives to TMS (tetramethyl saline) or DSS (4,4-dimethyl-4-silapentane-1-sulfonic acid) as an internal standard. Multiplicities are indicted by s (singlet), d (doublets), t (triplet), q (quartet), m (multiplet), and brs (broad singlet). *J* value are given in Hz. The high-resolution mass spectra (HRMS) were obtained on a Bruker Daltonics solariX 12 tesla Fourier Transform Ion Cyclotron Resonance mass spectrometer (Department of chemistry, University at Buffalo, NY), and the low-resolution mass spectra were acquired on a Thermoquest Finnigan LCQ Deca mass spectrometer (Waltham, MA, USA). FTIR spectra were obtained on a NICOLET 380 FT-IR spectrometer (Thermo Fisher Scientific, Madison, WI). Melting point were obtained on a MEL-TEMP® melting apparatus (Electrothermal, Dubuque, IA).

HPLC/MS analysis was achieved on an Agilent 1260 infinity II HPLC coupled to Agilent infinity LC/MS. Chromatographic separations were achieved by using Luna 3u C8(2) column (100×4.6 mm i.d., Phenomenex, Torrance, CA). The mobile phase is consisted of phase A (ammonium water (pH 10.6)) and phase B (acetonitrile) with a flow rate of 1 mL/min. Phase B was initially set at 0% for 5 min, increased linearly to 90% over 20 min and held for 3 min, then returned to the initial conditions over 5 min. The system was re-equilibrated for 3 min before the next injection. The autosampler was thermostated at 4 °C and a volume of 50 μL was injected with a run time of 33 min. The HPLC was monitored at 210 nm.

2.3.2 Synthesis of GUNW-3

i. Synthesis of Cholesterol p-Touenesulfonate (Scheme 2.1, compounds 1)

A solution of cholesterol (5 g, 13.13 mmol), *p*-toluenesulfonylchloride (3.75 g, 19.7 mmol), triethylamine (2.98 ml), and pyridine (1.5 ml) in anhydrous dichloromethane (20 ml) was stirred for 24 h at room temperature. The solvents were removed by a rotary evaporator under a reduce pressure. The residue was purified using a silica gel column (mesh 200-400) with hexane/ethyl acetate to yield compound 1 as a white powder in 95% yield. The compound was characterized by ^{1}H NMR (600 MHz, $CDCl_3$) δ 7.72 (d, *J* = 8.3 Hz, 2H), 7.25 (d, *J* = 8.0 Hz, 2H), 5.25 – 5.20 (d, 1H), 4.24 (tt, *J* = 11.4, 4.6 Hz, 1H), 2.36 (4H), 2.22 – 2.15 (m, 1H), 1.90 – 0.74 (m, 38H), 0.58 (s, 3H).

ii. Synthesis of Cholesterol-ethylene Glycol (Scheme 2.1, compound 2)

To a stirred solution of ethylene glycol (11.77 g,110.9 mmol) in 30 ml dioxane was added dropwise compound 1 *(*3 g, 5.5 mmol) in dioxane (5 mL). The mixture was kept at 70 ˚C for 48 h before removing the solvents using a rotary evaporator under a

reduce pressure. The resulting residue was purified using a silica gel column (silica size 200-400 mesh) with hexane/ethyl acetate to yield a slightly yellow viscous product in 79% yield. The product was characterized by ^{1}H NMR (400 MHz, $CDCl_3$) δ 5.35 (d 1H), 3.68 (ddd, *J* = 15.1, 8.6, 4.1 Hz, 8H), 3.26 – 3.12 (m, 1H), 2.38 (d, *J* = 12.8 Hz, 1H), 2.22 (t, *J* = 12.0 Hz, 1H), 2.10 – 1.71 (m, 5H), 1.64 – 0.82 (m, 33H), 0.65 (s, 3H).

iii. Synthesis of Cholesterol-ethylene glycol-acrylate (Scheme 2.1, compound 3)

A solution of acryloyl chloride (0.524 g,6.49 mmol) in anhydrous dichloromethane (2 ml) was added dropwise to a stirred solution of compound 2 (2.05 g, 4.33 mmol) in anhydrous dichloromethane (15 ml) under argon in an ice bath. The mixture was stirred for 30 min before removal of dichloromethane under a reduced pressure by a rotary evaporator. The residue was purified by a silica gel column (silica size, mesh 200-400) using hexane/ethyl acetate to yield colorless viscous product in 69% yield. The product was characterized by ^{1}H NMR (600 MHz, $CDCl_3$) δ 6.43 (dd, *J* = 17.3, 1.4 Hz, 1H), 6.19 – 6.13 (m, 1H), 5.83 (dd, *J* = 10.4, 1.4 Hz, 1H), 5.43 – 5.24 (m, 1H), 4.48 – 4.22 (m, 2H), 3.79 – 3.73 (m, 2H), 3.67 – 3.61 (m, 4H), 3.31 – 3.07 (m, 1H), 2.37 – 2.30 (m, 1H), 2.21 (m, 1H), 2.03 – 1.78 (m, 5H), 1.61 – 0.84 (m, 33H), 0.67 (s, 3H).

iv. Synthesis of GUNW-3

Glutathione (0.911 g, 2.96 mmol) and sodium carbonate (0.314 g, 2.96 mmol) were dissolved in water (6 mL) before added to a stirred solution of compound 3 (1.5 g, 2.96 mmol) in tetrahydrofuran (7 mL). Th mixture was stirred overnight at room temperature followed by addition of water (50 mL). The solution was frozen and lyophilized to yield the crude GUNW-3. GUNW-3 was purified through precipitation

using water (pH4)/acetonitrile (1:1 ratio) and separated by filtration to yield white powder in 40% yield. The product was characterized by ^{1}H NMR, and HRMS. The purity of the compound was determined by HPLC to be 97%. The melting point of the compound was determined to be 200 ˚C by a MEL-TEMP® melting apparatus. ^{1}H NMR (600 MHz, D_2O) δ 5.34 (s, 1H), 4.28 (s, 1H), 3.72 (dd, *J* = 97.5, 31.9 Hz, 11H), 3.23 (d, *J* = 72.2 Hz, 2H), 3.00 (s, 1H), 2.87 (s, 4H), 2.44 (d, *J* = 82.1 Hz, 2H), 2.18 (d, *J* = 23.9 Hz, 3H), 1.91 (s, 3H), 1.82 – 0.10 (m, 39H). HRMS calculated for $C_{44}H_{73}N_3O_{10}S$ $(M+Na)^+$ (*m/z*) 858.4914, found 858.4909.

2.3.3 Purification and chemical stability of GUNW-3

Stock solutions of GUNW-3 were prepared by dissolving GUNW-3 in a solution of methanol and ammonium water (1:1 ratio, pH 10.8) to obtain the concentration of 1 mg/ml. Calibration curves were constructed in a solution of methanol and ammonium water (1:1 ratio, pH 10.8) by preparing a series of concentrations of GUNW-3 (62.5, 125, 250, 500, 750 and 1000 μg/ml).

FTIR analysis of GSH and GUNW-3 were conducted on a NICOLET 380 FTIR spectrometer and the OMIC was used for data analysis.

LC/MS analysis of GUNW-3 was conducted on a (xxx Instrument name). SIM was used for MS analyses and performed in both negative-ion mode (SIM: 834.6) and positive mode (SIM:837.4). The capillary temperature was set at 4000V and the fragmentor of the compound was set at 135V. The temperature of the ESI source during the run was set at 350 °C for the desolvation gas. The gas flow was set at 11L/h.

GUNW-3 mass spectrum was obtained by direct infusion into Finnegan TSQ quantum.

2.3.4 In-vitro toxicity study

An African green monkey kidney fibroblast cell line (CV-1) from American Type Culture Collection (ATCC) and a human lung squamous carcinoma cell line (NCI-H226) from the National Cancer Institute were used for the cytotoxicity studies. Cells were grown seeded on a 96-well plate at a concentration of 3000 cells/well. RPMI 1640 growth medium supplemented used with 10% FBS, 100 unit/ml of penicillin (Mediatech, Inc, Herndon, VA) in humidified atmosphere containing 5% CO_2 at 37˚C. After 24hrs, cells were treated with different concentrations of GUNW-3. The MTT assay was used to determine the cell viability after a 4-day treatment.

2.3.5 In-vivo toxicity study

GUNW-3 (26 mg/ml, injection volume) was intravenously injected to female C57BL/6 mice (6-8 weeks old, 17 g from Jackson Laboratory (Bar Harbor, ME, USA)) for 4 days. The mice were monitored for any sign of toxicity (food intake, weight, abnormal activities and etc) for 4 days. Mice were sacrificed on day 5 and submitted to the Animal Disease Research & Diagnostic Laboratory at South Dakota State University for a pathological examination by a university veterinarian.

2.4 Result and Discussion

2.4.1 Synthesis of GUNW-3

GUNW-3 was synthesized in a total of 4 steps. The first step was tosylation of the commercially available cholesterol with 4-methylbenzene-1-sulfonyl chloride (Scheme 2.1, step a) in the presences of pyridine and triethylamine to produce tosylated cholesterol (**1**) in 95% yield (Scheme 2.1). Compound 1 was added with ethylene glycol (2,2'-oxydiethanol) in Dioxin (Scheme 2.1, step b) to produce cholesterol-ethylene glycol

(**2**) in 79 % yield. Cholesterol-ethylene glycol (**2**) reacted with acryloyl chloride (Scheme 2.1, step c) in the presence of triethylamine to form cholesterol-ethyleneglycol-acrylate (**3**) in 69% yield. Michael addition coupling of GSH to compound **3** was achieved in the presence of sodium carbonate to complete the synthesis of GUNW-3 in 40% yield (Figure 2.3). The reaction conditions for the synthesis were not optimized. GUNW-3 was characterized by ^{1}H NMR and HRMS. The purity of GUNW-3 was confirmed to be 97% by HPLC.

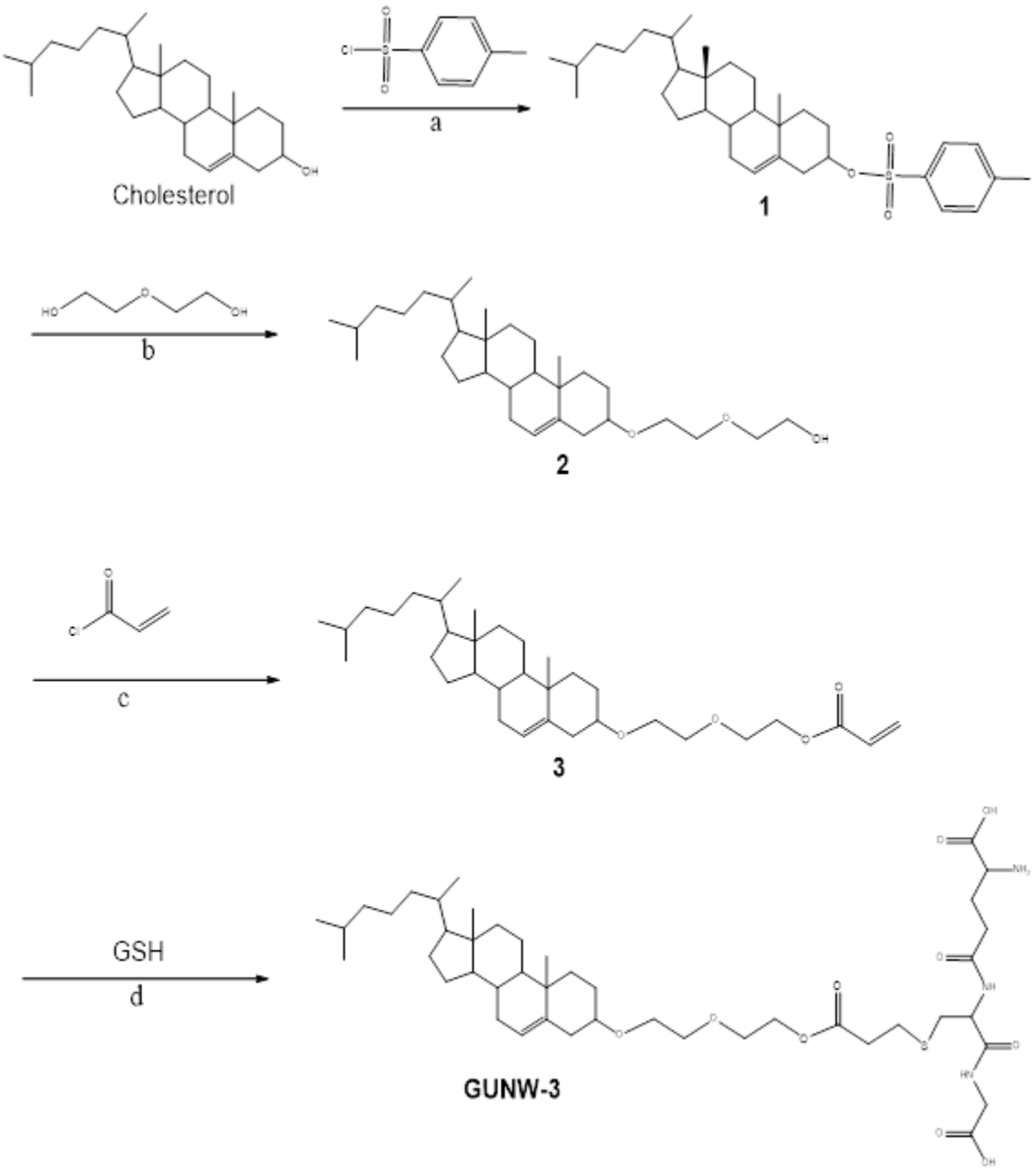

a: Pyridine, Triethylamine, Dichloromethane
b:Dioxin
c:Triethylamine, Dichloromethane
d:Sodium carbonate, Tetrahydrofuran, Water

Figure 2.3 Synthetic schemes of GUNW-3.

2.4.2 Purity and stability of GUNW-3

The purity of GUNW-3 was checked by HPLC and determined to be 97% as shown by a representative HPLC chromatogram (top one in Figure 2.3). For a comparison, a representative HPLC chromatogram derived from solvent only was also given (bottom one in Figure 2.4). As one can see that GUNW-3 (the peak at 21 min in the top chromatogram) was the only peak observed besides the solvent peaks.

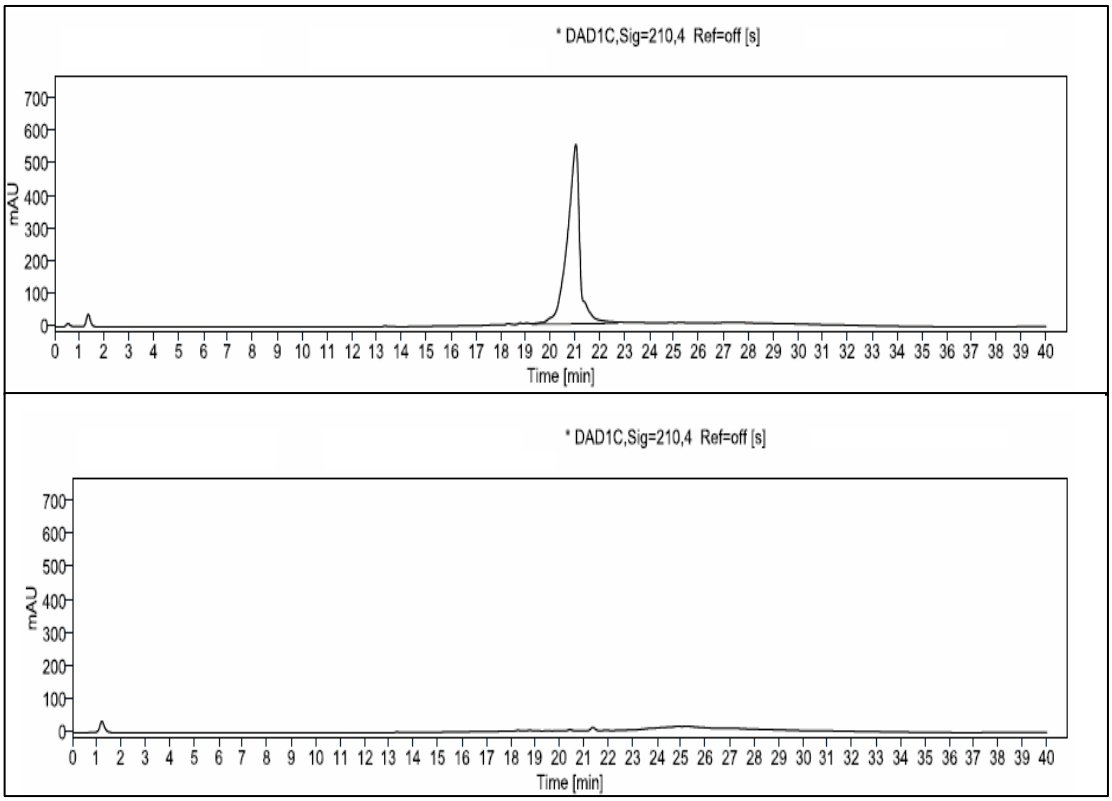

Figure 2.4 Representative HPLC chromatogram of GUNW-3 at concentration of 1 mg/ml and the blank solvent.

The stability of GUNW-3 in a solution of methanol-ammonium water (1:1 ratio, pH 10.8) was checked continuously for 7 days (Figure 2.3). As shown in the figure, GUNW-3 was stable in the first 3 days. However, it started to decompose quickly after 3 days. The accelerated decomposition after day 3 suggests a possibility of decomposition product-facilitated decomposition (Figure 2.5).

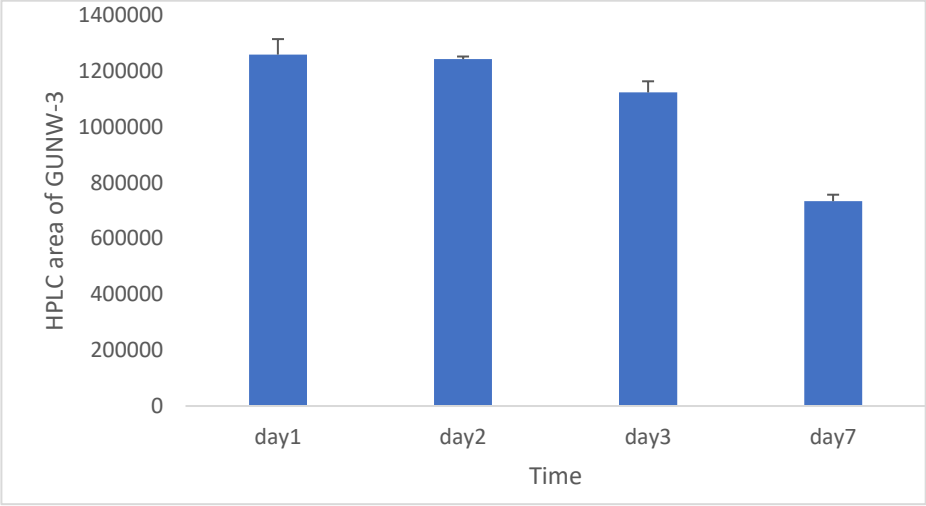

Figure 2.5 Stability of GUNW-3 in a solution of methanol-ammonium water (1:1 ratio, pH:10.8, ±SD, n=3).

2.4.3 Confirmation of *S*-link isomer vs *N*-link isomer

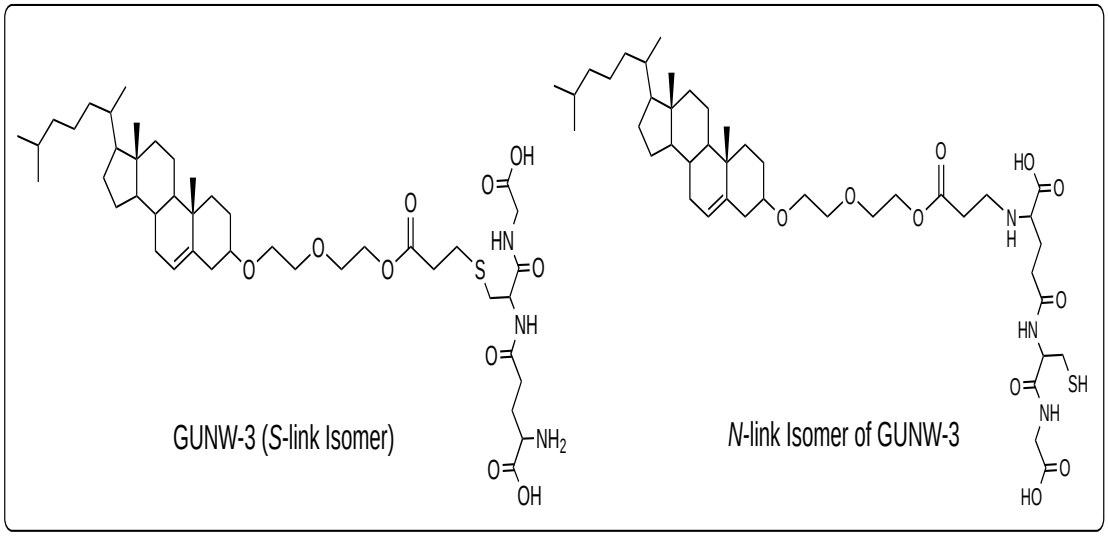

Figure 2.6 Chemical structures of GUNW-3 and its N-link isomer

The Michael addition coupling of GSH to compound 3 (Scheme 2.1) may proceed with two possibilities: addition of the SH group to yield GUNW-3 (*S*-link isomer) and addition of the basic amino group of the glutamate residue to produce GUNW-3's *N*-link isomer (Figure 2.6), although addition of the GSH group is expected to be the dominating reaction. To confirm GUNW-3 is the product, two analytical methods were employed: FTIR and MS. In FTIR, the -SH group has a distinct peak at 2516.7 cm^{-1} as observed in the FTIR spectrum of GSH (Figure 2.7A). The peak at 2516.7 cm^{-1} disappeared in the product obtained from the Michael addition reaction (Figure 2.7B) confirming that the -SH is no longer present in the obtained product which suggests that the reaction occurred through the addition of the -SH group to compound 3 and the product is GUNW-3 (the *S*-link isomer).

A

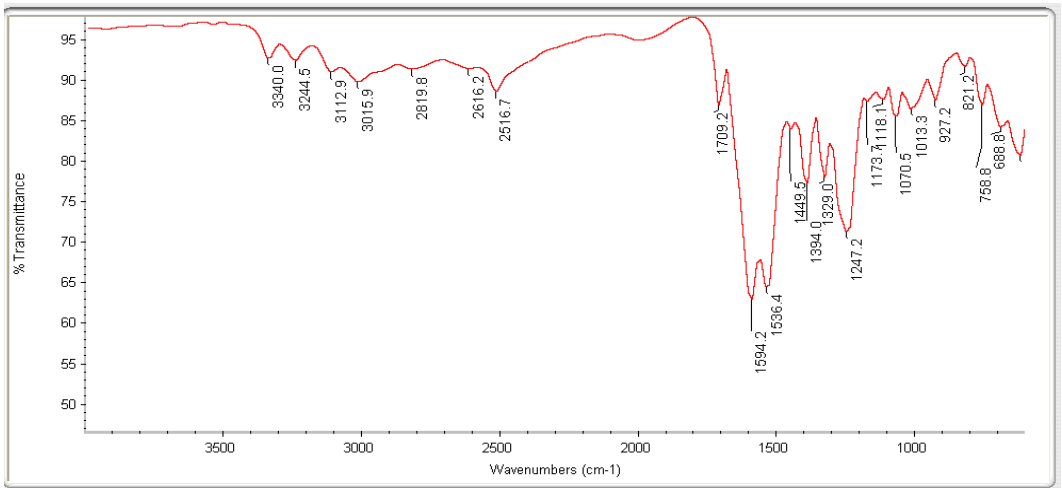

B

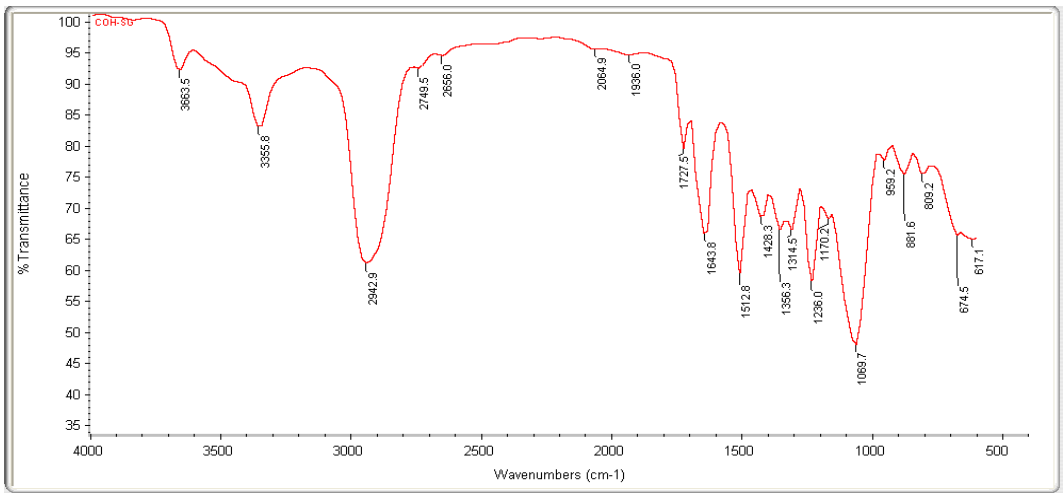

Figure 2.7 FITR spectra of GSH (**A**) and GUNW-3 (**B**)

The confirmation of the obtained product was GUNW-3 was further achieved by LC/MS/MS. Based on the structures of the *S*-link isomer and *N*-link isomer, the fragmentation of these two isomers are expected to be different. For the *S*-link isomer, two neutral losses are expected: a neutral loss of glycine ($C_2H_5NO_2$, 75Da) and a neutral loss of pyroglutamate ($C_5H_7NO_3$, 129Da). These two neutral losses were observed in the MS/MS spectrum: *m*/*z* fragment at 762.45 for the neutral loss of glycine and *m*/*z* fragment at 708.29 for the neutral loss of pyroglutamate (Figure 2.7). It needs to be noted that these expected two neutral losses were also reported in the literature for the *S*-link isomer (Yue's reference). The *m*/*z* fragments at 468.70 and 369.82 in the mass spectrum of GUNW-3 (Figure 2.8) were the fragment generated from a neutral loss of cholesterol and cholesterol ion respectively. Therefore, the mass spectrum matches well with the structure of the *S*-link isomer (GUNW-3) not the *N*-link isomer. If it would be the *N*-link isomer, a neutral loss of 178.0412Da (C5H10N2O3S) would have been observed as reported in the literature for the *N*-link isomer [57].

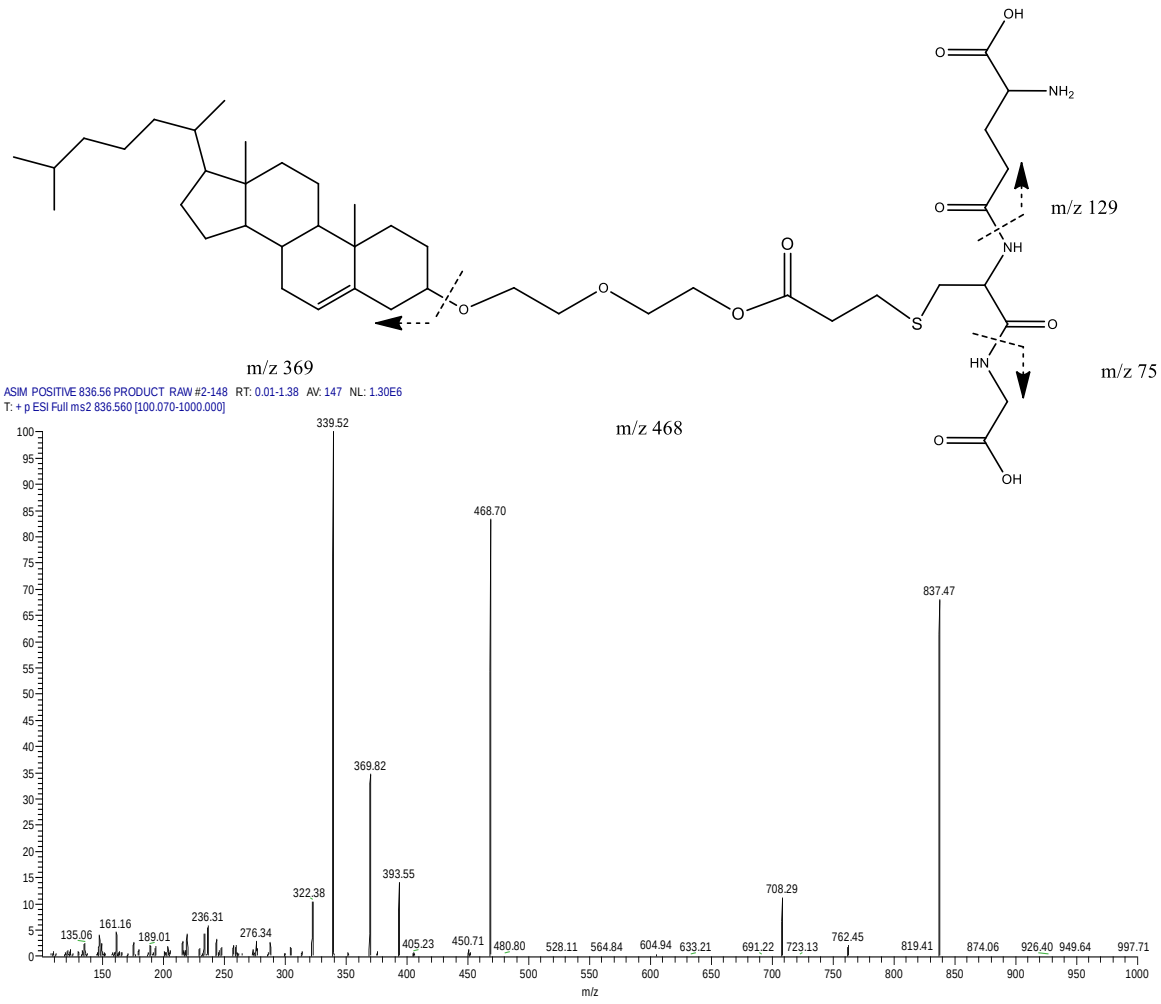

Figure 2.8 Mass spectrum of GUNW-3 obtained from LC/MS/MS on a positive mode.

2.4.4 Cell viability test of GUNW-3

The cell viability test of GUNW-3 was conducted with two cell lines: one normal cell line (CV-1 cells) and one cancer cell line (NCI-H226 cells). A dose-response curve revealed IC_{50} values of 0.65 mM and 0.47 mM for NCI-H226 cells and CV-1 cells respectively which are much higher than the critical micellar concentration (CMC) (3.9 μM) of GUNW-3 (in Chapter 3) and much higher than the concentration of GUNW-3 used in brain targeting micelles (GUNW-3 micelles) or liposomes (GUNW-3 liposomes). Figure 2.9 presents representative dose-response curves for the determination of the IC_{50} values.

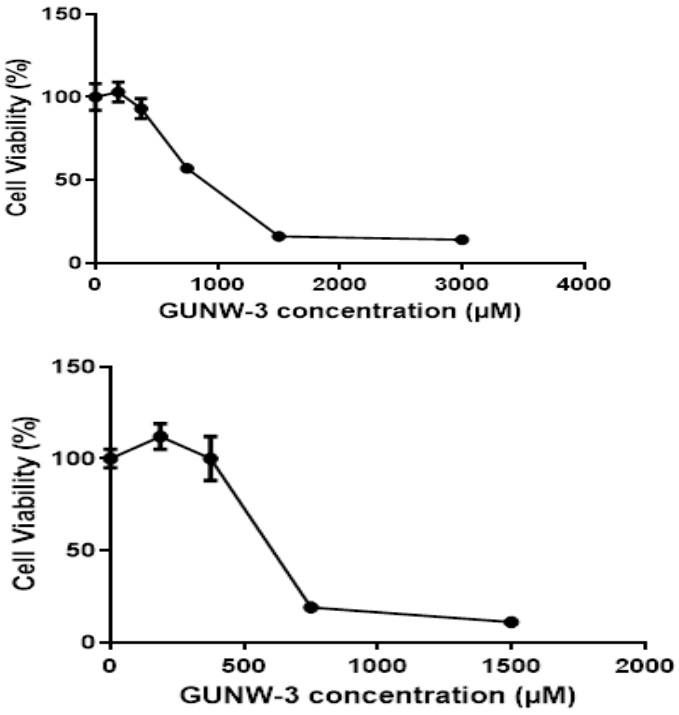

Figure 2.9 Dose-response curves for the determination of IC_{50} values of GUNW-3 with NCI-H226 cell line (**A**) and CV-1 cell line (**B**) (mean ±SD, n=3).

2.4.5 In-vivo toxicity

A preliminary *in vivo* toxicity study was conducted with one mouse. For this work we used a dosage that is 3.7 time higher than the dose used for GUNW-3 micelles (Chapter 3) and GUNW-3 liposomes (Chapter 4) and the dose was used daily for four days instead of a single dose in the *in vivo* brain-targeting studies (Chapters 3 and 4). Mice were closely monitored daily. No abnormal activities (loss of food intake, weight loss, and behavior abnormality) were observed during the 4 days. Mice were sacrificed on day 5 and subjected for a pathological examination in the Animal Disease Research & Diagnostic Laboratory at South Dakota State University by a university pathologist. No significant gross and microscopic lesion were noted for all organs examined (Figure 2.10).

ANIMAL DISEASE RESEARCH & DIAGNOSTIC LABORATORY
Veterinary and Biomedical Sciences Department
South Dakota State University
Box 2175, North Campus Drive • Brookings, SD 57007-1396
Phone: (605) 688-5171
Fax: (605) 688-6003
Accounting: (605) 688-5392
http://sdstate.edu/vs

XIANGMING GUAN PhD
SDSU PHARMACY 337T65
SAV, BOX 2202C
BROOKINGS, SD 57007

FAX:
Report Date: 06/23/19
Collection Date:
Status: Complete

Case: 19-12089
Accession Date: 06/07/19
Owner: SDSU PHARMACY 337T65
Owner Address: BROOKINGS, SD 57007

Species: MOUSE SP.
Wt: lbs
Age:

Case Coordinator:_____
David Knudsen, DVM, MS, DACLAM

TEST REPORT

Diagnostic Findings

SUMMARY
June 23, 2019 dk

Signalment: two dead adult C57x mice, ID #1 and #2

No significant gross or microscopic lesions were noted in either animal, and tissues were free of potential bacterial pathogens. Please call me here at the lab if you have any questions.

Pathology

GROSS PATHOLOGY
June 23, 2019 dk

Two dead mice were submitted for examination. Animals were identified by marker sports on the tail as either #1 or 2. Both animals were free of gross lesions. Samples were collected for histologic examination and culture.

HISTOPATHOLOGY
June 23, 2019 dk

Animal #1:
Liver: mild multifocal extramedullary hematopoiesis.
No observed lesions: lung, spleen, pancreas, brain, stomach, kidney, intestine, duodenum, cecum

Animal #2:
No observed lesions: lung, liver, kidney, spleen, brain, stomach, duodenum, pancreas, intestine, cecum

Bacteriology

AEROBIC CULTURE — Verified on: 06/10/19 12:03 PM

Animal ID	Specimen	Test	Isolate	Level	Result
1	LUNG	AEROBIC CULTURE			NO PATHOGEN ISOLATED

19-12089 Page 1 of 3

2	LUNG	AEROBIC CULTURE			NO PATHOGEN ISOLATED
1	LIVER	AEROBIC CULTURE			NO PATHOGEN ISOLATED
2	LIVER	AEROBIC CULTURE			NO PATHOGEN ISOLATED
1	KIDNEY	AEROBIC CULTURE			NO PATHOGEN ISOLATED
2	KIDNEY	AEROBIC CULTURE			NO PATHOGEN ISOLATED
1	CECUM	AEROBIC CULTURE			NO PATHOGEN ISOLATED
2	CECUM	AEROBIC CULTURE			NO PATHOGEN ISOLATED

Figure 2.10 The report from the Animal Disease Research & Diagnostic Laboratory for a pathological examination of mice treated with GUNW-3 micelles or GUNW-3 liposomes

In summary, GUNW-3 was designed as a brain targeting agent. The compound was successfully synthesized in a total of 4 steps. In this chapter we confirmed the chemical structure of GUNW-3. We also confirmed that GUNW-3 is relatively stable. A cell viability study showed the IC_{50} values of GUNW-3 in the NCI-H226 cell line and CV-1 cell line were to be 0.65 mM and 0.47 mM respectively. A preliminary *in vivo* toxicity study of GUNW-3 showed that no organ toxicity was observed as reported by the pathologist at a dosage that was 3.7 times higher than the dose used and four time more frequent than that used for brain targeting of GUNW-3 micelles and GUNW-3 liposomes.

Chapter 3 Brain Targeting of GUNW-3 Micelles

3.1. Introduction

3.1.1 Micelles

Amphiphilic molecules are the molecules that have a hydrophilic group and a hydrophobic group. Amphiphilic molecules can undergo self-assembly to form micelles when they dissolve in a solvent [58]. Micelles are an aggregation form of the molecule in solution. In an aqueous solution, amphiphilic compounds arrange themselves in a way that the hydrophobic groups will make a core while the hydrophilic groups will be oriented toward water. This type of micelles is known as the normal micelles. However, when present in an organic solvent the arrangement of amphiphilic molecules will be the opposite which is known as reverse micelles.

Micelles are nanoparticles with a typical particle size of 20 nm to 200 nm[58]. Micelles can be classified based on its materials, the manner of self-assembly, and the surface charge. Based on the materials, micelles can be classified as lipid micelles, polymer micelles, oligopeptide micelles, and polysaccharides micelles. The materials used to make micelles can be employed to control the particle size, ability of drug encapsulation, biological stability, and drug releasing rate of micelles. Based on the manner of self-assembly, micelles can be classified as normal micelles, reverse micelles, and unimolecular micelles of which one molecule can assemble to form one micelle. Unimolecular micelles are a polymer that has multiple hydrophilic and hydrophobic groups. The surface charge of micelles can lead to three types of micelles: nonionic (neutral), cationic (positive), and anionic (negative) micelles.

Critical micelles concentration (CMC) [59] is a critical parameter for micelles. CMC is a concentration that an amphiphilic molecule starts to form micelles. At concentration lower than the CMC, the molecule will exist as a monomer not micelles.

3.1.2 Micelles in drug delivery

Micelles are considered as an effective drug delivery system. Regular micelles are the most commonly used micelles and used to deliver poorly water-soluble drugs which can be encapsulated in the hydrophobic core of micelles. On the other hand, hydrophilic drugs can be effectively encapsulated in reverse micelles in the hydrophilic core. Reverse micelles are usually used in an oily injection. Clinical applications of reverse micelles are USP steroid injection and some biocompatible oily formulations used for oral delivery [60]. CMC is one of the critical parameters to be used to determine if the micelles can be used for a clinical application. Micelles with low CMC (in μM) are required for a clinical application since micelles with high CMC will dissociate to become a monomer upon dilution in bloodstream. Only a few micelle formulations, manly polymeric micelles, have made it to clinical studies (Table 3.1) [58, 61].

Table 3.1 Micelles formulations in clinical trials

Name	Clinical phase	Condition	Completed date	NCT#
Paclitaxel polymeric micelles	Phase IV	Recurrent breast cancer	Unknown	00912639
Genexol-PM	Phase III	Taxanepre treated recurrent breast cancer	2013	00876486
Paclitaxel polymeric micelles	Phase II	Advanced ovarian cancer	2013	00886717
Docetaxel-PM	Phase II	Esophagus Squamous cell carcinoma	Ongoing	03585673

3.1.3 Micelles for Brain Targeting

3.1.3a Ligand-Micelle-Based Active Brain Targeting

Ligand-mediated delivery of bio-actives using micelles can enhance the efficacy of bio-actives. For example, MPEGPCL-Tat (methoxy poly(ethylene glycol)/poly(ε-

caprolactone)) polymer micelles modified with human immunodeficiency virus Tat protein as the brain-targeting agent and coumarin as a model drug showed higher brain distribution of coumarin [62]. Polymeric micelles modified with p-hydroxybenzoic acid (p-HA) as the brain-targeting agent was found effective in improving cellular uptake of docetaxel in brain capillary endothelial cells (BCECs) by 1.2 times over the unmodified micelles, 1.2 times more cytotoxic than unmodified micelles, and 1.7 times more effective than free drug. Ex vivo near infrared fluorescence imaging showed 1.3-1.8 times higher brain uptake than unmodified micelles [63]. Similarly, cyRGD-installed polymeric micelles were constructed and chemically conjugated with epirubucin via a pH-sensitive hydrazone bond for the effective brain delivery in glioblastoma (GBM). The micelles easily penetrated the U87MG cell-derived spheroid model and *in vivo* studies clearly showed that accumulation of the drug was four folds higher than the non-CyRGD tagged micelles [64, 65]

3.1.3.b Passive Targeting

Passive targeting of micelles crosses the BBB mostly through adsorptive-mediated endocytosis mechanism. A number of these micelles have been developed and found effective in brain targeting. Novel polyion complex micelles composed of methoxy poly(ethylene glycol)-grafted chitosan and encapsulated with all-trans retinoic acid (ATRA) were developed for brain tumor treatment. *In vivo* imaging of polymeric

micelles (CS-SA) of stearic acid (SA)-modified chitosan (CS) loaded with doxorubicin revealed that CS-SA micelles were capable of crossing the BBB and delivered the drug effectively into the brain. Polymeric micelles NK012 loaded with an anticancer agent SN-38 was found effective against xenografted rat glioblastoma with less toxicity. Polymeric micelles constructed with novel cross-linked hyaluronan styrylpyridinium (HA-SbQ) copolymer and loaded with PTX were found to give higher cellular uptake by bone marrow-derived macrophages (BMM) and U87 cells. Cytotoxic studies revealed that the formulation was more potent than the naı¨ve drug. Cholesterol-conjugated polyoxyethylene sorbitol oleate (CPSO) amphiphilic copolymer was used to prepare self-assembled CPSO micelles for PTX delivery in glioblastomas. The researcher claimed, after *in vitro* studies in U87 cells and *in vivo* studies, that the CPSO micelles were more biocompatible, safe, and better capable of delivering the drug across the BBB than Taxol along [65].

3.1.4 GUNW-3 micelles

GUNW-3 is a molecule with cholesterol at one end of the molecule and glutathione at the other end (Figure 3.1). The cholesterol part and glutathione part are connected by a short ethylene glycol link (figure 3.1). Cholesterol is an endogenous compound and plays an important role in the cell membrane structure[66]. Structurally, cholesterol is a very hydrophobic molecule with a molecular weight of 386.6 and log P

value around 7. On the other side, glutathione is a very hydrophilic endogenous antioxidant tripeptide with a molecular weight of 307.3 and a log P value of -6.3 [67]. This big difference in the log P values of cholesterol and glutathione, with one being highly hydrophobic and the other highly hydrophilic, is the basis for GUNW-3 to be amphiphilic. We have found that GUNW-3 can form micelles by itself with a low CMC. The ability of GUNW-3 to form micelles is properly due to the amphiphilic structure feature with a hydrophobic part (cholesterol) at one end of the GUNW-3 molecule and the hydrophilic part (glutathione) at the other end of the molecule. This part of the project was aimed to investigate the basic properties of GUNW-3 micelles and the brain-targeting ability of GUNW-3 micelles by using DiR, a near infrared (NIR) fluorescent cyanine dye, as a model compound to track distribution of GUNW-3 micelles and also to investigate the ability of GUNW-3 micelles to deliver DiR.

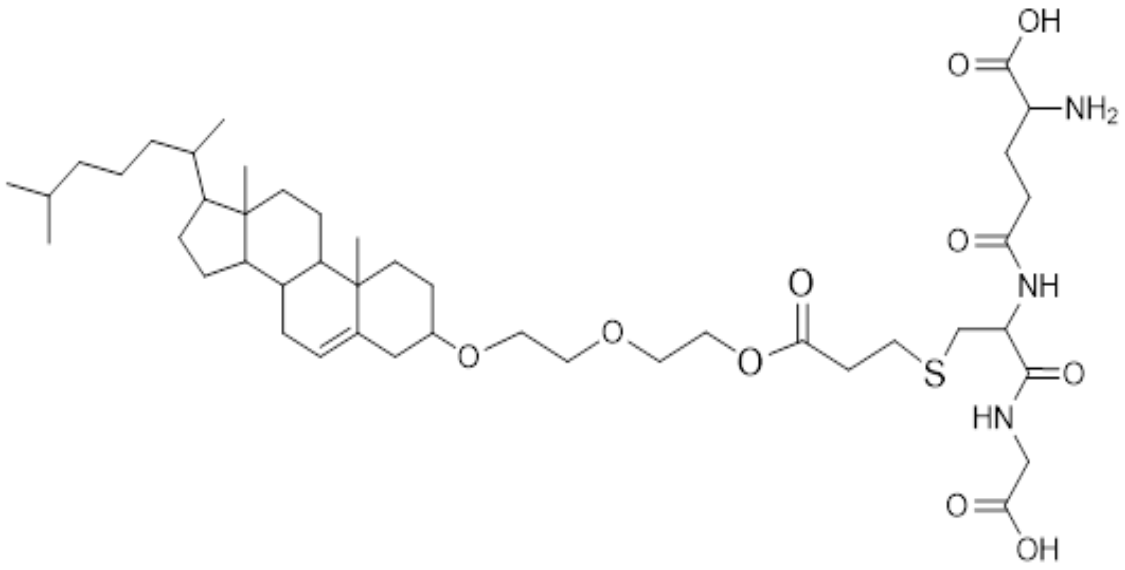

Figure 3.1 Chemical Structure of GUNW-3.

3.2 Experimental Section

3.2.1 Materials and instruments

Unless otherwise stated, all chemical reagents and solvents were obtained from commercial sources and used without further purification. GUNW-3 was prepared based on a procedure in Chapter 2 of this dissertation. DiR [or DilC18(7)], Ethanol, tetrahydrofuran (THF), cholesterol, Dulbecco's phosphate buffer saline (Gicob™D PBS, no calcium, no magnesium,1x) were purchased from Thermo Fisher Scientific (Waltham, MA, USA). Pyrene and lecithin (phospholipid 90G) were obtained from lipoid (Ludwigshafen, Germany). Dimethyldioctadecylammonium bromide (DDAB) was obtained from AppliChem (Darmstadt, Germany). Sephadex column (PD10 column, GE health care, Little Chalfont, UK), RPMI 1640 growth medium supplement with 10% FBS 100 units/ml of penicillin was obtained from Mediatech, Inc. (Hendon, VA). In-vivo and ex-vivo imaging was obtained on a Xtreme in-vivo imaging (Bruker).

3.2.2 Procedures

3.2.2.1 The Critical micellar concentration of GUNW-3

The CMC of GUNW-3 was determined by using pyrene as a fluorescent probe. Briefly, 1 mg/ml of pyrene in acetone (6×10^{-6} M) was added to a series of vials and evaporated under nitrogen. Different concertation of GUNW-3 from 0.00001 mg/ml to 1 mg/ml was added to the vials. The mixtures were vortexed for 2 min. The fluorescence intensity from each vial was determined by a spectrofluorometer using the excitation wavelength of 334 nm and emission wavelengths of 375 nm for I_1 and 384 nm for I_3 respectively. The CMC is the concentration at the intersection of the two straight lines of the I_3/I_1 ratio low concentration and high concentration[68-70].

3.2.2.2 Preparation and characterization of GUNW-3 DiR micelles

GUNW-3 Dir micelles were prepared by a film-dispersion method. Briefly, 7 mg of GUNW-3 and 0.025 mg of DiR were suspended in ethanol (50µl) and vortex-mixed. The ethanol was evaporated by using nitrogen. The residue was hydrated with Dulbecco's phosphate buffer saline (DPBS). The solution was centrifuged at 14000 rpm for 10 min to remove insoluble DiR to give GUNW-3 DiR micelles [71].

The particle size and zeta potential of GUNW-3 DiR micelles were determined by using Zetasizer. Briefly, a freshly prepared GUNW-3 DiR micelle solution was diluted (0.5:100) with deionized water before used for particle size and zeta potential determination by the dynamic light scattering (DLS) method using Zetasizer (Malvern instrument, Westborough, MA).

3.2.2.3 Preparation of control DiR liposomes

In addition to free DiR, control DiR liposomes were employed as a control for GUNW-3 DiR micelles. Control DiR liposomes were prepared by the Thin Layer Hydration method. Briefly, Lecithin (7 mg/ml), cholesterol (1 mg/ml), DDAB (2 mg/ml), and DiR (0.025 mg/ml) were dissolved in chloroform. The thin film was formed after rotavapory evaporation of solvents overnight under a reduced pressure. The thin film was then hydrated using DPBS solution for 10 min and vortex-mixed for 2 min. Liposome size reduction was achieved by a bath sonicator for 20 min (4 min sonication with 1 min break) followed by extrusion through a 200 nm, and then 100 nm filter. Sephadex column (PD 10 column, GE health care, Little Chalfont, UK) was used to separate untrapped DiR

by centrifugation at 2500 rpm for 2 min to yield the control DiR liposomes. The particle size and zeta potential were determined by the Dynamic light scattering (DLS) method using Zetasizer (Malvern instrument, Westborough, MA) after a dilution (0.5:100) of the DiR liposomes with deionized water.

3.2.2.4 Determination of DiR encapsulation efficiency and loading capacity

The encapsulation efficiency (EE%) and loading capacity (LC%) of GUNW-3 DiR micelles and control DiR liposomes were determined by fluorescence. The GUNW-3 DiR micelles or the control DiR liposomes were dissolved in DMSO to a concentration of 7 mg/ml. The GUNW-3 micelles solution or control liposomes solution (60 μl) and DMSO (40 μl) were pipetted into a well of a 96-well plate for fluorescence intensity measurement on a fluorescent plate reader by using 730 nm and 780 nm as the excitation and emission wavelengths. A calibration curve was constructed by spiking a known concentration of DiR to a blank liposomes in DMSO[72].

3.2.2.5 Stabilities of GUNW-3 DiR micelles and control DiR liposomes

A stability study of GUNW-3 DiR micelles was conducted at 4 ˚C to determine the storage stability of the micelles. Since micelles will encounter proteins once in the blood circulation, the stability of GUNW-3 in the presence of serum at 37 ˚C was also checked. The particle size was used as a parameter for micelle stability studies.

3.2.2.5a Stabilities of GUNW-3 DiR micelles and control DiR liposomes

The stability of freshly prepared GUNW-3 DiR micelles or control DiR liposomes was checked, after a 0.5:100 dilution with deionized water as described earlier, every 24 h at 4 ˚C for 5 days. The particle size was determined by the dynamic light scattering (DLS) method using Zetasizer (Malvern instrument, Westborough, MA).

3.2.2.5b Stabilities of GUNW-3 DiR micelles and control DiR liposomes in the presence of FBS

The stabilities of GUNW-3 DiR micelles and control DiR liposome were checked in the presence of RPMI 1640 growth medium supplemented with 10% FBS at 37 ˚C. Samples were diluted with deionized water (0.5:100) before particle size determination The particle size was checked by the dynamic light scattering (DLS) method using Zetasizer (Malvern instrument, Westborough, MA).

3.2.2.6 Whole body fluorescence imaging of mice

Females BALB/Cj mice (6-8 weeks old, 17-20 g) were used for this work. Mice were purchased from Jackson Laboratory (Bar Harbor, ME, USA) and acclimatized to a laboratory condition for one week before the experiment. For the experiment, mice were divided into 3 groups and intravenously injected with GUNW-3 DiR micelles, control DiR liposome, or free DiR (250 μg DiR/Kg) respectively through the tail vein. Fluorescence images for the whole body were taken at 15 min, 1 h, 24 h, and 48 h post injection. Images were analyzed using the Bruker MI SE software. All procedures were approved by the Institutional Animal Care and Use Committee (IACUC) at South Dakota State University, Brookings, SD, USA.

3.2.2.7 EX-vivo brain and organs imaging

To assess organ distribution, mice were sacrificed 1 h and 48 h after a single dose tail vein injection. The heart was perfused with DPBS before organs were collected to remove blood in tissues. Images of organs were obtained using Xtreme in-vivo imaging (Bruker) and analyzed using the Bruker MI SE software.

3.2.2.8 Statistics

In this work, results from *in vitro* experiments were reported as mean ± standard deviation (SD) of n=3 and results from *in vivo* experiments were reported as means with standard error of mean (SEM). Student's *t*-test was used to compare two groups and one-way ANOVA with a Tukey post-test was used to compare all three groups. The results are reported using GraphPad Prism 8 to demonstrate the statistical difference ($p < 0.05$).

3.3 Result and Discussion

3.3.1 The critical micellar concentration (CMC) of GUNW-3 micelles

CMC is a critical micelle parameter to reflect the stability of micelles and is also a parameter to determine if the micelles are stable enough to be used for a clinical application. The CMC of micelles used for a clinical application needs to be in μM concentration so that the micelles are stable enough to remain as micelles once being diluted in the blood stream.

In this study, the CMC of the GUNW-3 micelles was measured using pyrene - a fluorescens probe. Pyrene is a hydrophobic molecule that has a very low water solubility. As demonstrated in Figure 3.2, pyrene showed a low but constant fluorescence intensity before GUNW-3 formed micelles (Figure 3.2). The fluorescence intensity took a turn and increased dramatically indicating that GUNW-3 started to form micelles – a phenomenon resulting from the fact that pyrene started to be encapsulated inside the micelles which increased significantly the solubility of pyrene that in turn significantly increased the fluorescence intensity. The CMC of GUNW-3 was determined to be 3.3 μg/ml (3.9 μM) (Figure 3.2). The low μM CMC of GUNW-3 suggests that GUNW-3 micelles are stable enough to be used for a clinical application.

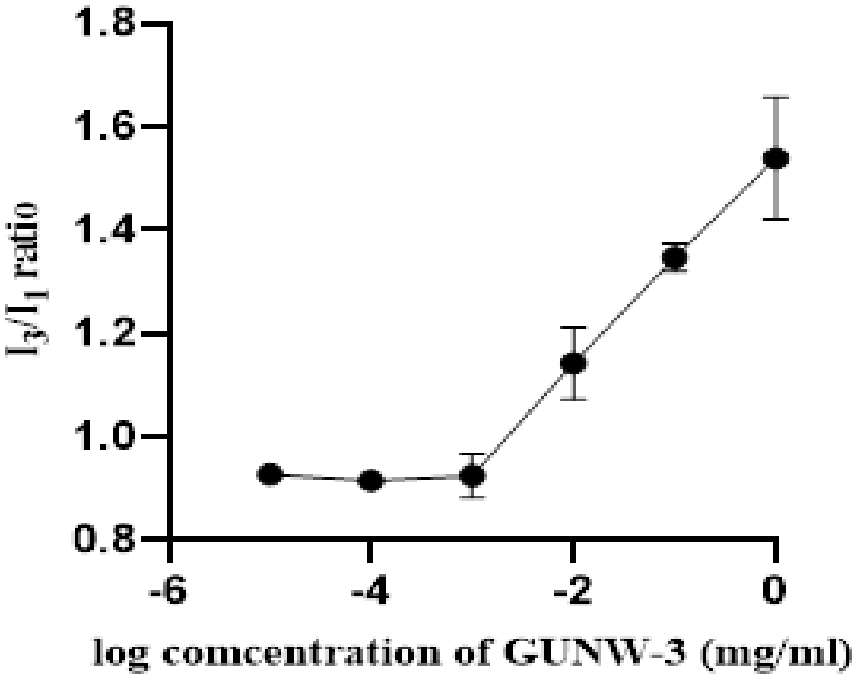

Figure 3. 2 A plot of I_3/I_1 versus concentration of GUNW-3. Pyrene was used as a fluorescent probe. Data were presented as the mean ± SD (n=3).

3.3.2 Preparation and characterization of GUNW-3 DiR micelles

Figure 3.3 provides a graphic demonstration for the preparation of GUNW-3 DiR micelles. GUNW-3 formed micelles through self-assembly once its concentration exceeded the CMC. The average particle size of GUNW-3 DiR micelles was 29.09 nm ± 5 (Figure 3.4.A) and the size distribution parameter PDI (poly distribution index) was 0.126. The particle size of GUNW-3 micelles was well below 150 nm which is the maximum particle size for brain targeting. The zeta potential of GUNW-3 micelles was found to be -19 mV ± 2.1 (Table 3.2).

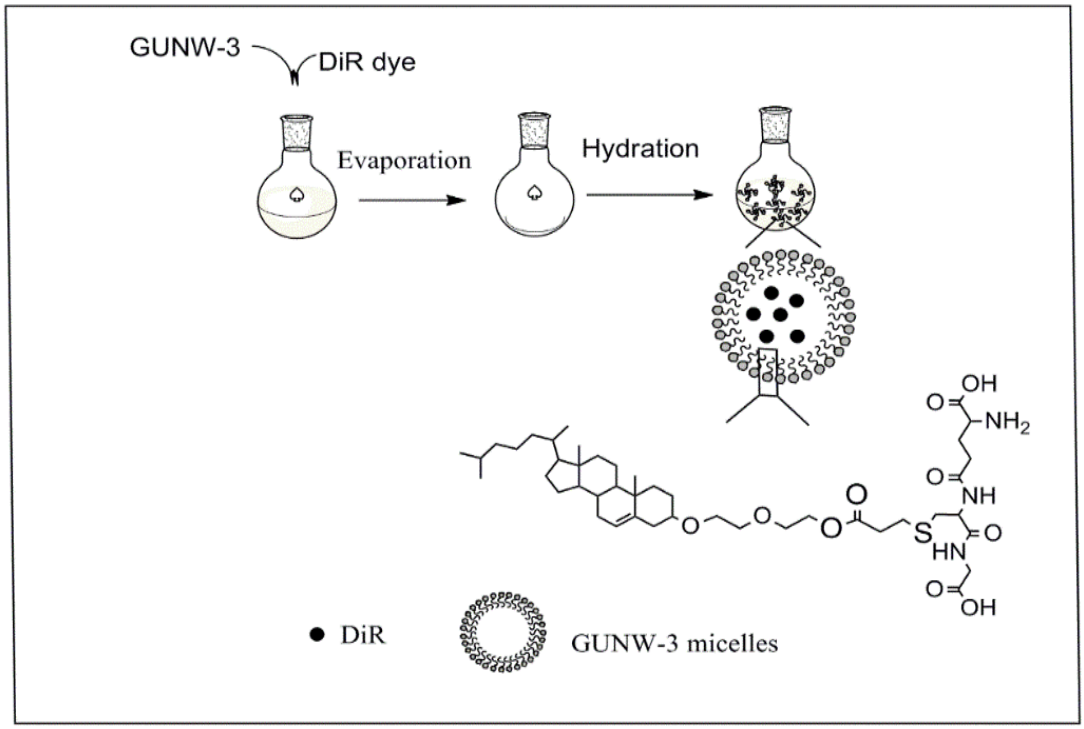

Figure 3. 3 Preparation of GUNW-3 micelles.

3.3.3 Preparation and characterization of control DiR liposomes

Control DiR liposomes were prepared based on the thin layer hydration method. The average size and size distribution of the prepared control DiR liposomes are illustrated in Figure 3.4. The average size of the control DiR liposomes was 99.56 nm ± 2.5 with a PDI value of 0.205. The zeta potential of the control DiR liposomes was +19.2 mV±6.53 (Figure 3.4.B, Table 3.2). The positive charge on the liposome surface was from cationic DDAB. Cationic liposomes are known to have better brain targeting when compared with neutral liposomes and anionic liposomes due to their electrostatic interaction with the negatively charged cell surface (adsorptive-mediated endocytosis) [73, 74].

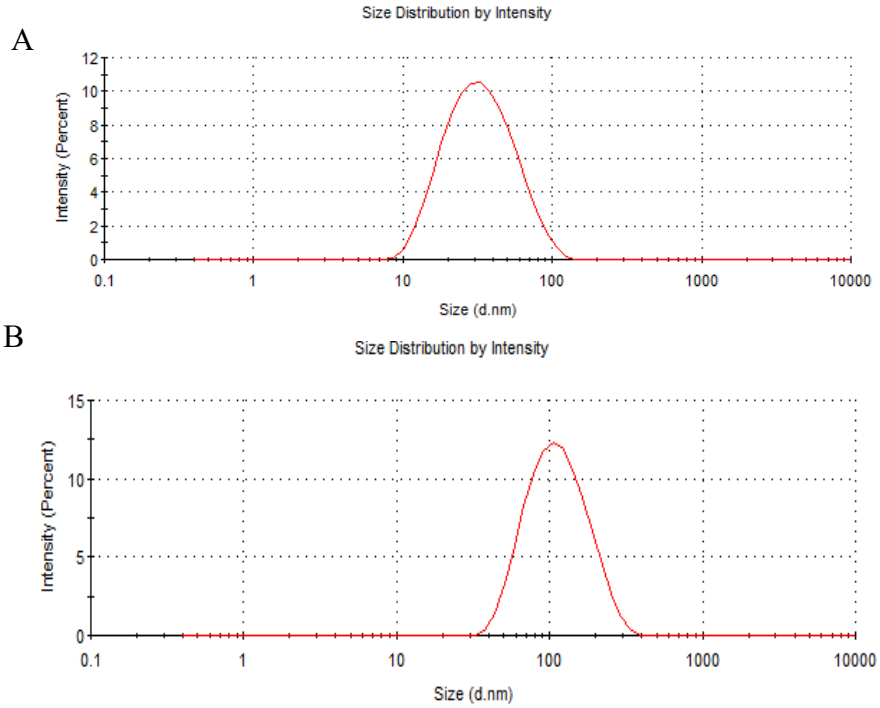

Figure 3.4 Particle size and size distribution of GUNW-3 DiR micelles (A) and control DiR liposomes (B).

Table 3.2 Nanoparticle parameters of GUNW-3 DiR micelles and control DiR liposomes. Results are presented as mean ±SD (n=3).

Nanoparticles	Theoretical loading (%)	Particle Size (nm)	PDI	Zeta potential (mV)	(EE%)	(LC%)
GUNW-3 DiR micelles	0.35	29.09 ± 5	0.126	-19 ± 2.1	68±0.6	0.24 ± 0.0015
Control DiR liposomes	0.25	99.5 ± 2.5	0.205	+19.2 ±6.53	69 ± 0.7	0.17 ± 0.0013

3.3.4 Determination of DiR encapsulation

The encapsulation efficiency (EE%) and loading capacity (LC%) of GUNW-3 DiR micelles and control DiR liposomes were determined by fluorescence using 730 nm and 780 nm as the excitation and emission wavelengths. The EE% and LC% of the GUNW-3 micelles were found to be 68±0.6 % and 0.24 ± 0.0015% respectively while the EE% and LC% of the control DiR liposomes were found to be 68±0.7% and 0.17 ± 0.0013% respectively (Table 3.2).

3.3.5 Stabilities of GUNW-3 DiR micelles and control DiR liposomes

3.3.5.1 Stabilities of GUNW-3 DiR micelles and control DiR liposomes

The stabilities of GUNW-3 DiR micelles and control DiR liposomes were studied at 4 ℃ for 5 days in the DPBS. The particle size was used as a parameter to reflect the stability. The data are shown in Figure 3.5.A. The particle size of the control DiR liposomes on day 1 was 99.56 nm ± 2.89 exhibiting no statistical difference when compared with 102.83 nm ± 1.2 on day 5. No statistically significant difference was observed either for the particle size of GUNW-5 micelles on day 1 (29.2 nm ± 5.08) vs that on day 5 (29.7 nm± 1.2). These results suggest that both GUNW-3 DiR micelles and control DiR liposomes were stable in the stock solution at 4 ℃ – a storage temperature (Figure 3.5.A).

3.5.5.2 Stabilities of GUNW-3 DiR micelles and control DiR liposomes in the presence of FBS

In order to achieve significant brain uptake, nanoparticles need to have good stability in the presence of proteins which are present in the blood circulation. To check the stability in the presence of proteins, GUNW-3 DiR micelles or control DiR liposomes

were incubated in the RPMI 1640 growth medium supplemented with 10% fetal bovine serum (FBS) at 37 °C. As shown in figure 3.5.B, the particle size of GUNW-3 DiR micelles increased from ~27.7 nm to ~105.6 nm then continued to increase to reach 229 nm at 24 h. The particle size of GUNW-3 micelles remained relatively constant (~229 nm) after 24 h until 48 h when the experiment ended demonstrating a two-phase increase in particle size. The two-phase increase in particle size suggests possibly two different mechanisms to account for these two phases in particle size increases. One is that GUNW-3 quickly complexed with FBS that increased the particle size initially (first phase size increase), then followed by a slow increase in particle size which might be caused by particle aggregation. Binding of GUNW-3 micelles to FBS appears to be consistent with a literature report on the binding of GSH to BSA. It was reported that GSH can bind to BSA at site I in subdomain IIA based on the molecular docking results. The binding process is dominated by hydrogen bonds and concluded that there is a strong interaction between GSH and BSA. Therefore, it is quite likely GUNW-3 binds to BSA in a similar manner [75]. Similar to GUNW-3 DiR micelles, control DiR liposomes quickly changed the particle size from ~120 nm to ~367.6 nm (Figure 3.5.C). However, no second phase particle size increase was observed for control DiR liposomes. It is noted that the required particle size for brain-targeting should be below ~150 nm. Larger particles will not be able to enter the brain. Therefore, an increase in particle size observed with GUNW-3 micelles and control DiR liposomes will have impacts on their abilities to enter the brain. The increase in size will also have an impact on the clearance of nanoparticles [76].

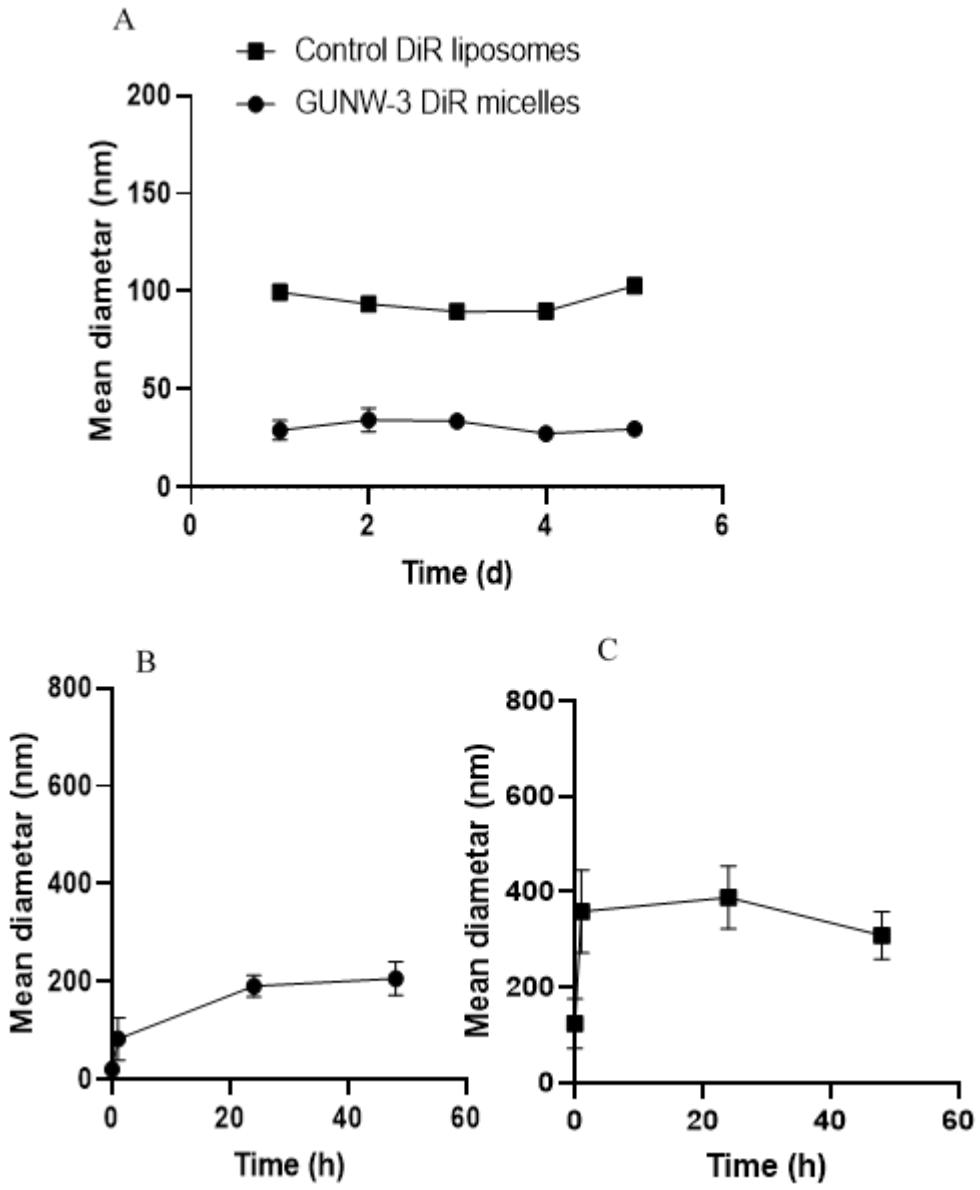

Figure 3.5 (A) Stabilities of GUNW-3 DiR micelles and control DiR liposome in the absence of FBS. (B) GUNW-3 DiR micelles stability in the presence of FBS. (C) control DiR liposomes stability in the presence of serum. Data are presented as mean ±SD (n=3).

3.3.6 Whole-body fluorescence imaging

In-vivo imaging of mice is a widely used method to investigate the *in vivo* brain targeting ability of nanoparticles. DiR, a near infrared fluorescent lipophilic carbocyanine and commonly used dye, is often encapsulated in nanoparticles to track the distribution of nanoparticles *in vivo*. In this dissertation, DiR is encapsulated in GUNW-3 micelles (GUNW-3 DiR micelles) to help track the distribution of GUNW-3 micelles in mice through *in vivo* imaging. Additionally, DiR is a hydrophobic cationic molecule. The abilities of GUNW-3 micelles to encapsulate DiR and to deliver DiR demonstrate the ability of GUNW-3 micelles in delivering compounds with similar properties. In other words, GUNW-3 DiR liposomes serve two purposes: i). help track the bio-distribution of GUNW-3 micelles and determine if GUNW-3 micelles exhibit brain-targeting effects; ii). demonstrate the ability of GUNW-3 to deliver DiR and DiR similar molecules. For a comparison, control DiR liposomes and DiR dissolved in 5% ethanol (free DiR) were employed as two controls. Since control DiR liposomes are cationic liposomes and cationic liposomes have been reported to exhibit a brain targeting effect[73, 74, 76], control DiR liposomes served as a good positive control. Since free DiR cannot pass BBB, it was not expected to exhibit any brain target effects.

In the whole-body imaging experiment, mice were treated with GUNW-3 DiR micelles, control DiR liposomes, or free DiR intravenously through tail vein injection. Whole body imaging was performed at 15 min, 1 h, 24 h, and 48 h (Figure 3.6). As demonstrated in Figure 3.6 C, GUNW-3 DiR micelles distributed to the brain rapidly within 15 min. A minimum amount of control DiR liposomes were observed in the brain (Figure 3.6.B) while no free DiR (Figure 3.6.A) was observed in the brain consistent with

the literature report for the brain targeting ability of cationic liposomes and free DiR. The fluorescence intensity remained strong for 48 h in the brain of the mouse treated with GUNW-3 DiR micelles when compared with those from the control DiR liposomes and free DiR suggesting a significant brain-targeting effect by GUNW-3 micelles. The brain targeting of GUNW-3 micelles was further confirmed by the lateral images obtained at 1 h (Figure 3.7). As demonstrated in the lateral images, strong brain fluorescence was observed for the mouse treated with GUNW-3 DiR micelles. The fluorescence was barely visible in both brains of the mice treated with the control DiR liposomes and free DiR. One interesting thing observed in the lateral images was that fluorescence was also seen in the spinal cord of the mouse treated with GUNW-3 DiR micelles which further confirms the entry of GUNW-3 DiR micelles into the CNS (Figure3.6. Lateral image).

Figure 3.7 shows the fluorescence intensity obtained from the brains of the whole-body images in Figure 3.6. The fluorescence intensity in the brain of the mouse treated with GUNW-3 DiR micelles was 5.8 and 19 times higher than that from the control DiR liposome and free DiR respectively. Interestingly, while both controls showed a decrease in fluorescence intensity, GUNW-3 DiR micelles showed an increase in fluorescence from 1 h to 48 h. At 48 h, the fluorescence intensity in the brain of the mouse treated with GUNW-3 DiR micelles was 13 and 22 times higher than that from the control DiR liposome and free DiR respectively (Figure 3.7).

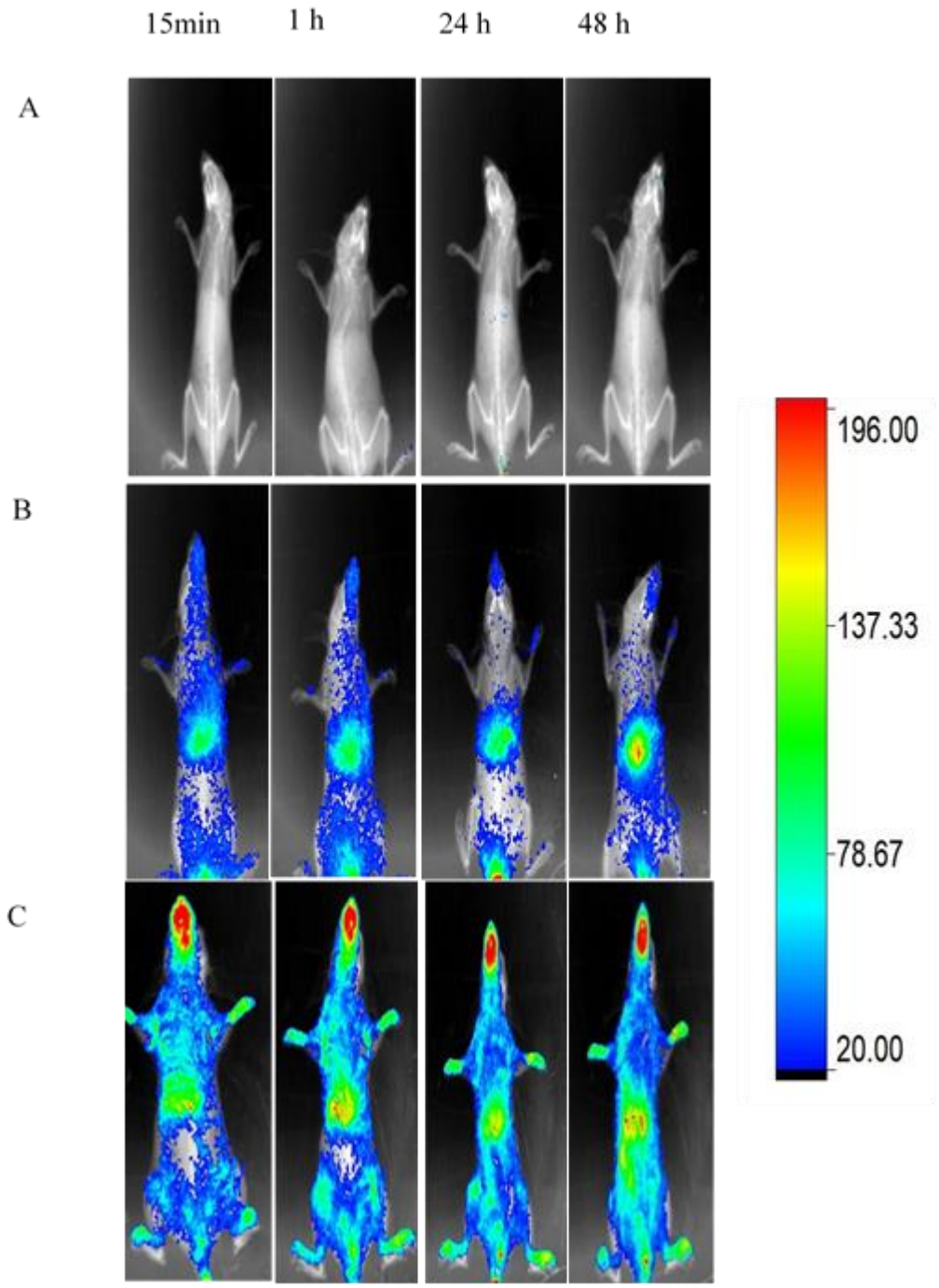

Figure 3. 6 In-vivo whole-body fluorescence imaging of mice at 15 min, 1 h, 24 h, and 48 h. A: Free DiR, B: Control DiR liposome, and C: GUNW-3 DiR micelles. Representative image, n=3.

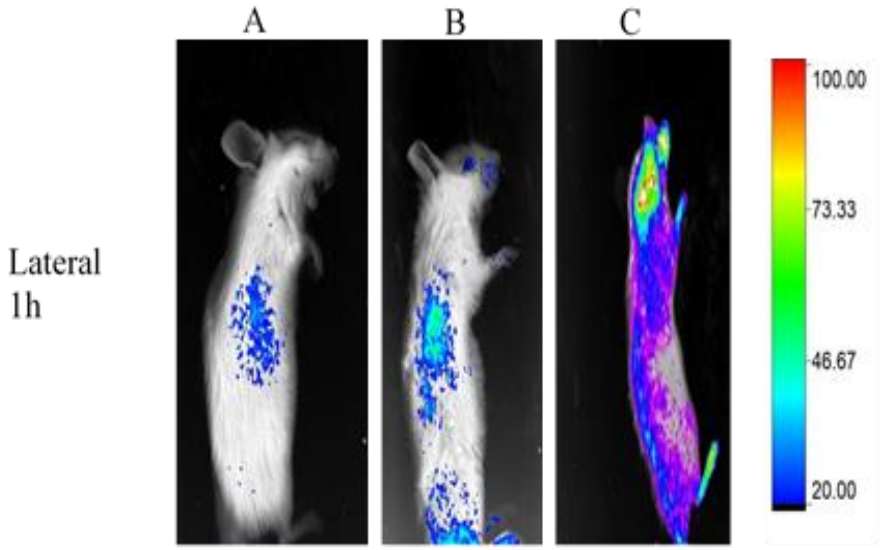

Figure 3.7 Lateral image for each group at 1h. A: Free DiR, B: Control DiR liposome, and C: GUNW-3 DiR micelles. Representative image, n=3.

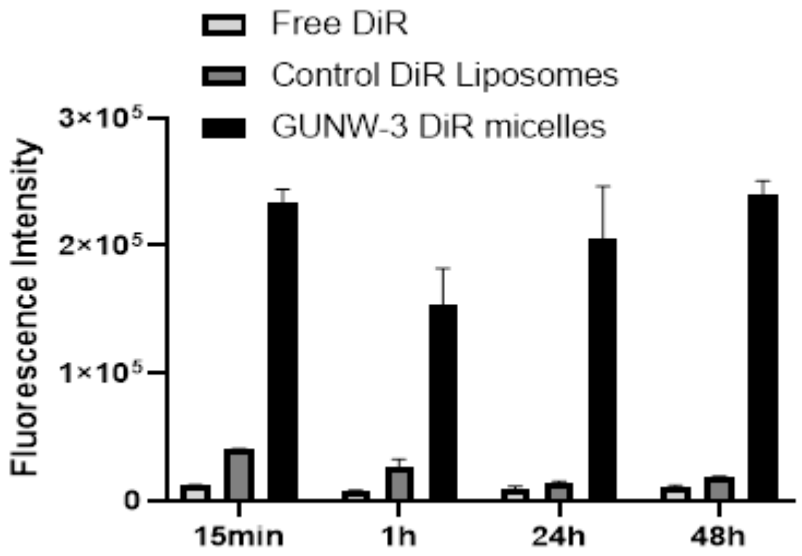

Figure 3.8 Fluorescence intensity from the brains of mice treated with GUNW-3 DiR micelles, control DiR liposomes, or free DiR at different time points. Results are presented as mean ± SEM (n=3).

3.3.7 Ex-vivo imaging.

To further confirm brain targeting, the brain and some of the other major organs (brain, heart, lung, liver, spleen, and kidney) were collected for ex-vivo imaging at 1 h and 48 h. Blood was removed by heart perfusion with DPBS before organ collection. Fluorescence images of the organs were obtained using Xtreme in-vivo imaging (Bruker).

3.3.7.1 Ex-vivo brain imaging at 1 h

The fluorescence images of the collected brains at 1 h demonstrates that the fluorescence intensity was significantly higher from the brain of the mouse treated with GUNW-3 DiR micelles when compared with control DiR liposome and free DiR ($p = 0.0002$, one-way ANOVA with Tukey post-test, n=3) (Figure 3.8. A, B, C, D). Around 5-fold of increase of the total fluoresce intensity in the brains of mice treated with GUNW-3 micelles was observed when compared with the control DiR liposomes ($p = 0.0006$, Tukey post-test) and 12-fold of increase when compared with free DiR ($p =0.0003$, Tukey post-test) (Table 3.3). These ex-vivo results conclude that GUNW-3 micelles exhibit a significant brain targeting effect.

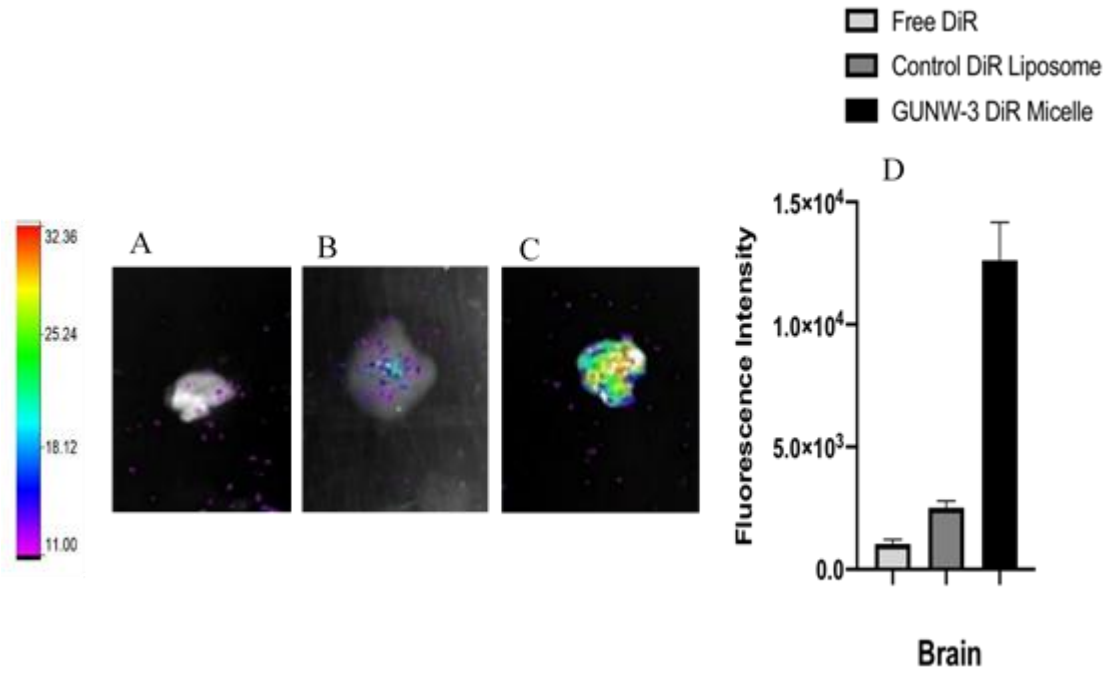

Figure 3.9 Ex-vivo imaging of the brains at 1 h after a single dose IV injection by tail vein injection (0.250 mg/Kg DiR). A: Free DiR; B: Control DiR liposomes; C: GUNW-3 DiR micelles. D: Semi-quantitative fluorescence intensity of the brains (n=3, mean ± SEM).

Table 3 3 Comparison of fluorescence intensity from the brains of mice with different treatments as presented in Figure 3.8

Comparison of brain fluorescence intensity	**Statistical significance**
Free DiR vs. control DiR liposomes	ns ($p = 0.5268$)
Free DiR vs. GUNW-3 DiR micelles	*** ($p = 0.0003$)
Control DiR liposome vs. GUNW-3 DiR micelles	*** ($p = 0.0006$)

ns: no statistically significant difference *<0.05, **<0.01, ***<0.001, (n=3). One-way ANOVA with a Tukey post-test was used to compare all three groups.

3.3.7.2 Ex-vivo brain imaging at 48h

Ex-vivo brain imaging at 48 hours showed a 6.5-fold and 14-fold increase in brain fluorescence from the mice treated with GUNW-3 DiR micelles when compared with the control DiR liposomes (p = 0.0005, according to the Tukey post-test (Table 3.4)) and free DiR (p = 0.0003, according to the Tukey post-test ((Table 3.4) (Figure 3.9)).

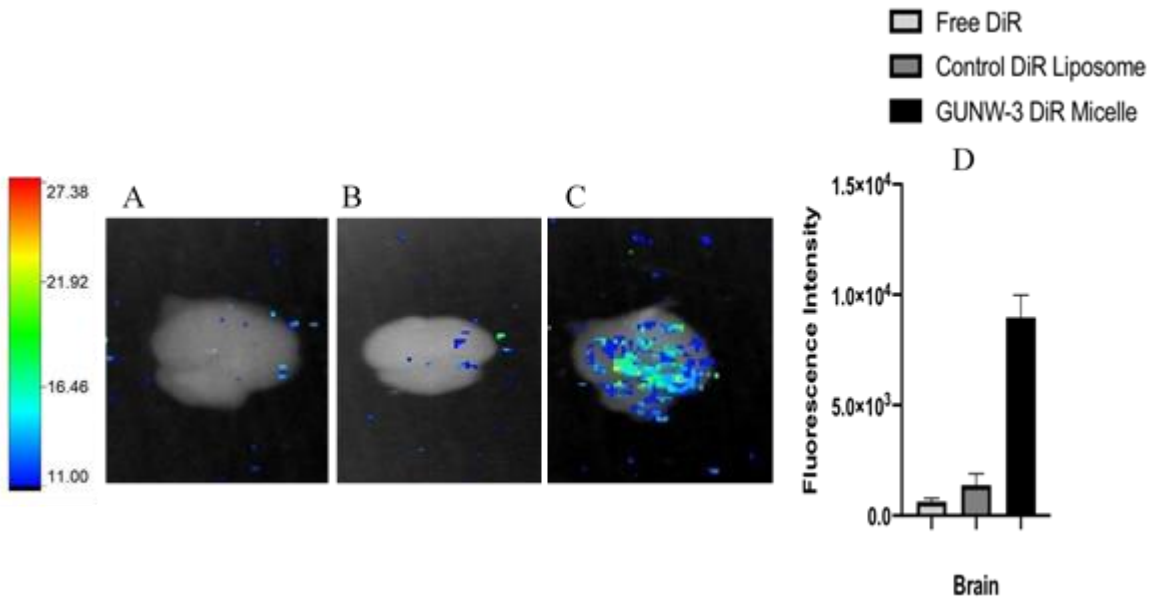

Figure 3.10 Ex-vivo imaging of the brains at 48 h after a single dose IV injection by tail vein injection (0.250 mg/Kg DiR). A: Free DiR; B: Control DiR liposomes; C: GUNW-3 DiR micelles. D: Semi-quantitative fluorescence intensity of the brains (n=3, mean ± SEM).

Table 3.4 Comparison of fluorescence intensity from the brains of mice with different treatments as presented in Figure 3.9

Comparison of brain fluorescence intensity	Statistical significance
Free DiR vs. Control DiR Liposome	ns (p = 0.7185)
Free DiR vs. GUNW-3 DiR Micelles	***(p = 0.0003)
Control DiR Liposome vs. GUNW-3 DiR Micelles	***(p = 0.0005)

ns: no statistically significant difference *<0.05, **<0.01, ***<0.001, (n=3). One-way ANOVA with a Tukey post-test was used to compare all three groups,

3.3.7.3 Ex-vivo tissue imaging at 1 h

In addition to brain distribution, tissue distribution in other major organs (heart, lung, liver, spleen, and kidney) at 1 h was investigated. The results are presented in Figure 3.10. As shown in the figure, GUNW-3 micelles appear to distribute to the heart, lungs, liver, and kidneys with a high accumulation in the liver. The control DiR liposomes also distributed to the heart, lungs, liver and kidneys with a high accumulation in the lungs while free DiR distributed mainly to the lungs and liver with a high accumulation in the lungs. The total fluorescence intensity from the collected organs appears to be strongest from the mouse treated with GUNW-3 DiR micelles, followed by that from the control DiR liposomes, and then that from free DiR. The observed organ distribution differences from these three formulations appear to be in line with the particle size as reported in the literature. Several studies have shown that the size of the nanoparticle significantly affects organs distribution and smaller nanoparticles (less than 30 nm) were more favored in organ distribution [77].

One of the other possibilities that may contribute to the organ distribution difference could be from the different clearance rates of these formulations. A pharmacokinetic study is needed to further provide insights.

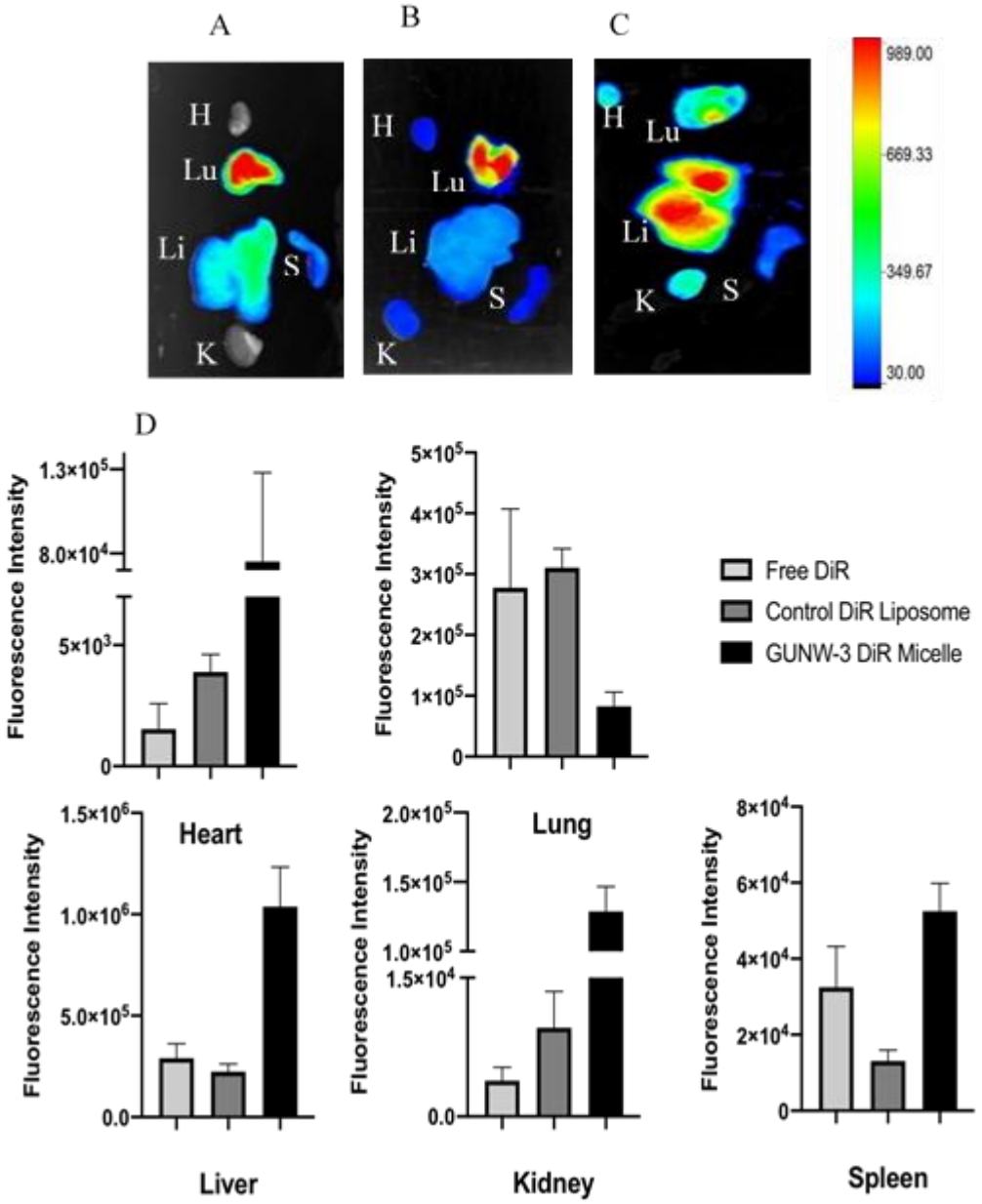

Figure 3.11 Ex-vivo imaging of the major organs collected 1 h after a single dose IV injection (0.250 mg/Kg DiR) of A: free DiR, B: control DiR liposome, and C: GUNW-3 DiR micelles. Organs (H: heart, Lu: lung, Li: liver, S: spleen, and K: kidney) were collected after heart perfusion with DPBS to remove blood in tissues, D: Semi-quantitative fluorescence intensity of different organs (n=3, mean ± SEM).

Table 3.5 Comparison of fluorescence intensity from the brains of mice with different treatments as presented in Figure 3.11

	Heart	Lung	Liver	Kidney	Spleen
Free DiR vs. Control DiR Liposome	ns (0.9984)	ns (0.953)	ns (0.923)	ns (0.9244)	ns (0.2506)
Free DiR vs. GUNW-3 DiR Micelles	ns (0.2789)	ns (0.2587)	* (0.0116)	*** (0.0004)	ns (0.2355)
Control DiR Liposome vs. GUNW-3 DiR Micelles	ns (0.2979)	Ns (0.1786)	** (0.078)	*** (0.0005)	* (0.0255)

ns: no statistically significant difference, *<0.05, **<0.01, ***<0.001, (n=3). One-way ANOVA with a Tukey post-test was used to compare all three groups

3.3.7.4 *Ex-vivo* tissue imaging at 48 h

Tissue distribution in other major organs at 48 h was also examined (Figure 3.11). It appears that significant accumulation was still observed at 48 h in the liver for mice treated with GUNW-3 DiR micelles and control DiR liposomes. The liver from mice treated with GUNW-3 DiR micelles showed much stronger fluorescence intensity than that with the control DiR liposomes. The total fluorescence intensity from the organs collected was strongest from the mice treated with GUNW-3 DiR micelles, followed by control DiR liposomes, then free DiR – the same trend as observed at 1 h. This trend appears to be consistent with the possibility that GUNW-3 DiR micelles being retained in mice longer than control DiR liposomes and free DiR. This might have occurred due to a stronger interaction of GUNW-3 with BSA as observed in section **3.5.5.2** and was consistent with the knowledge that conjugation with albumin increased the serum half-life of the nanoparticles [78]. Again, a pharmacokinetic study is needed to provide more insights on this.

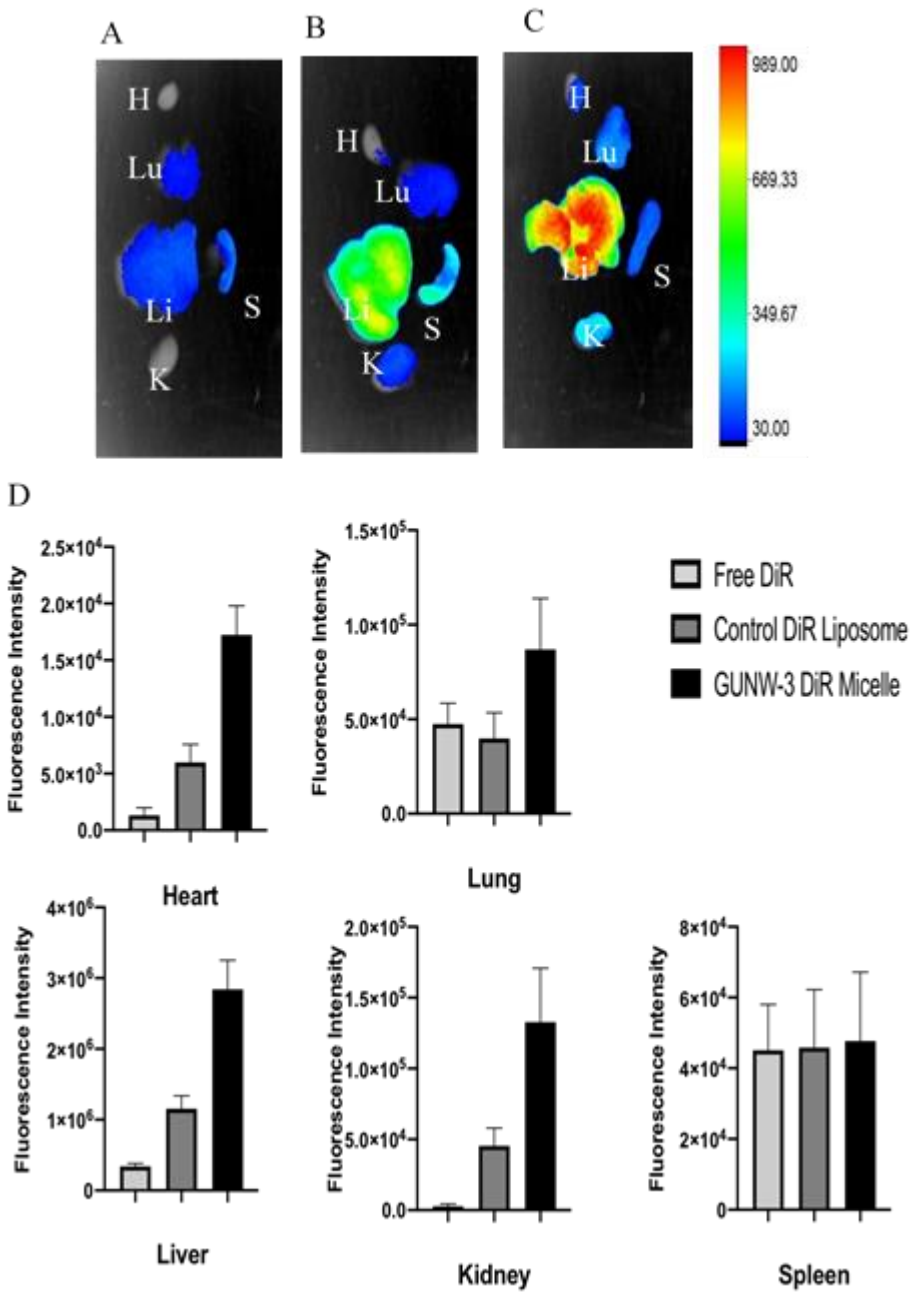

Figure 3.12 Ex-vivo imaging of the major organs 48 h after a single dose IV injection (0.250 mg/Kg DiR) of A: Free DiR, B: control DiR liposome, and C: GUNW-3 DiR micelles. Organs (H: heart, Lu: lung, Li: liver, S: spleen, and K: kidney) were collected after heart perfusion with DPBS to remove blood in tissues. D: Semi-quantitative fluorescence intensity of different organs (n=3, mean ± SEM).

Table 3.6 Comparison of fluorescence intensity from the brains of mice with different treatments as presented in Figure 3.12

	Heart	Lung	Liver	Kidney	Spleen
Free DiR vs. Control DiR Liposome	ns (0.2326)	ns (0.9547)	ns (0.1476)	ns (0.4447)	ns (0.9994)
Free DiR vs. GUNW-3 DiR Micelles	** (0.0018)	ns (0.3535)	** (0.0012)	* (0.0173)	ns (0.9931)
Control DiR Liposome vs. GUNW-3 DiR Micelles	* (0.0101)	ns (0.2491)	** (0.0091)	ns (0.0824)	ns (0.9965)

ns: no statistically significant difference *<0.05, **<0.01, ***<0.001, (n=3). One-way ANOVA with a Tukey post-test was used to compare all three groups,

In summary, GUNW-3 is an amphiphilic compound that can form micelles. Its low CMC value (3.9 μM) suggests that GUNW-3 micelles are stable enough to be used as a drug delivery system for a therapeutic application. We also demonstrate that GUNW-3 micelles were stable in the stock solution for 5 days at 4 °C and exhibited a better stability in the presence of FBS at 37 °C when compared with the control liposomes. Most importantly, we demonstrate that the brain uptake of GUNW-3 DiR micelles were 5-times higher than that of the control DiR liposome and 12-times higher than that of free DiR at 1 h after a single dosage IV injection. At 48 h after a single dosage IV injection, the brain uptake of GUNW-3 micelles was 6.5 times higher than that of control DiR liposomes and 14 times higher than that of free DiR. Our data provide a proof of concept for potential application of GUNW-3 micelles as an effective drug delivery system for delivering therapeutic and preventive agents to the brain for the treatment and prevention of brain diseases.

Chapter 4 Brain-Targeting of GUNW-3 Liposomes

4.1 Introduction

Liposome is a word that originally derives from two Greek words: lipo (fat) and soma (body)[79]. Liposomes are well established and widely used nanoparticles for drug delivery [80, 81]. A search for liposomes in PubMed reveals more than 48,000 results as of today. There are around 40 liposomal formulations in clinical studies and more than 12 liposomal products in the market worldwide [34]. Structurally, a liposome consists of an aqueous core surrounded by a bilayer of natural or synthetic lipids (Figure4.1).

Liposomes can encapsulate various molecules: small, large, hydrophilic, hydrophobic, and biologicals like peptides, proteins, DNA, and RNA without any modification to these molecules [76]. Liposomes deliver compounds with hydrophilic molecules being carried within the aqueous core and hydrophobic molecules being carried within the hydrophobic double lipid layers (Figure 4.1). Liposomes can also be modified for targeted delivery by coating the liposome surface with a targeting molecule to take the liposomes to a disease site such as cancer or to a tissue such as the brain (Figure 4.1).

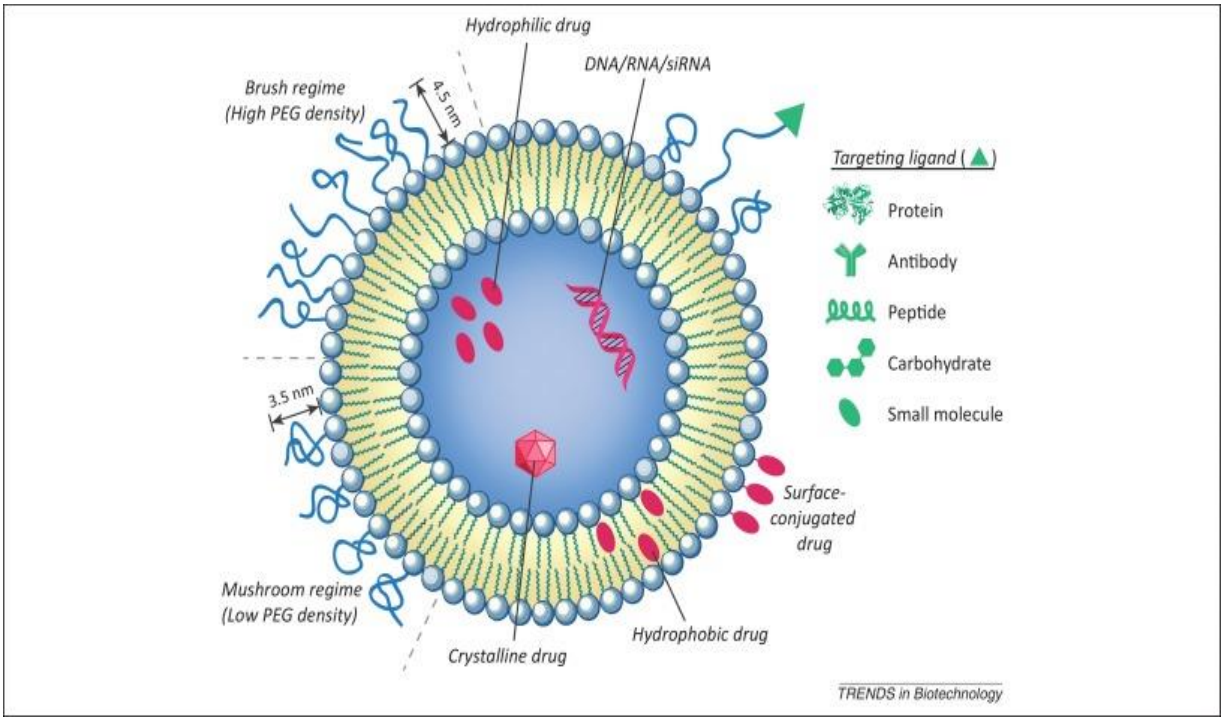

Figure 4.1 A graphic description of a liposome[82].

4.1.1 Classification of liposomes

Liposomes can be classified based on their composition, delivery mechanism, structural property, surface charge, and preparation methods [83]. A brief description of these classifications is presented below.

A. Based on the intracellular delivery mechanism that usually depends on its composition, liposomes can be classified into: (i). conventional liposomes; (ii). immune liposomes; (iii). long circulation liposomes; (iv). pH-sensitive liposomes; (v). charge liposomes; and (vi) fusogenic liposomes.

B. Based on the property of the stretcher, liposomes can be divided into: (i). Multilamellar vesicles with a particle size >0.5 μm (MLV); (ii). Oligolamellar vesicles with a particle size of 0.1-1 μm (OLV); (iii). Unilamellar vesicles

(ULV); (iv). Small unilamellar vesicles with a particle size of 20-100 mm (SUV); (v) Medium size unilamellar vesicles (MUV); (vi). Large unilamellar vesicles with a particle size >100 mm; (vii). Giant unilamellar vesicles with a particle size >1 μm (GUV); and (viii). Multivesicular vesicles with a particle size > 1 μm (MVV).

C. Based on surface charge, liposomes can be divided into positively charge liposomes (cationic liposomes), negatively charge liposomes (anionic liposome), and neutral liposomes. Liposomes surface charge (zeta potential) is dependent on the lipid composition used in preparing the liposomes.

D. Based on the method of preparation, liposomes can be prepared by: (i). Reverse-phase (REV); (ii). Frozen and Thawed MLV (FATMLV); (iii). Extrusion method (VET); (iv) French press (FPV); (v). Fusion method (FUV); and (vi). Dehydration-rehydration method (DRV).

4.1.2 Liposomes for brain targeting

Liposomes have been used to improve drug accumulation in the brain, especially positively charged liposomes which have been found to increase brain penetration by adoptive-mediated endocytosis due to an electrostatic interaction between the positively charged liposomes and negatively charged cell membrane [73, 74, 76]. However, even positively charged liposomes had a limited ability to pass the blood brain barrier (BBB) if the liposomes contain no brain-targeting ligand[34] . Thus, the coating liposome surface with a brain-targeting ligand is a common approach in improving the brain targeting ability of liposomes [34]. Effective brain-targeting ligands have been found to be those substrates of a receptor or transporter that is highly expressed in the BBB. These

substrates include glucose, amino acids, transferrin, insulin, low density lipoprotein, and glutathione (GSH) etc [44, 84]. The first work to improve the brain-targeting ability of liposomes by coating its surface with a brain targeting ligand was reported in 1996 and the brain-targeting agent was transferrin [38]. GSH is a relatively recent brain targeting agent.

4.1.3 GUNW-3 liposomes for brain targeting

In this investigation, we studied the improvement of brain-targeting of a cationic liposome by GUNW-3 – GUNW-3 liposomes. GUNW-3 liposomes are expected to be formed by imbedding the hydrophobic cholesterol moiety of GUNW-3 into the double lipid layer of the liposomes and the hydrophilic GSH part floating on the surface of the liposome for brain targeting. The reason for selecting cationic liposomes was based on the fact the cationic liposomes exhibit certain brain-targeting effects.

GUNW-3 liposomes are made up of lecithin, cholesterol, dimethyldoioctadecyl-ammonium bromide (DDAB), and GUNW-3. Below is a brief description of these components.

A. Lecithin

Soy lecithin is a phospholipid and is the main part of liposomes. A phospholipid is an amphiphilic molecule with a hydrophilic group located at one end of the molecule and a hydrophobic group located at the other end (Figure 4.2). The hydrophilic phosphate group of the phospholipid is negatively charged. When the phospholipid is hydrated, molecules of phospholipid arrange themselves to a structural bilayer forced by Van-der Waals, hydrophilic, and hydrophobic interactions [85].

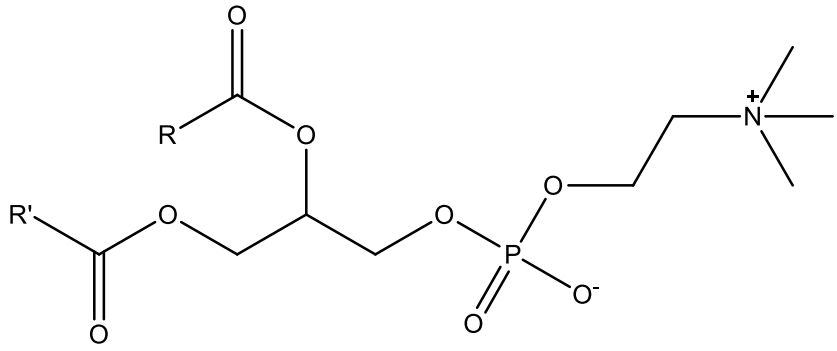

R,R' = Fatty acid residues

Figure 4.2 Chemical structure of Lecithin.

B. Cholesterol

Cholesterol helps decrease the fluidity of the lipid bilayer and increases the stability of liposomes in the biological system (Figure 4.3) [86].

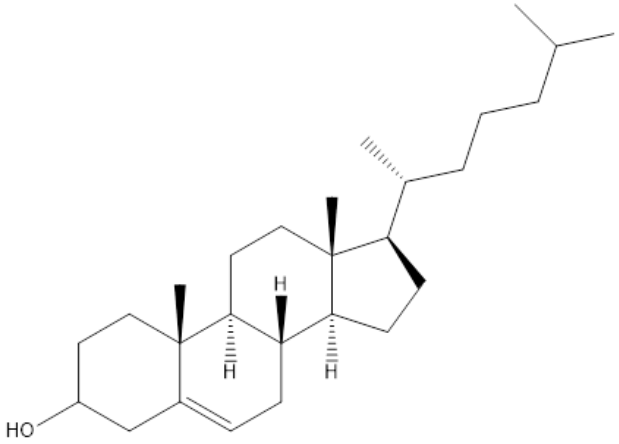

Figure 4.3 Chemical structure of cholesterol

C. DDAB

Dimethyldoioctadecylammonium bromide (DDAB) is a cationic lipid. Along with the negatively charged lecithin, DDAB helps increase interlamellar resistance between successive bilayers (Figure 4.4). This effect will result in an overall entrapped

volume[87]. Moreover, DDAB helps generate the positively charged liposomes that helps improve brain uptake when compared with neutral or anionic liposomes [73, 74, 76].

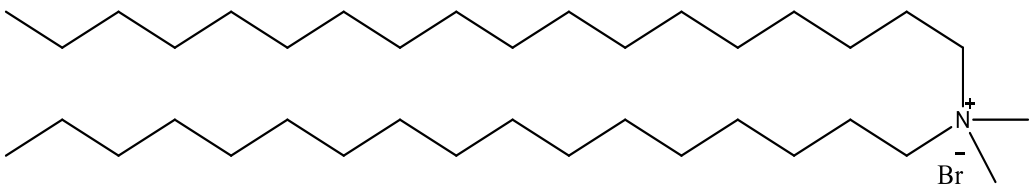

Figure 4.4 Chemical structure of dimethyldoioctadecylammonium bromide (DDAB)

D. GUNW-3

GUNW-3 is a glutathione transporter-based brain-targeting agent designed and synthesized by us (Figure 4.5). The synthetic procedure of GUNW-3 was described in chapter 2 of this dissertation. Insertion of GUNW-3 to the liposome surface is expected to improve brain-targeting of liposomes.

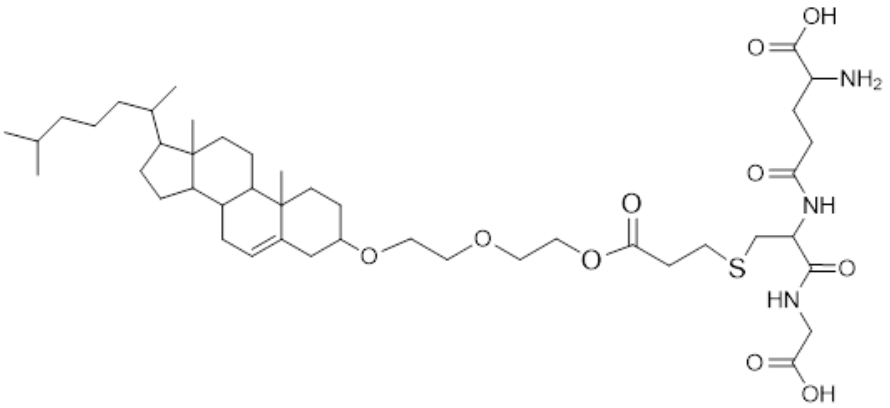

Figure 4.5 Chemical structure of GUNW-3

By using the whole-body imaging technique and DiR as a tracking agent to track distribution, we have demonstrated that GUNW-3 liposomes quickly distributed into the

brain and significantly increase the brain distribution when compared with control liposomes (the cationic liposomes). Ex-vivo imaging of the collected brains showed a 3-fold increase in brain distribution of GUNW-3 liposomes when compared with control liposomes. Our data from this project confirm the ability of GUNW-3 to improve the brain-targeting ability of liposomes.

4.2 Experimental section

4.2.1 Material and instruments

Unless otherwise stated, all chemical reagents and solvents were obtained from commercial sources and used without further purification. GUNW-3 was synthesized based on the procedure presented in Chapter 2. Lecithin (Phospholipon 90G) was obtained from Lipoid (Ludwigshafen, Germany), cholesterol from MP biomedicals (solon, OH, USA), DDAB from Applichem (Darmstadt, Germany), DiR from Fisher Scientific (Pittsburgh, PA, USA), filter paper, filter support, and extrusion apparatus from Avanti Polar Lipid, Inc (Alabaster, Al, USA), Sephadex columns (PD10 column) from GE health care (Little Chalfont, UK). PRMI 1640 growth medium, penicillin/streptomycin, phosphate buffered saline (PBS), trypsin, and fetal bovine serum (FBS) were obtained from Mediatech (Herndon, VA). , Dulbecco's phosphate buffered saline (Gicob™D DPBS, no calcium, no magnesium,1x) was purchased from Thermo Fisher Scientific (Waltham, MA, USA). In-vivo and ex-vivo imaging was obtained on a Xtreme in-vivo imaging (Bruker).

4.2.2 Procedures

4.2.2.1 DiR liposomes

Both GUNW-3 DiR liposomes and control DiR liposomes were prepared by using the Thin Layer Hydration technique. Briefly, Lecithin (7 mg/ml), cholesterol (1 mg/ml), DDAB (2 mg/ml), and DiR (0.025 mg/ml) were dissolved in chloroform. To form a thin film, solvents were evaporated by rotavapory evaporation overnight under a reduced pressure. The thin film was hydrated with a DPBS solution for control DiR liposomes or a DPBS solution with GUNW-3 (7 mg/mL) for GUNW-3 DiR liposome for 10 min

followed by vortexing for 2 min. To obtain the desired size, a bath sonicator was employed to sonicate the mixture for 20 min (4 min sonication with 1 min break) followed by extrusion with a 200 nm then 100 nm filter. A Sephadex column (PD 10 column, GE health care, Little Chalfont, UK) was used to remove untrapped DiR by centrifugation (2500rpm for 2 min) to give the control DiR liposomes or GUNW-3 DiR liposomes.

The liposomes were diluted (0.5:100) with deionized water before used for particle size and zeta potential determination using the dynamic light scattering (DLS) method on a Zetasizer (Malvern instrument, Westborough, MA).

4.2.2.2 Determination of the encapsulation efficiency (EE%) and loading capacity (LC%) of DiR liposomes

The EE% and LC% of GUNW-3 DiR liposomes and control DiR liposomes were determined by the fluorescence intensity of DiR. GUNW-3 DiR liposomes or control DiR liposomes were dissolved in DMSO to a concentration of 7 mg/ml. The GUNW-3 liposomes solution or control liposomes solution (60 μl) and DMSO (40 μl) were pipetted into a well of a 96-well plate for fluorescence intensity measurement on a fluorescent plate reader by using 730 nm and 780 nm as the excitation and emission wavelengths. A calibration curve was constructed by spiking a known concentration of DiR to a blank liposomes in DMSO[72].

4.2.2.3 Liposomes stability study

The storage stability of liposomes was studies at 4 °C – the storage temperature. Since liposomes will encounter proteins once in the blood circulation, the stability of

liposomes in the presence of proteins (FBS) was investigated at 37 °C. The particle size was used as a parameter for micelle stability studies.

4.2.2.3.1 Stabilities of GUNW-3 DiR liposomes and control DiR liposomes

The particle size of a freshly prepared GUNW-3 DiR liposomes and control liposomes were checked, after a 0.5:100 dilution with deionized water as described early, every 24 h at 4°C for 7 days. The size was checked by the dynamic light scattering (DLS) method using Zetasizer (Malvern instrument, Westborough, MA).

4.2.2.3.2 Stabilities of GUNW-3 DiR liposomes and control DiR liposomes in the presence of FBS

Using the partial size as an indicator, the stability of GUNW-3 DiR liposomes (1 mg/mL) and control DiR liposome (1 mg/mL) were checked in the presence of RPMI 1640 growth medium supplemented with 10% FBS at 37 °C. Samples were diluted to a concentration of 0.5:100 with deionized water and the size was checked by the dynamic light scattering (DLS) method using Zetasizer (Malvern instrument, Westborough, MA).

4.2.2.4 Whole body optical imaging of mice

Females BALB/Cj mice (6-8 weeks old, 17-20 g) were used for this work. Mice were purchased from Jackson Laboratory (Bar Harbor, ME, USA) and acclimatized to a laboratory condition for one week before the experiment. For the experiment, mice were divided into two groups and intravenously injected with GUNW-3 DiR liposomes and control DiR liposomes (250 μg DiR/Kg) respectively through the tail vein. Optical images for the whole body were taken at 5 min, 15 min, 30 min, 60 min, and 180 min. The images were analyzed using the Bruker MI SE software. All procedures were

approved by the Institutional Animal Care and Use Committee (IACUC) at South Dakota State University, Brookings, SD, USA.

4.2.2.5 EX-vivo brain and organ imaging

To assess the organ distribution, mice were sacrificed 1 h and 48 h after a single dose IV injection by the tail vein injection The heart was perfused with DPBS to remove blood before organs were collected. The images were using the Bruker MI SE software.

4.2.2.6 Statistics

In this work, results from *in vitro* experiments were reported as mean ± standard deviation (SD) and results from *in vivo* experiment were reported as standard error of mean (SEM). Student's t-test was used to compare two groups. The results reported using GraphPad Prism 8 to demonstrate the statistical difference ($p < 0.05$).

4.3 Result and Discussion

4.3.1 Liposome preparation

Control and GUNW-3 liposomes were prepared based on the thin layer hydration method. Lecithin, DDAB, and cholesterol, and DiR were added to chloroform. The chloroform was evaporated to from the lipid film. The lipid film was hydrated with DPBS with or without GUNW-3 to form GUNW-3 DiR liposomes or control DiR liposomes. A graphic description of the procedures is presented in Figure 4.6.

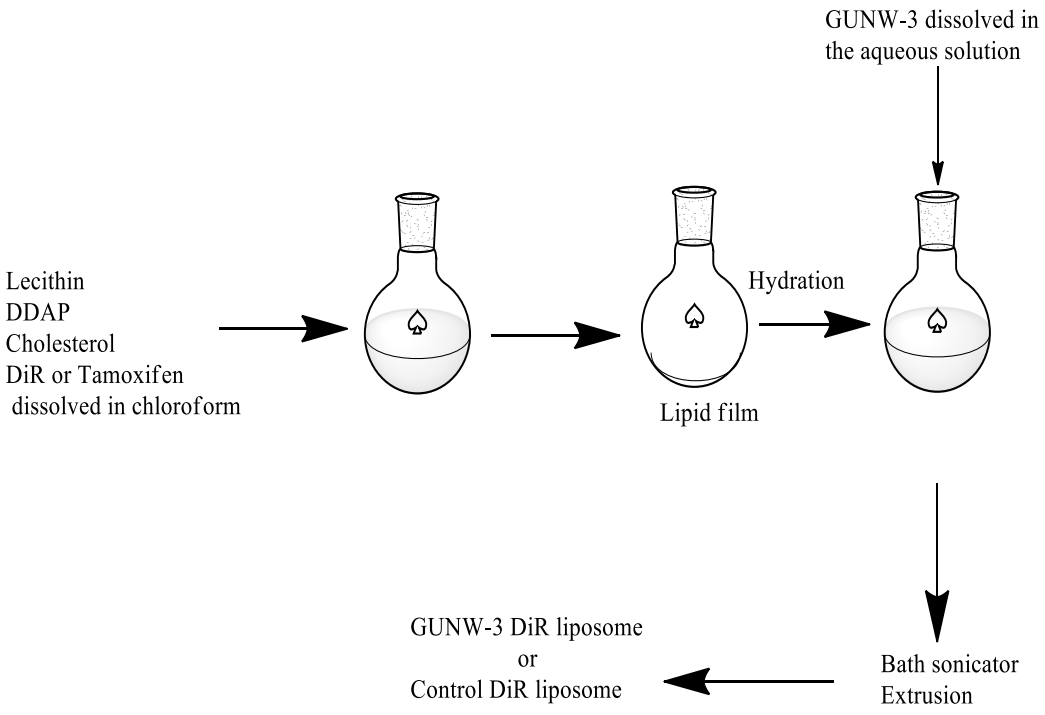

Figure 4.6 Graphic description of the preparation of GUNW-3 DiR liposomes and control DiR liposomes using the thin hydration method.

4.3.2 Characterization of DiR liposomes

The average particle size and size distribution of the control DiR liposomes and GUNW-3 DiR liposomes are presented in Figure 4.7. The particle size of the control DiR liposomes and GUNW-3 DiR liposomes was found to be 99.56 nm ± 2.5 and 102.3 nm ± 0.6 respectively. The parameter for the size distribution (PDI) for control DiR liposomes and GUNW-3 DiR liposomes were 0.205 and 0.228 respectively (Figure 4.6.B, Table 4.1). The zeta potential of the control DiR liposomes and GUNW-3 DiR liposomes were +19.2 mV ± 6.53 and -27.4mV ±1.6 (Figure 4.7.B). It is noted that the charge of the liposomes changed from positive (control DiR liposomes) to negative (GUNW-3 DiR liposomes) after the liposomes were added with GUNW-3. The negative charge on the GUNW-3 DiR liposome surface was a result of negative charges from the GUNW-3 molecule. A change of the surface charge of the liposomes is an indication that the liposome surface is now containing the brain targeting molecule GUNW-3.

The EE% and LC% of the control DiR liposomes were 69% ±0.7 and 0.17% while the EE% and LC% of GUNW-3 DiR liposomes were 71±0.5% and 0.16% respectively (Table 4.1). Both liposomes contained the same amount of phospholipid (7 mg/ml), cholesterol (1 mg/ml), and cationic lipid (DDAB) (3mg/ml). GUNW-3 was determined to be 4.48 mg/mL by LC/MS.

A

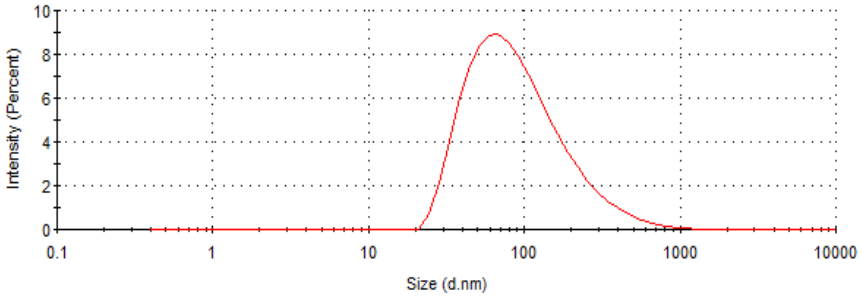

B

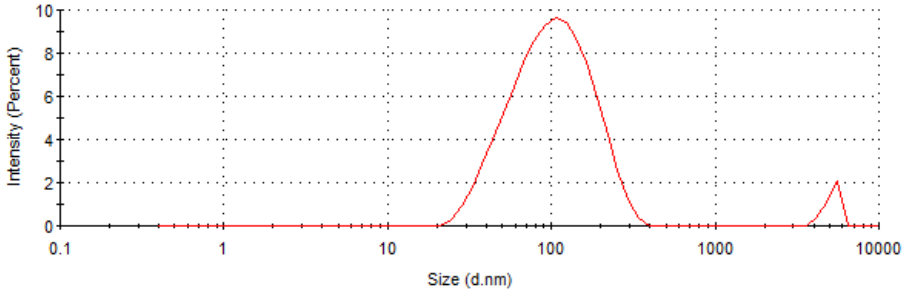

Figure 4.7 Particle size and size distribution of control DiR liposomes (A), and GUNW-3 DiR liposome (B).

Table 4.1 Parameters of control DiR liposomes and GUNW-3 liposomes (n = 3, mean ±SD).

Formulation	Theoretical loading (%)	Size (nm)	PDI	Zeta potential (mV)	EE%	LC%
Control DiR liposomes	0.25	99.5 ± 2.5	0.205	+19.2 ±6.5	69 ± 0.7	0.17 ± 0.0013
GUNW-3 DiR liposomes	0.22	102 ± 0.6	0.288	-27.4±1.9	71 ± 0.5	0.16 ± 0.0008

4.3.2 Liposome stability

4.3.2.1 DiR liposome storage stability

The storage stabilities of GUNW-3 DiR liposomes and control DiR liposomes were monitored at 4 °C for 7 days and the results are presented in Figure 4.8A. The particle size was the parameters used to determine the stability. The size of the control DiR liposomes was 99.56 ± 2.89 nm on day 1 compared with 102.83 ± 1.2 nm on day 7, no statistical difference was found on day 1 and day 7. The same was true with GUNW-3 DiR liposomes: particle size was 102 ± 0.6 nm on day 1 vs 96 ± 1.6 nm on day 7 with no statistical difference. These results suggest that both liposomes were stable at its storage temperature for 7 days.

4.3.2.2 Stability of DiR liposome in the presence of proteins (FBS)

The stability of GUNW-3 DiR liposomes and control DiR liposomes were studied in RPMI 1640 growth medium supplemented with 10% FBS. The results are presented in Figure 4.8 B, and C). GUNW-3 DiR liposomes increased the size from 127 nm to 250 nm in the first hour while control DiR liposomes increased the size from 124 nm to 358 nm in the first hour. Similar to GUNW-3 DiR micelles, GUNW-3 DiR liposomes then appeared to slowly and continuously increase its size to 389 nm by 48 hours demonstrating a two-phase increase in particle size while control DiR liposomes remained almost unchanged. As we suggested in GUNW-3 DiR micelles, this two-phase increase in particle size indicates possibly two different mechanisms in particle size increases. One possible explanation might be that GUNW-3 liposomes may quickly complex with FBS that quickly increased the particle size initially (first phase size

increase), then followed by a slow increase in particle size which might be caused by particle aggregation.

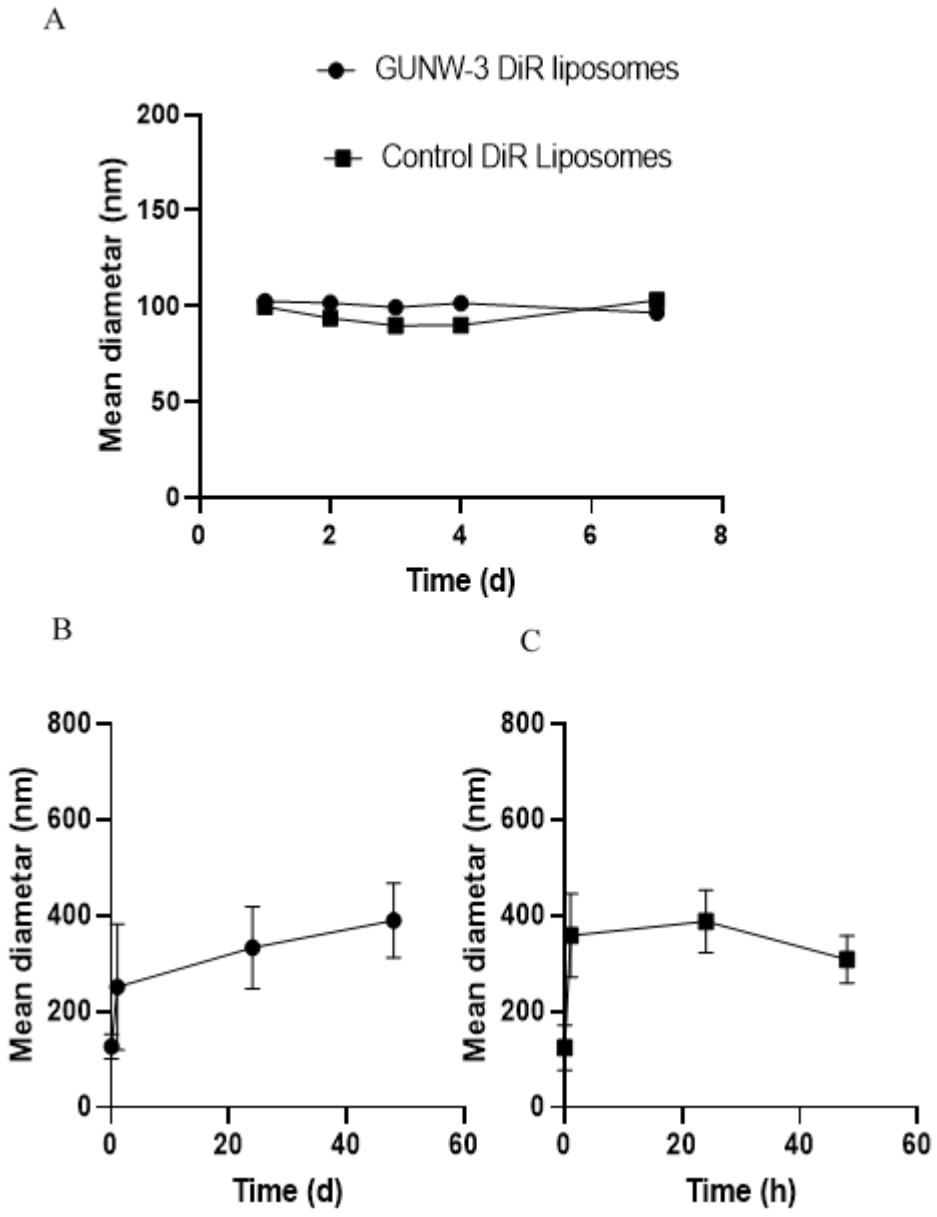

Figure 4.8 Stability of GUNW-3 DiR liposomes and control DiR liposomes. A: storage stability at 4 C for 7 days; B: GUNW-3 DiR liposomes; C: Control DiR liposomes

stability in the presence of proteins (FBS) at 37 C for 7 days. Results are presented as mean ±SD (n = 3).

4.3.3 In-vivo imaging

Whole body imaging of the mice treated with GUNW-3 DiR liposomes or control DiR liposomes was conducted to investigate the brain targeting effect of GUNW-3 DiR liposomes. Mice were treated with GUNW-3 DiR liposomes or control DiR liposomes with a single dose IV injection (0.25 mg/kg DiR) by the tail vein injection. Whole body images were taken at 15 min, 30 min, 60 min, and 180 min (Figure 4.11). In-vivo imaging showed a fast brain distribution (15 min) for GUNW-3 DiR liposomes while control DiR liposomes showed a fast liver distribution. Control DiR liposomes also showed a minimum brain distribution (Figure 4.9) which is consistent with the knowledge that cationic liposomes exhibit some brain-targeting effects. The fluorescence intensity in the brain continued to grow for GUNW-3 DiR liposomes till 30 min and maintained the same intensity till 60 min then started to drop (Figure 4.9). The fluorescence intensity from the brain treated with control DiR liposomes appeared to increase till 30 min then remain unchanged for the rest of the experiment (180 min). The increase in brain targeting based on the brain fluorescence intensity are 23 times at 15 min and 9 times at 30 min (Figure 4.10).

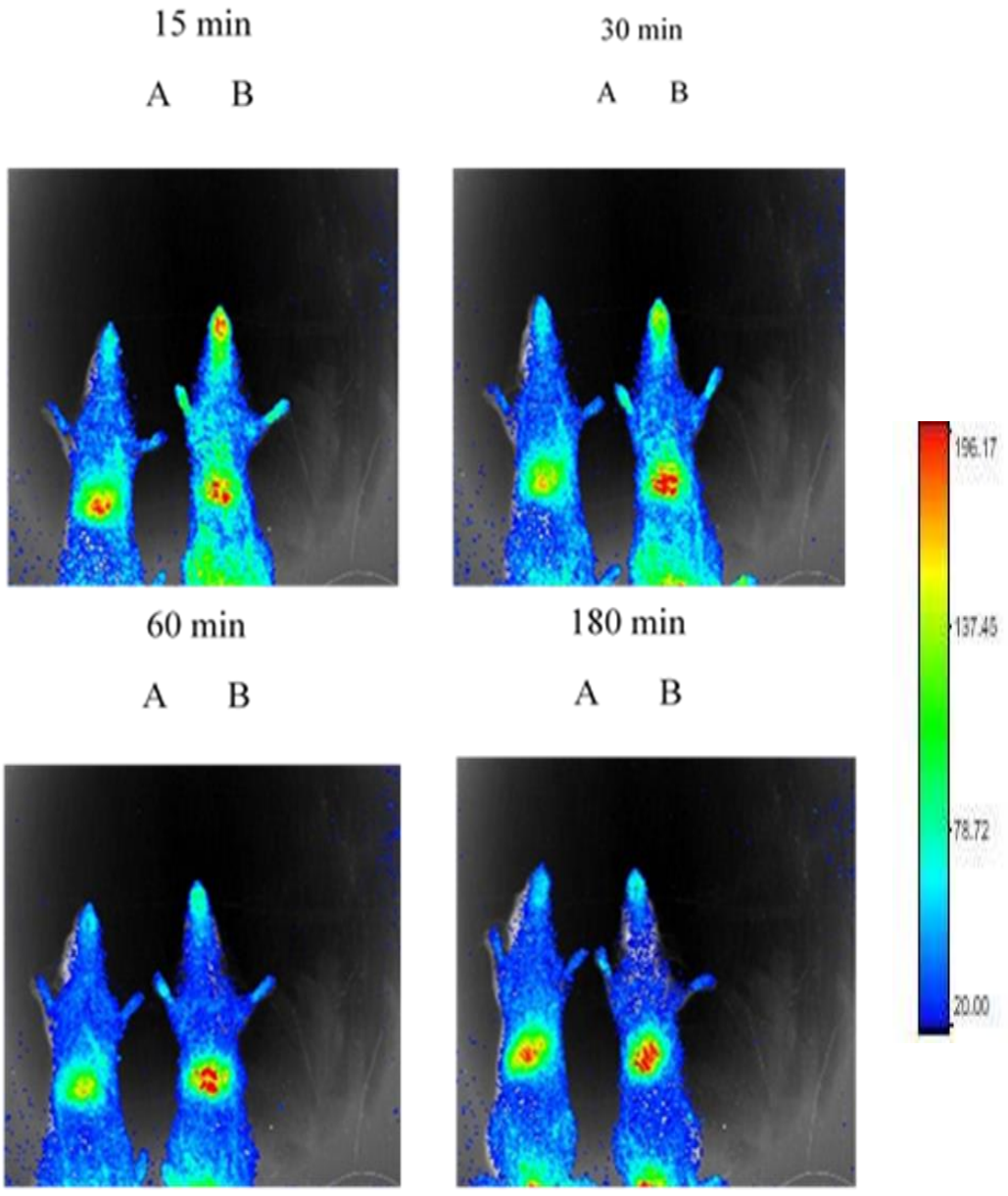

Figure 4.9 In-vivo whole-body imaging of mice at 15 min, 30 min, 60 min, and 180 min. A: control DiR liposomes; and B: GUNW-3 DiR liposomes. Representative image, n=3.

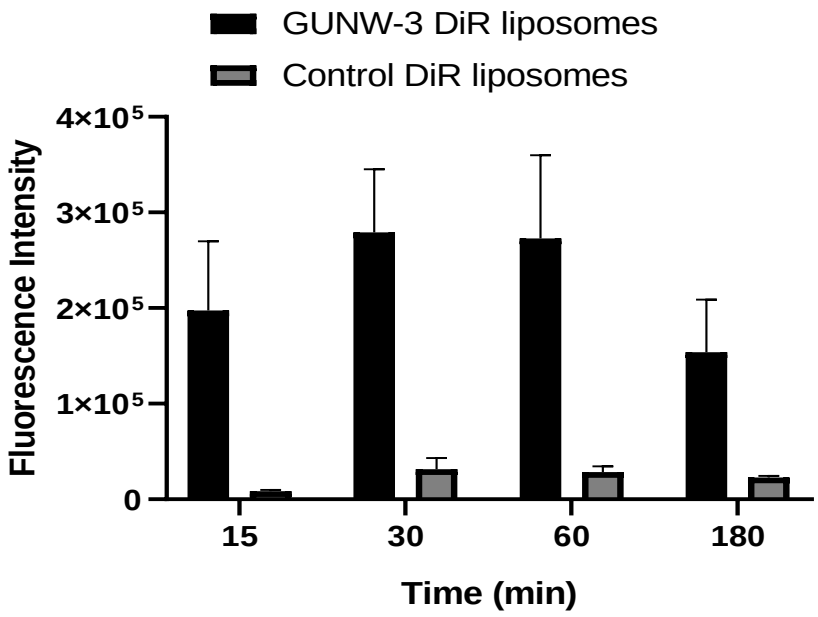

Figure 4.10 In-vivo semi-quantitative fluorescence intensity of brains. Results are presented as mean ± SEM (n=4).

4.3.4 Ex-vivo imaging.

To further confirm brain targeting, brain and some of the other major organs (brain, heart, lung, liver, spleen, and kidney) were collected for ex-vivo imaging at 1 h. Blood was removed by hear perfusion with DPBS before organ collection. Fluorescence images of the organs were obtained using Xtreme in-vivo imaging (Bruker).

4.3.4.1 Ex-vivo brain imaging at 1 h

As shown in figure 4.11. A and B, a significant increase in brain distribution was observed with mice treated with GUNW-3 DiR liposomes when compared with that from the control DiR liposomes (Figure 4.11). Based on the fluorescence intensity, GUNW-3 DiR showed a 3-times brain distribution when compared with the control liposomes ($p=0.0443$, n=3, Figure 4.11. C). The results suggested that GUNW-3 liposomes exhibit a significantly high brain targeting ability than control DiR liposomes.

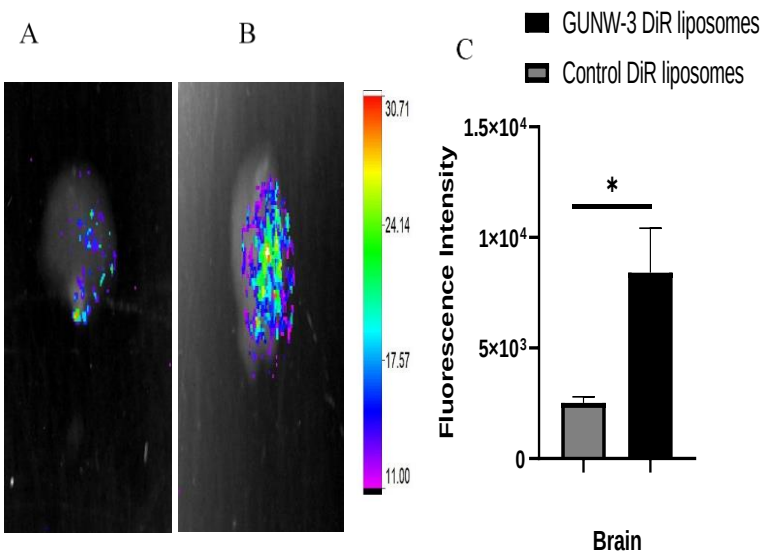

Figure 4 11 Ex-vivo imaging of the brains at 1 h after a single dose IV injection of A: control DiR liposomes or B: GUNW-3 DiR liposomes. D: Semi-quantitative fluorescence intensity of brains presented as mean ± SEM. *<0.05, **<0.01, ***<0.001 (n = 3).

4.3.4.2 Ex-vivo organ imaging at 1 h

In addition to brain distribution, distribution to other major organs (heart, lung, liver, spleen, and kidney) was examined. The images of these organs and their corresponding fluorescence intensities were presented in Figure 4.12 and Figure 4.13. Based on the fluorescence intensity in Figure 4.13, it appears the major distribution of both liposomes was in the liver and lung though distribution in the heart, kidney and spleen was also observed. It appeared control DiR liposomes distributed to the liver and lungs more than GUNW-3 DiR liposomes while GUNW-3 DiR liposomes distributed to the kidney more than control DiR liposomes. The higher organ distribution of the control DiR liposomes comparing to GUNW-3 DiR liposomes may be explained by the interaction between the GUNW-3 DiR liposomes to albumin which decreases the distribution of GUNW-3 DiR liposomes to organs. This interaction happens because of

the presence of GSH on the surface of GUNW-3 liposomes. It has been reported that GSH can bind to BSA at site I in subdomain IIA according to the molecular docking results. The binding process is dominated by hydrogen bonds, which is consistent with the fluorescence studies. It was concluded that there was a strong interaction between GSH and BSA. The binding of a drug to albumin is believed to reduce the level of free drug available [88-90].

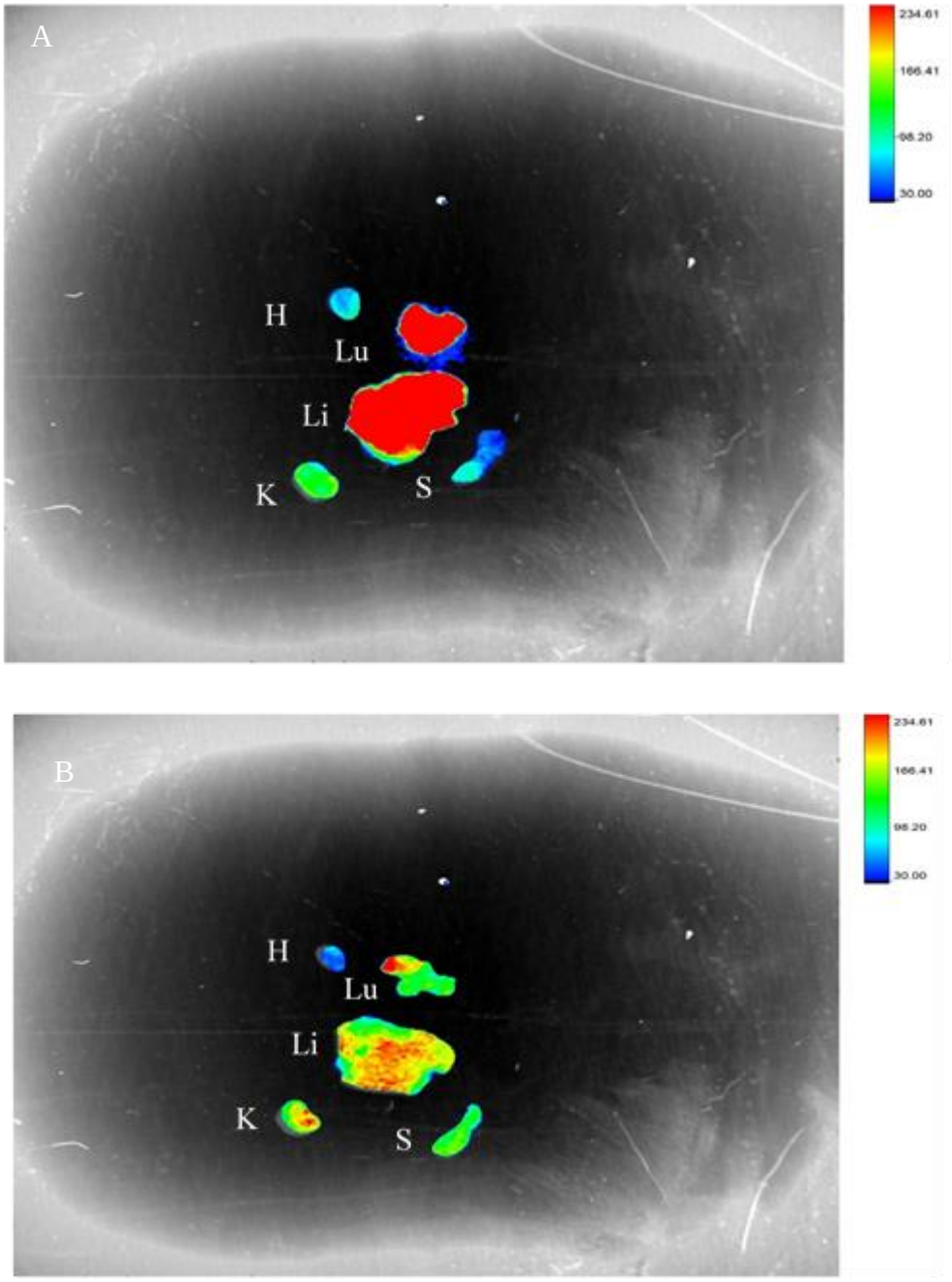

Figure 4.12 Ex-vivo imaging of the major organ 1h after (i.v) injection of the (A) Control DiR liposomes (B) GUNW-3 DiR liposomes. Organs (H: heart, Lu: lung, Li: liver, S: spleen, and K: kidney). Representative image, n=3.

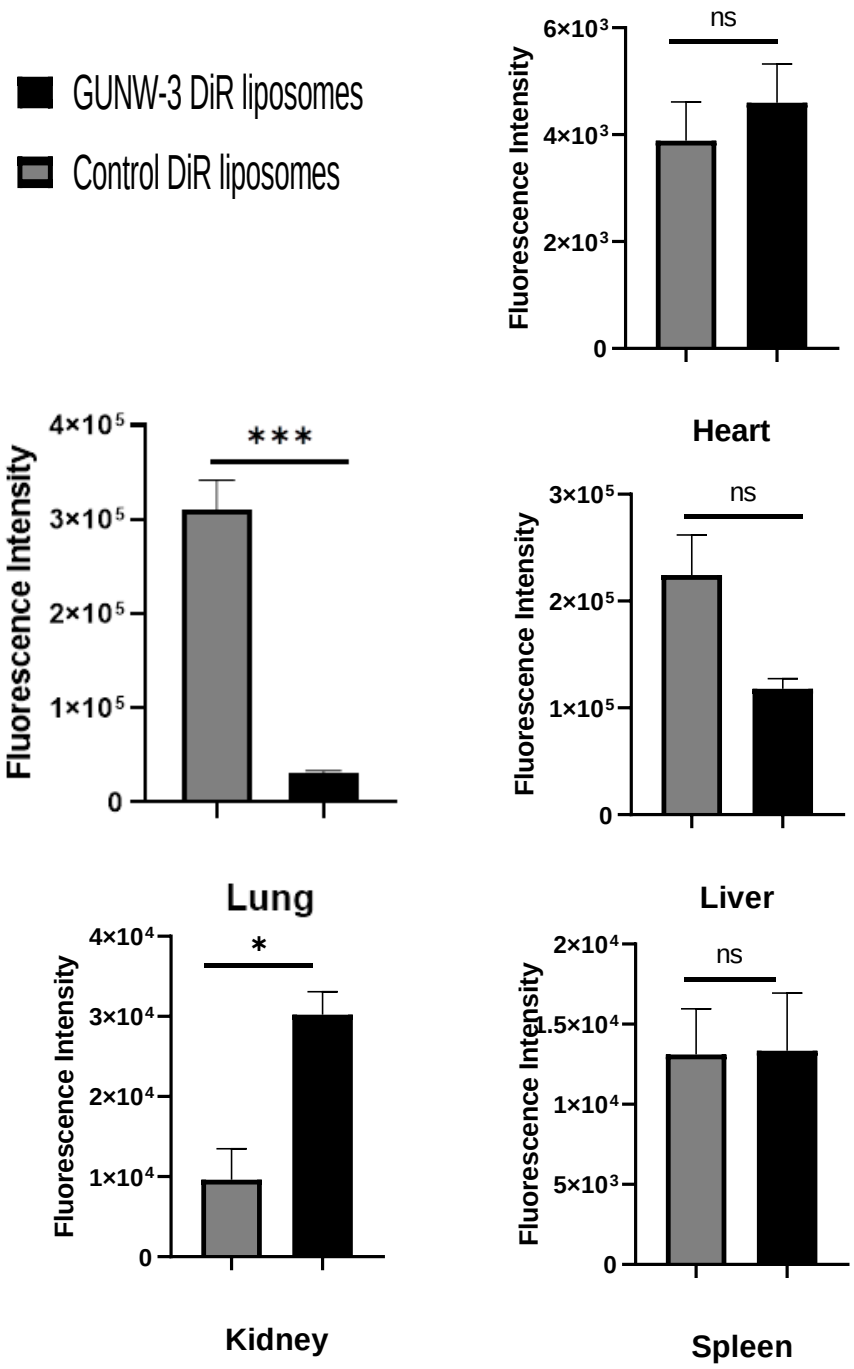

Figure 4.13 Semi-quantitative fluorescence intensity from different organs. Data were presented as mean ± SEM, ns: no statistically significant difference, *<0.05, **<0.01, ***<0.001 (n = 3).

In summary, we have demonstrated that GUNW-3 liposomes were able to encapsulate DiR and deliver DiR to the brain. Ex-vivo imaging showed GUNW-3 DiR liposomes reached the brain 3 times of control DiR liposomes. Our data show that GUNW-3 liposomes have the potential to be developed into an effective drug delivery system for brain-targeting.

Chapter 5. Conclusion, Significance, and Future Direction

5.1 Conclusion

The BBB is a selective barrier made by endothelial cells that separates the peripheral blood circulation from the CNS. The BBB serves as a physical barrier through the tight junction of endothelial cells and overdistribution of different drug efflux pumps such as P-glycoproteins and multidrug-resistance protein. Because of that reason, nearly all big drug molecules and more than 98% of small drug molecules are not able to reach the brain to effectively treat brain diseases. Utilizing endogenous ligands of receptors or transporters that are expressed on the surface of the BBB is one of the most commonly employed methods to overcome the BBB issue. GSH is found in both endothelium cells and astroglia with mM concentration. GSH transporters are highly expressed on the BBB surface.

This dissertation presented a rational design and synthesis of GSH-based brain targeting molecule, GUNW-3. GUNW-3 was designed to contain a GSH molecule as a hydrophilic head group and a cholesterol molecule as a hydrophobic tail group. These two groups are connected with a small linker of a diethylene glycol group. As an amphiphilic molecule, GUNW-3 can form micelles by itself. Micelles are an effective drug delivery system. GUNW-3 micelles were expected to be brain targeting due to the presence of the hydrophilic GSH part on the surface of the micelles. Moreover, we used GUNW-3 to modify the liposome surface to to form GUNW-3 liposomes for brain targeting.

Ex-vivo brain targeting evaluation of GUNW-3 micelles showed 5-times higher in brain targeting than that of the control liposomes and 12-times higher than that of free

DiR at the first hour after an i.v dosing. Forty eight hours post dosing, GUNW-3 micelles showed 6.5 times higher in brain targeting than that of control liposome and 14 times higher than that of free DiR. Our data confirm the ability of the brain delivery of the GUNW-3 micelles. Brain targeting was also observed with GUNW-3 liposomes. Ex-vivo imaging of the brains showed a 3 times increase in brain targeting by GUNW-3 liposomes when compared with the control liposomes.

In summary, we have successfully synthesized and characterized the rationally designed GUNW-3 as a brain targeting agent. GUNW-3 micelles and GUNW-3 liposomes are promising drug delivery systems for delivering therapeutic and diagnostic agents to the brain for therapeutic, preventive, and diagnostic applications.

5.2 Limitation

This work focuses on confirming the brain-targeting ability of GUNW-3 as a micelle (GUNW-3 micelles) or as a brain-targeting agent to facilitate liposomes to cross the BBB. The abilities of GUNW-3 to improve brain targeting of both formulations (micelles and liposomes) were confirmed by using DiR as a tracking agent. DiR is very widely used dye to confirm the in vivo distribution of nanoparticles. However, drugs with different lipophilicities are needed to determine the applicability of these two formulations. Further, an in vitro experiment with brain endothelial cells need to be conducted to confirm that these two formulations enter the cells through the GSH transporter.

5.3 Significance

The BBB is the major cause of treatment failure for various brain diseases such as brain cancer and caner metastasis, Parkinson’s disease, and Alzheimer’s disease etc. The

failure is resulted from the inability of a drug molecule to pass the BBB to achieve the effective therapeutic concentration. This dissertation demonstrates a proof of concept that both GUNW-3 micelles and GUNW-3 liposomes can effectively deliver molecules to the brain. The preliminary data also show that GUNW-3 micelles and GUNW-3 liposomes are not cytotoxic at the dosages employed both *in vitro* and *in vivo*. GUNW-3 micelles and GUNW-3 liposomes may find a great application in helping treatment of various brain diseases.

5.4 Future direction

GUNW-3 micelles and GUNW-3 liposomes showed a promising brain targeting ability. Our future plan for this project includes:

- Further characterization GUNW-3 liposomes and micelles
    - *In vitro* mechanistic study of brain-targeting
    - *In vivo* pharmacokinetics study
    - Evaluation of GUNW-3 micelles and GUNW-3 liposomes to encapsulate therapeutic and diagnostic compounds.
- Prepare more GUNW-3 derivatives for more effective brain targeting agents.

References

1. Zaidi, Z.F.J.T.o.a.j., *Gender differences in human brain: a review.* 2010. **2**(1).
2. Dekaban, A.S., D.J.A.o.N.O.J.o.t.A.N.A. Sadowsky, and t.C.N. Society, *Changes in brain weights during the span of human life: relation of brain weights to body heights and body weights.* 1978. **4**(4): p. 345-356.
3. Shatz, C.J.J.S.A., *The developing brain.* 1992. **267**(3): p. 60-67.
4. Xing, C.-Y., et al., *Distribution of cardiac output to the brain across the adult lifespan.* 2017. **37**(8): p. 2848-2856.
5. Jain, V., et al., *MRI estimation of global brain oxygen consumption rate.* 2010. **30**(9): p. 1598-1607.
6. Brodal, P., *The central nervous system: structure and function*. 2004: Oxford University Press.
7. Abbott, N.J., et al., *Structure and function of the blood–brain barrier.* 2010. **37**(1): p. 13-25.
8. Hawkins, B.T. and T.P. Davis, *The blood-brain barrier/neurovascular unit in health and disease.* Pharmacological reviews, 2005. **57**(2): p. 173-185.
9. Bentivoglio, M. and K. Kristensson, *Tryps and trips: cell trafficking across the 100-year-old blood–brain barrier.* Trends in neurosciences, 2014. **37**(6): p. 325-333.
10. Abbott, N.J., L. Rönnbäck, and E.J.N.r.n. Hansson, *Astrocyte–endothelial interactions at the blood–brain barrier.* 2006. **7**(1): p. 41.
11. Abbott, N.J., *Evidence for bulk flow of brain interstitial fluid: significance for physiology and pathology.* Neurochemistry international, 2004. **45**(4): p. 545-552.

12. Löscher, W. and H.J.N.R.N. Potschka, *Drug resistance in brain diseases and the role of drug efflux transporters.* 2005. **6**(8): p. 591.

13. Ghose, A.K., V.N. Viswanadhan, and J.J. Wendoloski, *A knowledge-based approach in designing combinatorial or medicinal chemistry libraries for drug discovery. 1. A qualitative and quantitative characterization of known drug databases.* Journal of combinatorial chemistry, 1999. **1**(1): p. 55-68.

14. Lipinski, C.A., *Drug-like properties and the causes of poor solubility and poor permeability.* Journal of pharmacological and toxicological methods, 2000. **44**(1): p. 235-249.

15. Bradbury, M., et al., *The distribution of potassium, sodium, chloride and urea between lumbar cerebrospinal fluid and blood serum in human subjects.* Clinical science, 1963. **25**: p. 97.

16. Hansen, A.J., *Effect of anoxia on ion distribution in the brain.* Physiological reviews, 1985. **65**(1): p. 101-148.

17. Somjen, G.G., *Ions in the brain: normal function, seizures, and stroke*. 2004: Oxford University Press.

18. Abbott, N.J., et al., *Structure and function of the blood–brain barrier.* Neurobiology of disease, 2010. **37**(1): p. 13-25.

19. Bernacki, J., et al., *Physiology and pharmacological role of the blood-brain barrier.* Pharmacol Rep, 2008. **60**(5): p. 600-22.

20. Lim, D.A., Y.-C. Huang, and A. Alvarez-Buylla, *The adult neural stem cell niche: lessons for future neural cell replacement strategies.* Neurosurgery Clinics, 2007. **18**(1): p. 81-92.

21. Meng, J., V. Agrahari, and I. Youm, *Advances in targeted drug delivery approaches for the central nervous system tumors: the inspiration of nanobiotechnology.* Journal of Neuroimmune Pharmacology, 2017. **12**(1): p. 84-98.

22. Pardridge, W.M., *Brain drug targeting: the future of brain drug development*. 2001: Cambridge University Press.

23. Fung, L.K., et al., *Chemotherapeutic drugs released from polymers: distribution of 1, 3-bis (2-chloroethyl)-l-nitrosourea in the rat brain.* Pharmaceutical research, 1996. **13**(5): p. 671-682.

24. Pardridge, W.M., *The blood-brain barrier: bottleneck in brain drug development.* NeuroRx, 2005. **2**(1): p. 3-14.

25. Lossinsky, A., A. Vorbrodt, and H. Wisniewski, *Scanning and transmission electron microscopic studies of microvascular pathology in the osmotically impaired blood-brain barrier.* Journal of neurocytology, 1995. **24**(10): p. 795-806.

26. Nadal, A., et al., *Plasma albumin is a potent trigger of calcium signals and DNA synthesis in astrocytes.* Proceedings of the National Academy of Sciences, 1995. **92**(5): p. 1426-1430.

27. Lloyd, K. and O. Hornykiewicz, *Parkinson's disease: activity of L-dopa decarboxylase in discrete brain regions.* Science, 1970. **170**(3963): p. 1212-1213.

28. Fischer, H., R. Gottschlich, and A. Seelig, *Blood-brain barrier permeation: molecular parameters governing passive diffusion.* The Journal of membrane biology, 1998. **165**(3): p. 201-211.

29. Bodor, N. and J.J. Kaminski, *Prodrugs and site-specific chemical delivery systems,* in *Annual Reports in Medicinal Chemistry*. 1987, Elsevier. p. 303-313.

30. Pathan, S.A., et al., *CNS drug delivery systems: novel approaches.* Recent patents on drug delivery & formulation, 2009. **3**(1): p. 71-89.

31. Pardridge, W.M., et al., *Blood-brain barrier transport and brain metabolism of adenosine and adenosine analogs.* Journal of Pharmacology and Experimental Therapeutics, 1994. **268**(1): p. 14-18.

32. Zhang, Y. and W.M. Pardridge, *Rapid transferrin efflux from brain to blood across the blood–brain barrier.* Journal of neurochemistry, 2001. **76**(5): p. 1597-1600.

33. Jain, A. and S.K. Jain, *Ligand-appended BBB-targeted nanocarriers (LABTNs).* Critical Reviews™ in Therapeutic Drug Carrier Systems, 2015. **32**(2).

34. Rip, J., *Liposome technologies and drug delivery to the CNS.* Drug Discovery Today: Technologies, 2016. **20**: p. 53-58.

35. Mishra, V., et al., *Targeted brain delivery of AZT via transferrin anchored pegylated albumin nanoparticles.* Journal of drug targeting, 2006. **14**(1): p. 45-53.

36. Jones, A.R. and E.V. Shusta, *Blood–brain barrier transport of therapeutics via receptor-mediation.* Pharmaceutical research, 2007. **24**(9): p. 1759-1771.

37. Dufès, C., M. Al Robaian, and S. Somani, *Transferrin and the transferrin receptor for the targeted delivery of therapeutic agents to the brain and cancer cells.* Therapeutic delivery, 2013. **4**(5): p. 629-640.

38. Huwyler, J., D. Wu, and W.M. Pardridge, *Brain drug delivery of small molecules using immunoliposomes.* Proceedings of the National Academy of Sciences, 1996. **93**(24): p. 14164-14169.

39. Friden, P.M., et al., *Anti-transferrin receptor antibody and antibody-drug conjugates cross the blood-brain barrier.* Proceedings of the National Academy of Sciences, 1991. **88**(11): p. 4771-4775.

40. Lee, H.J., et al., *Targeting rat anti-mouse transferrin receptor monoclonal antibodies through blood-brain barrier in mouse.* Journal of Pharmacology and Experimental Therapeutics, 2000. **292**(3): p. 1048-1052.

41. Shi, N., et al., *Brain-specific expression of an exogenous gene after iv administration.* Proceedings of the National Academy of Sciences, 2001. **98**(22): p. 12754-12759.

42. Friden, P.M., et al., *Characterization, receptor mapping and blood-brain barrier transcytosis of antibodies to the human transferrin receptor.* Journal of Pharmacology and Experimental Therapeutics, 1996. **278**(3): p. 1491-1498.

43. Halmos, T., et al., *Synthesis of glucose-chlorambucil derivatives and their recognition by the human GLUT1 glucose transporter.* European journal of pharmacology, 1996. **318**(2-3): p. 477-484.

44. Patching, S.G., *Glucose transporters at the blood-brain barrier: function, regulation and gateways for drug delivery.* Molecular neurobiology, 2017. **54**(2): p. 1046-1077.

45. Sies, H.J.F.R.B. and Medicine, *Glutathione and its role in cellular functions.* 1999. **27**(9-10): p. 916-921.

46. Kannan, R., et al., *GSH transport in human cerebrovascular endothelial cells and human astrocytes: evidence for luminal localization of Na+-dependent GSH transport in HCEC.* 2000. **852**(2): p. 374-382.

47. Kannan, R., et al., *Evidence for carrier-mediated transport of glutathione across the blood-brain barrier in the rat.* 1990. **85**(6): p. 2009-2013.

48. Zlokovic, B.V., et al., *Evidence for transcapillary transport of reduced glutathione in vascular perfused guinea-pig brain.* 1994. **201**(1): p. 402-408.

49. Kannan, R., et al., *GSH transport in immortalized mouse brain endothelial cells: Evidence for apical localization of a sodium-dependent GSH transporter.* 1999. **73**(1): p. 390-399.

50. Slivka, A., C. Mytilineou, and G.J.B.r. Cohen, *Histochemical evaluation of glutathione in brain.* 1987. **409**(2): p. 275-284.

51. Raps, S.P., et al., *Glutathione is present in high concentrations in cultured astrocytes but not in cultured neurons.* 1989. **493**(2): p. 398-401.

52. Kannan, R., et al., *Evidence for the Existence of a Sodium-dependent Glutathione (GSH) Transporter EXPRESSION OF BOVINE BRAIN CAPILLARY mRNA AND SIZE FRACTIONS IN XENOPUS LAEVIS OOCYTES AND DISSOCIATION FROM-GLUTAMYLTRANSPEPTIDASE AND FACILITATIVE GSH TRANSPORTERS.* 1996. **271**(16): p. 9754-9758.

53. More, S.S. and R.J.J.o.m.c. Vince, *Design, synthesis and biological evaluation of glutathione peptidomimetics as components of anti-Parkinson prodrugs.* 2008. **51**(15): p. 4581-4588.

54. Geldenhuys, W., et al., *Brain-targeted delivery of doxorubicin using glutathione-coated nanoparticles for brain cancers.* Pharmaceutical development and technology, 2015. **20**(4): p. 497-506.

55. Rip, J., et al., *Glutathione PEGylated liposomes: pharmacokinetics and delivery of cargo across the blood–brain barrier in rats.* 2014. **22**(5): p. 460-467.

56. Nosrati, H., et al., *Glutathione (GSH) Peptide Conjugated Magnetic Nanoparticles As Blood–Brain Barrier Shuttle for MRI-Monitored Brain Delivery of Paclitaxel.* 2019.

57. Lassila, T., et al., *Tandem mass spectrometric analysis of S-and N-linked glutathione conjugates of pulegone and menthofuran and identification of P450 enzymes mediating their formation.* Rapid Communications in Mass Spectrometry, 2016. **30**(7): p. 917-926.

58. Trivedi, R. and U.B. Kompella, *Nanomicellar formulations for sustained drug delivery: strategies and underlying principles.* Nanomedicine, 2010. **5**(3): p. 485-505.

59. Domínguez, A., et al., *Determination of critical micelle concentration of some surfactants by three techniques.* Journal of chemical education, 1997. **74**(10): p. 1227.

60. Torchilin, V.P., *Micellar nanocarriers: pharmaceutical perspectives.* Pharmaceutical research, 2007. **24**(1): p. 1.

61. .

62. Kanazawa, T., et al., *Cell-penetrating peptide-modified block copolymer micelles promote direct brain delivery via intranasal administration.* Pharmaceutical research, 2011. **28**(9): p. 2130-2139.

63. Zhang, Z., et al., *p-Hydroxybenzoic acid (p-HA) modified polymeric micelles for brain-targeted docetaxel delivery.* Chinese Science Bulletin, 2013. **58**(21): p. 2651-2656.

64. Quader, S. and K. Kataoka, *Nanomaterial-enabled cancer therapy.* Molecular Therapy, 2017. **25**(7): p. 1501-1513.

65. Kesharwani, P. and U. Gupta, *Nanotechnology-Based Targeted Drug Delivery Systems for Brain Tumors*. 2018: Academic Press.

66. Bloch, K., *Cholesterol: evolution of structure and function*, in *New Comprehensive Biochemistry*. 1991, Elsevier. p. 363-381.

67. Franco, R. and J. Cidlowski, *Apoptosis and glutathione: beyond an antioxidant.* Cell death and differentiation, 2009. **16**(10): p. 1303.

68. Daman, Z., et al., *Preparation, optimization and invitro characterization of stearoyl-gemcitabine polymeric micelles: A comparison with its self-assembled nanoparticles.* International journal of pharmaceutics, 2014. **468**(1-2): p. 142-151.

69. Piñeiro, L., M. Novo, and W. Al-Soufi, *Fluorescence emission of pyrene in surfactant solutions.* Advances in colloid and interface science, 2015. **215**: p. 1-12.

70. Meng, X., et al., *Pluronic F127 and D-α-tocopheryl polyethylene glycol succinate (TPGS) mixed micelles for targeting drug delivery across the blood brain barrier.* Scientific reports, 2017. **7**(1): p. 2964.

71. Li, F., et al., *Preparation and Characterization of Lipophilic Doxorubicin Pro-drug Micelles.* JoVE (Journal of Visualized Experiments), 2016(114): p. e54338.

72. Householder, K.T., et al., *Intravenous delivery of camptothecin-loaded PLGA nanoparticles for the treatment of intracranial glioma.* International journal of pharmaceutics, 2015. **479**(2): p. 374-380.

73. Piazzini, V., et al., *Stealth and cationic nanoliposomes as drug delivery systems to increase andrographolide BBB permeability.* Pharmaceutics, 2018. **10**(3): p. 128.

74. Vieira, D.B. and L.F. Gamarra, *Getting into the brain: liposome-based strategies for effective drug delivery across the blood–brain barrier.* International journal of nanomedicine, 2016. **11**: p. 5381.

75. Jahanban-Esfahlan, A. and V. Panahi-Azar, *Interaction of glutathione with bovine serum albumin: Spectroscopy and molecular docking.* Food chemistry, 2016. **202**: p. 426-431.

76. Bozzuto, G. and A. Molinari, *Liposomes as nanomedical devices.* International journal of nanomedicine, 2015. **10**: p. 975.

77. Hoshyar, N., et al., *The effect of nanoparticle size on in vivo pharmacokinetics and cellular interaction.* Nanomedicine, 2016. **11**(6): p. 673-692.

78. An, F.-F. and X.-H. Zhang, *Strategies for preparing albumin-based nanoparticles for multifunctional bioimaging and drug delivery.* Theranostics, 2017. **7**(15): p. 3667.

79. Mozafari, M.R., et al., *Recent trends in the lipid-based nanoencapsulation of antioxidants and their role in foods.* Journal of the Science of Food and Agriculture, 2006. **86**(13): p. 2038-2045.

80. Milla, P., F. Dosio, and L. Cattel, *PEGylation of proteins and liposomes: a powerful and flexible strategy to improve the drug delivery.* Current drug metabolism, 2012. **13**(1): p. 105-119.

81. Schwendener, R.A., *Liposomes in biology and medicine*, in *Bio-Applications of Nanoparticles*. 2007, Springer. p. 117-128.

82. Noble, G.T., et al., *Ligand-targeted liposome design: challenges and fundamental considerations.* Trends in biotechnology, 2014. **32**(1): p. 32-45.

83. Budai, M. and M. Szogyi, *Liposomes as drug carrier systems. Preparation, classification and therapeutic advantages of liposomes.* Acta Pharmaceutica Hungarica, 2001. **71**(1): p. 114-118.

84. Yang, Z., et al., *Dual receptor-specific peptides modified liposomes as VEGF siRNA vector for tumor-targeting therapy.* Current gene therapy, 2014. **14**(4): p. 289-299.

85. Shahidi, F. and X.Q. Han, *Encapsulation of food ingredients.* Critical Reviews in Food Science & Nutrition, 1993. **33**(6): p. 501-547.

86. Kaddah, S., et al., *Cholesterol modulates the liposome membrane fluidity and permeability for a hydrophilic molecule.* Food and chemical toxicology, 2018. **113**: p. 40-48.

87. El-Laithy, H.M., O. Shoukry, and L.G. Mahran, *Novel sugar esters proniosomes for transdermal delivery of vinpocetine: preclinical and clinical studies.* European journal of pharmaceutics and biopharmaceutics, 2011. **77**(1): p. 43-55.

88. Merlot, A.M., D.S. Kalinowski, and D.R. Richardson, *Unraveling the mysteries of serum albumin—more than just a serum protein.* Frontiers in physiology, 2014. **5**: p. 299.

89. Lancon, A., et al., *Human hepatic cell uptake of resveratrol: involvement of both passive diffusion and carrier-mediated process.* Biochemical and biophysical research communications, 2004. **316**(4): p. 1132-1137.

90. Vuignier, K., et al., *Drug–protein binding: a critical review of analytical tools.* Analytical and bioanalytical chemistry, 2010. **398**(1): p. 53-66.